

## Manuscript # ACP-2015-793

### Responses to Referee #2: Report #1

The authors have made an effort to address the questions raised by the reviewers. The model sensitivity tests as performed by the authors should be helpful for further understanding the sources and formation mechanisms of nitrate aerosols in the UTLS over the TP/SASM region. The authors' responses are generally fine, but additional issues arising need to be addressed further. Below are my specific comments and suggestions.

It is interesting to see that compared to surface  $\text{NO}_3^-$ , nitrate aerosols in the UTLS over the TP/SASM region are not so sensitive to a 50% reduction of anthropogenic  $\text{NO}_x$  emissions in Asia. What could one learn from this result with regards to the sources and formation mechanism of nitrate aerosols (and their gas precursors) in the UTLS over the TP/SASM region? Specifically, does it mean that anthropogenic  $\text{NO}_x$  emissions in Asia (including South and Southeast Asia) do not have large impacts on nitrate aerosols in the UTLS over the TP/SASM region? The authors may want to give a short discussion on the implications of this sensitivity result, instead of merely arguing that nitrate is more important than sulfate for the UTLS aerosol layer even under a situation of 50%  $\text{NO}_x$  emission reduction. The authors are suggested to use a different title for Sect. 7, .e.g. "Sensitivities of simulated nitrate in the UTLS to anthropogenic  $\text{NO}_x$ ,  $\text{NH}_3$  and  $\text{SO}_2$  emissions in Asia".

Response:

Thanks for the suggestions. We have made the following changes in the text:

(1) We have added discussions on why nitrate aerosol in the UTLS over the TP/SASM region is not sensitive to a 50% reduction of anthropogenic  $\text{NO}_x$  emissions in Asia: "As shown in Table 3, for the surface layer, simulated nitrate concentration over the TP/SASM region decreases by 46.8% with a 50% reduction in anthropogenic  $\text{NO}_x$  emissions in Asia, and it decreases by 22.3% when anthropogenic  $\text{NH}_3$  emissions are reduced by the same percentage, indicating that surface-layer nitrate aerosol is more sensitive to anthropogenic emissions of  $\text{NO}_x$  than to those of  $\text{NH}_3$ . Relative to the baseline simulation, simulated nitrate concentrations at 200 hPa and 100 hPa decrease, respectively, by 49.0% and 17.7% with a 50% reduction in  $\text{NH}_3$  emissions, whereas only by 2.1% and 1.3% with a 50% reduction in  $\text{NO}_x$  emissions. Over the studied region, the role of  $\text{NH}_3$  in the sulfate-nitrate-ammonium aerosol system can be quantified by the gas ratio of  $\text{GR} = \frac{\text{free ammonia}}{\text{total nitrate}} = \frac{\text{TA} - 2 \times \text{TS}}{\text{TN}}$  (Ansari and Pandis, 1998), where  $\text{TA} = \text{NH}_3 + \text{NH}_4^+$ ,  $\text{TS} = \text{SO}_4^{2-}$ , and  $\text{TN} = \text{HNO}_3 + \text{NO}_3^-$ . Over the TP/SASM region, GR is generally positive both at the surface and in the UTLS, especially over 20–40°N where deep convection exits (Fig. 11), indicating that S(VI) is in form of sulfate and free ammonia is available to react with nitrate (Seinfeld and Pandis 2006). However, GR is generally less than 1.0 above 400 hPa in summer over the TP/SASM region, which indicates nitrate concentrations are most sensitive to changes in  $\text{NH}_3$  and explains the small sensitivity of nitrate aerosol to  $\text{NO}_x$  emissions in the UTLS."

(2) We have changed the title of Sec. 7 to "Sensitivities of simulated nitrate in the UTLS to anthropogenic  $\text{NO}_x$ ,  $\text{NH}_3$ , and  $\text{SO}_2$  emissions in Asia".

PM2.5 is an important parameter usually used for air quality study, and it might not have to be used to describe the aerosols in the UTLS. Was PM2.5 simulated as a tracer in GEOS-Chem or it was calculated just by summing simulated SO<sub>4</sub><sup>=</sup>, NO<sub>3</sub><sup>-</sup>, NH<sub>4</sub><sup>+</sup>, BC and OC? Mineral dust and sea salt aerosols, which were simulated and used for the calculation of extinction coefficient in this study, should also be taken into account for PM2.5. Otherwise, more clear definition/descriptions should be given in the text. In the abstract (Line37-38), for example, it might be written as “defined as the sum of sulfate, nitrate, ammonium, black carbon, and organic carbon aerosols in this study”. In Fig. 7, the sub-panels for PM2.5 can be omitted, and instead the distributions of mineral dust and sea salt aerosols might be displayed.

Response:

We have revised the abstract to describe clearly that “PM<sub>2.5</sub> is defined as the sum of sulfate, nitrate, ammonium, black carbon, and organic carbon aerosols in this study”.

We agree that the consideration of sea salt and mineral dust aerosols may influence our calculated contribution of nitrate to total aerosol mass. We have done the calculation (see Figure A below) and added the following quantitative discussions at the end of Section 5: “Considering the large uncertainties in simulated sea salt (Jaeglé et al., 2011) and mineral dust (Fairlie et al., 2007) aerosols, we tend to be focused on anthropogenic aerosol species (SO<sub>4</sub><sup>2-</sup>, NO<sub>3</sub><sup>-</sup>, NH<sub>4</sub><sup>+</sup>, BC, and OC) in this work. In our model, concentrations of sea salt (or mineral dust) are simulated to be 1.0–1.7 ng m<sup>-3</sup> (or 5.0–7.0 ng m<sup>-3</sup>) over the studied region in the summer of 2005, which contribute less than 1.2% (or 5.0%) to total aerosol mass at 100 hPa. Therefore the consideration of sea salt and mineral dust can slightly reduce C<sub>NIT</sub> values, but C<sub>NIT</sub> values at 100 hPa are still as high as 45-65% over the TP/SASM region in summer.”

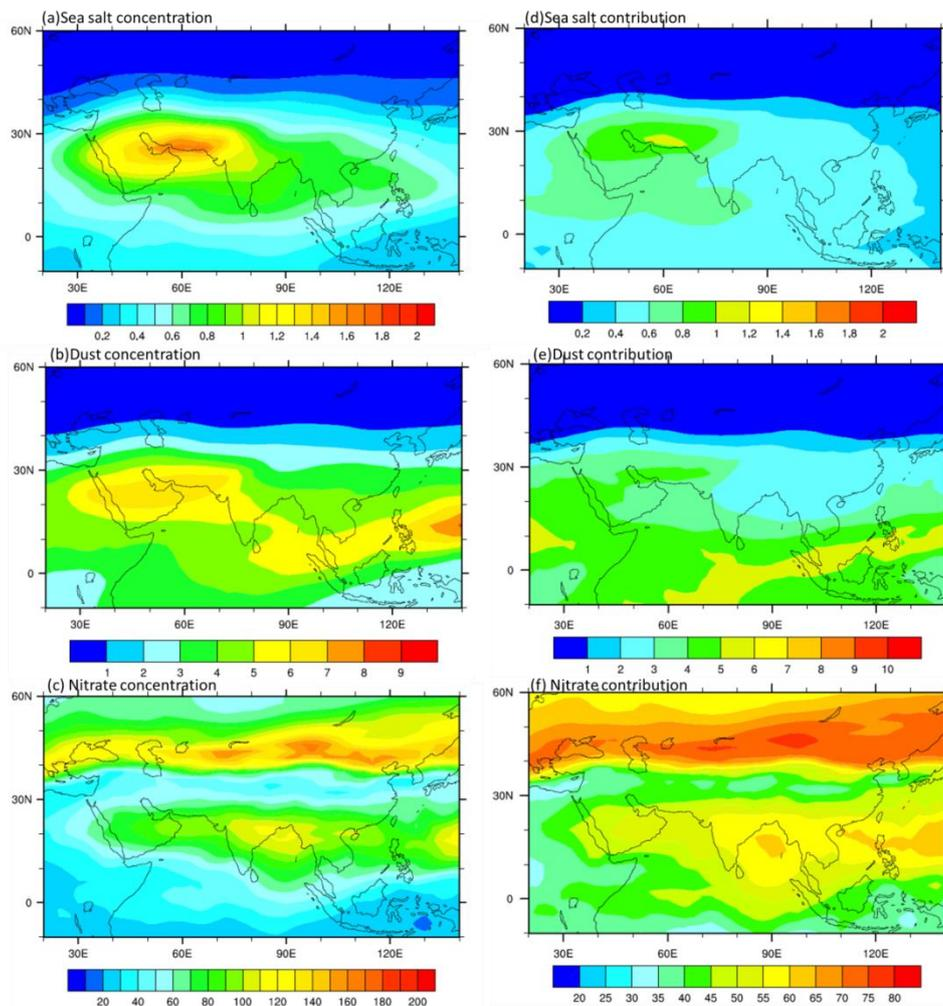


Figure A. Simulated seasonal mean concentrations ( $\text{ng m}^{-3}$ ) of (a) sea salt (sum of mass over two size bins of 0.1–0.5, 0.5–8  $\mu\text{m}$ ), (b) mineral dust (sum of mass over four size bins of 0.1–1.0, 1.0–1.8, 1.8–3.0, 3.0–6.0  $\mu\text{m}$ ), and (c) nitrate for summer (June–August) of year 2005. (c)–(f) show, respectively, the seasonal mean contributions (%) of sea salt, mineral dust, and nitrate to total aerosol mass (sum of sulfate, nitrate, ammonium, OC, BC, sea salt, and mineral dust) at 100 hPa.

The physical, chemical and dynamical processes related to the formation of the UTLS aerosol layer are complex and need further investigations in future studies. Therefore, I would suggest that a more detailed description of the aerosol module used in this study be given for the convenience of comparisons of future work with this study. How many size bins or modes of the aerosols were adopted in the GEOS-Chem used in this study? What ionic aerosols were considered in the ISORROPIA II used in this study,  $\text{NH}_4^+/\text{SO}_4^-/\text{NO}_3^-$ , or  $\text{NH}_4^+/\text{Na}^+/\text{K}^+/\text{Ca}^{2+}/\text{Mg}^{2+}/\text{SO}_4^-/\text{NO}_3^-/\text{Cl}^-/\text{CO}_3^-$ , or others? Were the aerosols treated as internal, or external mixed, or both (the same question as in my first round review)? One can see from Table 3 that OC and BC concentrations are constant for different simulations, indicating that they are external mixed.

Response:

Thanks for the suggestions. In the GEOS-Chem model, anthropogenic

aerosols are treated as bulk mass concentrations (particles of  $\text{SO}_4^{2-}$ ,  $\text{NO}_3^-$ ,  $\text{NH}_4^+$ , BC, and OC are not size-resolved). These anthropogenic aerosol species are usually summed to represent  $\text{PM}_{2.5}$  in previous studies on aerosols in the United States and in China (Liu et al., 2004; Zhang et al., 2010; Tai et al., 2012; Jiang et al., 2013; Lou et al., 2014). Anthropogenic aerosols are treated as bulk mass concentrations (particles of  $\text{SO}_4^{2-}$ ,  $\text{NO}_3^-$ ,  $\text{NH}_4^+$ , BC, and OC are not size-resolved). Sea Salt mass is simulated for two size bins (0.1–0.5 and 0.5–8  $\mu\text{m}$ ) and mineral dust is simulated for four size bins (0.1–1.0, 1.0–1.8, 1.8–3.0, and 3.0–6.0  $\mu\text{m}$ ). In the version of the GEOS-Chem model used in this work, ions considered in ISOROPIA II include  $\text{H}^+/\text{Na}^+/\text{NH}_4^+/\text{Cl}^-/\text{SO}_4^{2-}/\text{HSO}_4^-/\text{NO}_3^-/\text{OH}^-$ . Aerosol species are treated as an external mixture in the calculation of aerosol optical properties. We have revised the description of GEOS-Chem model (Sec. 2.1) to include the above information.

With respect to the formation mechanisms for  $\text{SO}_4^{2-}$  and  $\text{NO}_3^-$  in the UTLS (Line 547-553), simple comparison of the changes in the gas-phase oxidation of  $\text{SO}_2$  and the gas-particle equilibria of  $\text{NO}_3^-$  with temperature (altitude) might not be sufficient to explain the difference in their vertical distributions. Note that the reaction of  $\text{NO}_2$  (not  $\text{NO}$  as written in Line 546) with  $\text{OH}$  also changes with temperature, the same as for the reaction of  $\text{SO}_2$  with  $\text{OH}$ . Was  $\text{H}_2\text{SO}_4$  simulated in the GEOS-Chem? If so, comparisons of both the formation and nucleation rates of  $\text{H}_2\text{SO}_4$  and  $\text{HNO}_3$  might be helpful. It seems that the gas-phase oxidation of  $\text{SO}_2$  was not addressed in the work of X.Y. Zhang et al. (2012), not mentioned to the change of its reaction rate with temperature. Therefore, this work should not be cited here (Line 550).

Response:

We agree with the reviewer. Nearly all the chemical reactions are influenced by changes in temperature. Dawson et al. (2007) examined the sensitivities of sulfate and nitrate concentrations to temperature by using the Particulate Matter Comprehensive Air Quality Model with extensions (PMCAMx). The sensitivity test was performed by fixing all meteorological parameters but perturbing temperature. Their sensitivity simulations showed that the increases in temperature led to increases in sulfate concentrations and decreases in nitrate concentrations. Compared to nitrate, sulfate concentrations showed smaller sensitivity to temperature changes (Dawson et al., 2007); as temperature increased, nitrate concentrations decreased by 19%  $\text{K}^{-1}$  and 17%  $\text{K}^{-1}$  in January and July respectively, while sulfate concentration increased by 0.12%  $\text{K}^{-1}$  and 1.3%  $\text{K}^{-1}$  in January and July, respectively. We have clarified this in the second paragraph of Sec. 6.1.

$\text{H}_2\text{SO}_4$  is simulated in the GEOS-Chem (Park et al., 2004).

Thanks for pointing out the mistake with the reference of X.Y. Zhang et al. (2012). We have deleted it.

References:

- Ansari, A. S., and Pandis, S. N.: Response of Inorganic PM to Precursor Concentrations, *Environ. Sci. Technol.*, 32(18), 2706–2714, 1998.
- Dawson, J., Adams, P., and Pandis, S.: Sensitivity of  $\text{PM}_{2.5}$  to climate in the

- Eastern US: a modeling case study, *Atmos. Chem. and phys.*, 7, 4295–4309, 2007.
- Fairlie, T. D., Jacob, D. J., and Park, R. J.: The impact of transpacific transport of mineral dust in the United States, *Atmos. Environ.*, 41, 1251–1266, 2007.
- Jaeglé, L., Quinn, P., Bates, T., Alexander, B., and Lin, J.-T.: Global distribution of sea salt aerosols: new constraints from in situ and remote sensing observations, *Atmos. Chem. Phys.*, 11, 3137–3157, 2011.
- Jiang, H., Liao, H., Pye, H., Wu, S., Mickley, L. J., Seinfeld, J. H., and Zhang, X.: Projected effect of 2000-2050 changes in climate and emissions on aerosol levels in China and associated transboundary transport, *Atmos. Chem. Phys.*, 13, 7937–7960, 2013.
- Liu, Y., Park, R. J., Jacob, D. J., Li, Q., Kilaru, V. and Sarnat, J. A.: Mapping annual mean ground-level PM<sub>2.5</sub> concentrations using Multiangle Imaging Spectroradiometer aerosol optical thickness over the contiguous United States, *J. Geophys. Res.*, 109, D22206, doi:10.1029/2004JD005025, 2004.
- Lou, S., Liao, H., and Zhu, B.: Impacts of aerosols on surface-layer ozone concentrations in China through heterogeneous reactions and changes in photolysis rates, *Atmos. Environ.*, 85, 123–138, 2014.
- Park, R. J., Jacob, D. J., Field, B. D., Yantosca, R. M., and Chin, M.: Natural and transboundary pollution influences on sulfate–nitrate–ammonium aerosols in the United States: Implications for policy, *J. Geophys. Res.*, 109, D15204, doi:10.1029/2003JD004473, 2004.
- Seinfeld, J. H., and Pandis, S. N.: *Atmospheric chemistry and physics: from air pollution to climate change*, second ed. John Wiley: A Wiley-Interscience Publication Press, 2006.
- Tai, A. P. K., Mickley, L. J., Jacob, D. J., Leibensperger, E. M., Zhang, L., and Fisher, J. A., and Pye, H. O. T.: Meteorological modes of variability for fine particulate matter (PM<sub>2.5</sub>) air quality in the united states: implications for PM<sub>2.5</sub> sensitivity to climate change, *Atmos. Chem. Phys.*, 12(6), 3131-3145, doi:10.5194/acp-12-3131-2012, 2012.
- Zhang, L., Liao, H., and Li, J.: Impacts of Asian summer monsoon on seasonal and interannual variations of aerosols over eastern China, *J. Geophys. Res.*, 115, D00K05, doi:10.1029/2009JD012299, 2010.

### **Responses to Referee #3: Report #2**

The paper "Summertime nitrate aerosol in the upper troposphere and lower stratosphere over the Tibetan Plateau and the South Asian summer monsoon region" by Gu et al. describes results from global model simulations of aerosol chemical composition over the Tibetan plateau.

However, the title is misleading as not only UTLS but also surface concentrations are analyzed and compared with observations, which are a substantial contribution to the total manuscript.

Generally, the paper is reasonably well written and provides a basic evaluation of the aerosol chemical composition with a focus on aerosol nitrate over the Tibetan plateau. However, the applied horizontal resolution of the global model,

i.e.  $2^\circ$  by  $2.5^\circ$  is quite coarse for a focus on a specific region, such that no detailed information on the regional distribution over the TP can be addressed properly.

Overall, the paper can be published after addressing the major (and minor) points below.

Responses to general comments:

(1) Although we are focused on aerosols in the UTLS, we have to show and evaluate aerosol concentrations at the surface, because previous studies have shown that chemical species in the UTLS over the TP/SASM region are influenced by their concentrations at the surface (convection associated with the SASM is a vital pathway to transport chemical species from the lower troposphere into the stratosphere) (Chen et al., 2006; Randel and Park, 2006; Randel et al., 2010; Bian et al., 2011). Observational and modeling studies have shown that persistent maxima of atmospheric constituents ( $\text{H}_2\text{O}$ , CO,  $\text{CH}_4$ , HCN, etc.) exist in the UTLS above the TP/SASM region because of the deep convection during boreal summer (Gettelman et al., 2004; Li et al., 2005; Randel and Park, 2006; M. Park et al., 2004, 2007, 2008, 2009, Randel et al., 2010).

(2) We use the version of the GEOS-Chem model with  $2^\circ \times 2.5^\circ$  resolution because of the following reasons:

a. The models with a  $2^\circ \times 2.5^\circ$  horizontal resolution have been shown to have the ability to address the distributions of atmospheric constituents in the UTLS over the TP/SASM region in previous modeling studies. Li et al. (2005) used the GEOS-Chem model with a horizontal resolution of  $2^\circ \times 2.5^\circ$  to examine the transport of South Asian pollutants to the upper troposphere during 25 August – 6 September, 2004, and showed that the horizontal distribution of CO at 150 hPa agreed well with the MOPITT and MLS observations. Fadnavis et al. (2013) used the ECHAM5-HAMMOZ model with a horizontal resolution of  $2.8^\circ \times 2.8^\circ$  to study the transport of aerosols into the UTLS over the TP/SASM during the Asian summer monsoon season of 2003, and showed that the vertical distribution of aerosol extinction was in agreement with that obtained from HALOE and SAGE II measurements.

b. We agree with the reviewer that it's better to use a higher resolution model to address the regional distribution over the TP/SASM region. The nested version of the GEOS-Chem has a higher resolution of  $0.5^\circ \times 0.666^\circ$ , but the region with nested grids covers only  $70\text{--}150^\circ\text{E}$ , which cannot cover the whole anticyclone region studied in the manuscript.

c. We have compared the horizontal distribution of nitrate simulated with a  $2^\circ \times 2.5^\circ$  resolution with that simulated with a  $0.5^\circ \times 0.666^\circ$  resolution by using the GEOS-Chem model (See Figure B below). Over the nested domain (including China, India, and the Tibetan Plateau), the distribution and magnitude of nitrate with these two horizontal resolutions agree fairly well.

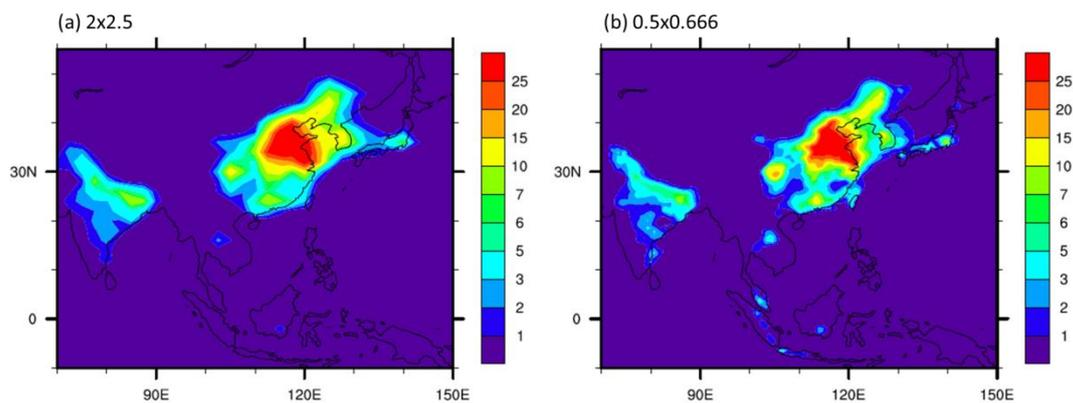


Figure B. The horizontal distribution of surface-layer nitrate aerosol concentration ( $\mu\text{g m}^{-3}$ ) in July of 2005 simulated from the GEOS-Chem model with horizontal resolutions of (a)  $2^\circ \times 2.5^\circ$  and (b)  $0.5^\circ \times 0.666^\circ$ .

Overall, the paper can be published after addressing the major (and minor) points below:

There are three major points in the current manuscript, which inhibit publication in the current form. These are:

1) The effect of nitrate aerosols is difficult to address from a simulation with and without nitrate as the chemical regime of the aerosol thermodynamic partitioning depend strongly on the availability of nitrate. Consequently, a completely different aerosol composition is derived, and from this a modified aerosol microphysical processing results as well as properties of the size distribution with implications for aerosol extinction. Consequently, this whole part should better be addressed by conclusions drawn from the experiments with a modified emission strength ( $\pm 20\%$ ), as this will not completely alter the chemical regime of the thermodynamics. The comparison with SAGE data for extinction suffers from the same problem. However, total extinction is reasonably well matched. A key question is whether the model is able to represent the stratospheric aerosol layer (originating mostly from COS oxidation and to a minor extent also anthropogenic  $\text{SO}_2$ ), as this will contribute to a major extent to the aerosol layer in the UTLS.

Response:

(1) Our description on numerical experiment may not be clear enough, which leads to a misunderstanding by the reviewer. There are five experiments discussed in the manuscript: one is our baseline simulation, and the other four are sensitivity experiments as presented in Sec. 7. All the simulations are conducted with full chemistry including all the gas-phase species and aerosols in the GEOS-Chem. When we show vertical distributions of aerosol extinction coefficients “with nitrate” (or “without nitrate”) in Fig. 9(b), we mean that we account for (or do not account for) the contribution of nitrate aerosol in our calculation of aerosol extinction. To avoid confusion, we have revised our description on Figure 9 in Sec. 4.3: “The vertical distributions of aerosol extinction coefficients “with nitrate” and “without nitrate” are both from the baseline run with full chemistry. The vertical distribution of aerosol extinction coefficient “with nitrate” (or “without nitrate”) indicates that the contribution of

nitrate aerosol to aerosol extinction is (or is not) accounted for.”

(2) We agree with the reviewer that the oxidation of COS contributes to the concentrations of sulfate aerosol in the stratosphere. Currently, COS is not considered in the standard version of the GEOS-Chem model. However, the absence of COS in our simulations should not compromise our major conclusions for the following reasons:

a. Early studies considered that the oxidation of COS is the major source of the background stratospheric sulfate during non-volcanic period (Crutzen, 1976; Maroulis et al., 1977). However, studies during the past two decades had different opinions (Hoffman et al., 1991; Chin and Davis, 1995; Weisenstein et al., 1997; Thomason et al., 1997; Kjellström, 1998; Sturges et al., 2001). Based on numerical simulations, the stratospheric production of  $\text{SO}_2$  from COS oxidation was estimated to be  $0.01\text{--}0.05 \text{ Tg S yr}^{-1}$  (Crutzen and Schmailzl, 1983; Chin and Davis, 1995; Weisenstein et al., 1997; Kjellström, 1998), which was 3–5 times smaller than the amount ( $0.043\text{--}0.17 \text{ Tg S yr}^{-1}$ ) needed to sustain the stratospheric sulfate (Chin and Davis, 1995). Besides, Sturges et al. (2001) found that the changes in COS concentrations were relatively small compared to the increases in sulfate concentrations in the stratosphere in the 20<sup>th</sup> century, indicating that COS might not be the main source of the increases in stratospheric sulfate. Based on the observations in Laramie, Wyoming, Hoffman et al. (1991) suggested that the high-altitude aircraft emissions might account for 65% of the sulfur sources in the stratosphere. By using a three-dimensional general circulation model ECHAM, Kjellström (1998) suggested that  $\text{SO}_2$  transported from the troposphere was the most important for sulfate in the stratosphere below 20 km while COS oxidation was the most important source for sulfate above 25 km. Although COS is not considered in our work, the emissions of volcanoes and aircrafts (Table 1) as well as the detailed simulations of  $\text{SO}_2$  (R. J. Park et al., 2004) are all included in our model.

b. The UTLS over the TP/SASM region has been reported to be largely influenced by anthropogenic emissions, since the deep convection associated with the SASM is a vital pathway to transport air mass from the lower troposphere into the stratosphere (Chen et al., 2006; Randel and Park, 2006; Randel et al., 2010; Bian et al., 2011). The global COS source is estimated to be  $0.4\text{--}0.9 \text{ Tg S yr}^{-1}$  (Chin and Davis, 1995; Seinfeld and Pandis, 2006; Brühl et al., 2012), which is much lower than the anthropogenic emissions of  $\text{SO}_2$  (Table 1).

c. COS in the stratosphere leads to the formation of  $\text{SO}_2$  via photolysis and oxidation reactions. As a result, COS mixing ratio decreases rapidly with altitude, from about 500 pptv at the tropopause to less than 10 pptv at about 30 km altitude (Chin and Davis, 1995). About 2/3 of the stratospheric COS oxidation takes place at altitudes above 25 km (Kjellström, 1998; Brühl et al., 2012). Kjellström (1998), indicating that COS played a minor role in sulfate formation at altitudes below 20 km. Since we are focused on aerosols in the UTLS, COS is expected to play a small role in sulfate concentration here.

2) The other key problem is the comparison with satellite data with a coarse vertical resolution. As  $\text{HNO}_3$  (as well as ozone) has an increasing gradient from the troposphere to the stratosphere, the detection from the satellite could

easily be influenced by the upper part of the sampling layers which might be dominated by the stratospheric air masses. This is e.g. obvious from the Figures 4 and 5, which are clearly influenced by the differences in tropospheric and stratospheric air masses at the given altitude. However, also in Fig. 7 there is only a very reduced impact of surface emissions or lifting patterns along the TP or the SASM visible, but the distribution looks basically as influenced by the tropopause distinguishing tropospheric and stratospheric air masses (comparable to a plot of potential vorticity).

Response:

Indeed there are large uncertainties with satellite data. As described in Sect. 3 of our manuscript, the MLS datasets provide HNO<sub>3</sub> and O<sub>3</sub> mixing ratios at vertical resolutions of 3–4 km and 2.5-3 km, respectively, in the UTLS region. The uncertainties of the MLS HNO<sub>3</sub> and O<sub>3</sub> datasets in the UTLS are about ±0.5-1 ppbv and 0.02-0.04 ppmv, respectively (Livesey et al., 2011). However, the UTLS datasets of MLS have been considered to be valuable and been used in previous studies to evaluate model results (Jin et al., 2009; Feng et al., 2011; Miyazaki et al., 2012; Brakebusch et al., 2013; Liu et al., 2013).

Concentrations of chemical species are determined by emissions, chemical production, chemical removal, transport, and deposition. Observational and modeling studies have shown that persistent maxima of CO, NO<sub>x</sub>, CH<sub>4</sub>, C<sub>2</sub>H<sub>6</sub>, OC, and BC exist in the UTLS over the TP/SASM region (Kar et al., 2004; Li et al., 2005; M. Park et al., 2004, 2008; Fadnavis et al., 2013), which are closely associated with the transport of air mass by deep convection during the Asian summer monsoon season (Chen et al., 2006; Randel and Park, 2006; Randel et al., 2010; Bian et al., 2011). In addition to the important role of transport, we are emphasizing in our work the role of chemical production during the vertical transport (Sect. 6), such as the gas-to-aerosol conversion of HNO<sub>3</sub> (the high relative humidity and low temperature associated with the deep convection over the TP/SASM region are favorable for nitrate formation).

3) The authors claim that vertical transport of nitrate (as it is the second most abundant aerosol compound in near surface air) is responsible for enhanced values in the UT. This cannot be true, as the vertical transport cannot change the ratios of sulphate to nitrate by transport alone; the transport algorithms usually transport all compounds in the same way.

Precipitation scavenging of aerosol species is controlled by their size and the hygroscopic properties of nitrate aerosols are so close to those of sulphate particles such that also cloud activation cannot play a role in altering the ratios of nitrate to sulphate either. Both gaseous HNO<sub>3</sub> and H<sub>2</sub>SO<sub>4</sub> are so soluble that in case of precipitation events, the concentrations would be equally reduced to almost zero. SO<sub>2</sub> which is slightly less soluble might have a larger chance of reaching the UT without a complete scavenging, but as seen from previous studies UTLS sulphate mostly originates from COS and other long lived species.

Consequently, convective transport of nitrate has to be ruled out almost completely to lead to the enhanced nitrate concentrations, even though the authors attribute a substantial fraction to this process (see e.g. Fig.13). STE might offer an alternative pathway of HNO<sub>3</sub> entering the UT from above, but

most likely the HNO<sub>3</sub> is formed in situ by NO<sub>x</sub> chemistry or by the release of NO<sub>y</sub> from long lived, hardly soluble compounds such as PAN. However, chemical in situ production is missing completely in Fig.13 and the corresponding discussion.

Response:

We agree with the reviewer that the vertical transport alone cannot change the ratios of sulfate to nitrate. The change in the ratio of sulfate to nitrate during vertical transport is explained by that the chemical mechanisms for SO<sub>4</sub><sup>2-</sup> and NO<sub>3</sub><sup>-</sup> have different sensitivity to meteorological conditions (Sect. 6). During the vertical transport, temperature decreases, which reduces the gas-phase oxidation of SO<sub>2</sub> (Yao et al., 2002; Seinfeld and Pandis 2006) but promotes the formation of NO<sub>3</sub><sup>-</sup> by shifting gas-particle equilibria (Dawson et al., 2007; Liao et al., 2009).

The wet deposition of both gas-phase species and aerosols are accounted for in the GEOS-Chem model. The aerosol wet deposition scheme has been implemented in the GEOS-Chem model following Liu et al. (2001). It accounts for scavenging in convective updrafts, rainout and washout from convective anvils and large-scale precipitation, and allows for return of chemical species to the atmosphere following evaporation. For the scavenging of aerosols, SO<sub>4</sub><sup>2-</sup>, NO<sub>3</sub><sup>-</sup>, NH<sub>4</sub><sup>+</sup>, and hydrophilic OC and hydrophilic BC aerosols are assumed to be fully soluble. The model also includes soluble gases on the basis of their effective Henry's law partitioning in warm clouds, and surface coating or cocondensation of ice crystals in cold clouds (R. J. Park et al., 2004). As mentioned by the reviewer, precipitation scavenging of nitrate is close to that of sulfate, which should not be a factor to change ratio of sulfate to nitrate during vertical transport. Therefore again we conclude that the change in the ratio of sulfate to nitrate during vertical transport is explained by that the chemical mechanisms for SO<sub>4</sub><sup>2-</sup> and NO<sub>3</sub><sup>-</sup> have different sensitivity to temperature and relative humidity.

The STE, the formations of HNO<sub>3</sub> by NO<sub>x</sub> chemistry, and the release of NO<sub>y</sub> from long lived, hardly soluble compounds such as PAN are all considered in the GEOS-Chem. The chemical mechanism for nitrate formation in the GEOS-Chem model was described in R. J. Park et al. (2004), which is comprehensive and has been used extensively in previous studies to simulate nitrate aerosol (Liu et al., 2004; R. J. Park et al., 2004; Pye et al., 2009; Zhang et al., 2010; Tai et al., 2012; Jiang et al, 2013; Lou et al., 2014; Eastham, et al., 2014). The same chemistry mechanism was also used to examine the global distributions and concentrations of nitrate aerosol in Liao et al. (2004) and Liao and Seinfeld (2005). Nitrate forms from the partitioning of HNO<sub>3</sub> between gas and aerosol phases. Major reactions for the production and loss of HNO<sub>3</sub> were listed in Liao and Seinfeld (2005) (see Table R1 below). Therefore the formation of gas-phase HNO<sub>3</sub> and the partitioning of HNO<sub>3</sub> between gas and aerosol phases are the two major chemical processes that influence nitrate concentrations. We have evaluated the ability of the GEOS-Chem model to simulate gas-phase HNO<sub>3</sub> in Section 3.1 (by comparisons of our model results with MLS observations and concentrations from previous modeling studies), so we quantify in Section 6.2 the nitrate formation from gas-to aerosol conversion of HNO<sub>3</sub> based on the ISORROPIA II thermodynamic equilibrium module (Fountoukis and Nenes, 2007) in the GEOS-Chem model.

Table R1. Annual mean HNO<sub>3</sub> budget for present-day and year 2100 simulations (taken from Liao and Seinfeld, 2005)

	Present-Day		Year 2100	
	Baseline	NOHET	Baseline	NOHET
Chemical Productions, Tg yr <sup>-1</sup>	153.5	154.5	464.0	457.3
(R1) NO <sub>2</sub> + OH + M → HNO <sub>3</sub> + M	36.5%	55.5%	36.8%	61.8%
(R2) NO <sub>3</sub> + CH <sub>2</sub> O → HNO <sub>3</sub> + prod.	1.1%	3.8%	2.2%	8.9%
(R3) ALD2 + NO <sub>3</sub> → HNO <sub>3</sub> + prod.	0.8%	3.2%	1.8%	6.6%
(R4) RIO2 + NO → HNO <sub>3</sub> + prod.	9.3%	9.1%	3.9%	3.7%
(R5) RIO1 + NO → HNO <sub>3</sub> + prod.	0.8%	0.7%	0.4%	0.3%
(R6) IAO2 + NO → 0.08HNO <sub>3</sub> + prod.	0.3%	0.3%	0.1%	0.1%
(R7) VRO2 + NO → HNO <sub>3</sub> + prod.	0.9%	0.9%	0.4%	0.4%
(R8) MRO2 + NO → HNO <sub>3</sub> + prod.	0.6%	0.6%	0.3%	0.2%
(R9) MVN2 + NO → 0.1HNO <sub>3</sub> + prod.	0.0%	0.1%	0.0%	0.1%
(R10) INO2 + NO → 0.85HNO <sub>3</sub> + prod.	4.7%	5.8%	2.6%	3.6%
(R11) ALK4 + NO <sub>3</sub> → HNO <sub>3</sub> + prod.	0.0%	0.4%	0.1%	0.5%
(R12) RCHO + NO <sub>3</sub> → HNO <sub>3</sub> + prod.	0.1%	0.4%	0.2%	0.7%
(R13) MEK + NO <sub>3</sub> → HNO <sub>3</sub> + prod.	1.1%	3.3%	0.8%	2.9%
(R14) INO2 + MO2 → 0.425HNO <sub>3</sub> + prod.	0.6%	0.8%	0.2%	0.3%
(R15) GLYX + NO <sub>3</sub> → HNO <sub>3</sub> + prod.	0.0%	0.0%	0.0%	0.0%
(R16) MGLY + NO <sub>3</sub> → HNO <sub>3</sub> + prod.	0.2%	0.8%	0.3%	1.5%
(R17) MACR + NO <sub>3</sub> → HNO <sub>3</sub> + prod.	0.3%	0.7%	0.2%	0.8%
(R18) C <sub>2</sub> H <sub>6</sub> + NO <sub>3</sub> → HNO <sub>3</sub> + prod.	0.0%	0.0%	0.1%	0.2%
(R19) INO2 + MCO3 → 0.85HNO <sub>3</sub> + prod.	2.2%	2.8%	1.0%	1.1%
(R20) DMS + NO <sub>3</sub> → HNO <sub>3</sub> + prod.	7.4%	10.8%	4.1%	6.3%
(R21) NO <sub>2</sub> + (aerosols) → 0.5HNO <sub>3</sub> + prod.	6.2%	0.0%	8.2%	0.0%
(R22) NO <sub>3</sub> + (aerosols) → HNO <sub>3</sub> + prod.	0.3%	0.0%	0.4%	0.0%
(R23) N <sub>2</sub> O <sub>5</sub> + (aerosols) → 2HNO <sub>3</sub>	26.5%	0.0%	35.8%	0.0%
Total loss, Tg yr <sup>-1</sup>	153.5	154.5	464.0	457.3
Chem. loss, Tg yr <sup>-1</sup>	10.7	20.0	24.9	44.6
(R24) HNO <sub>3</sub> + OH → prod.	34.6%	37.0%	32.9%	36.8%
(R25) HNO <sub>3</sub> + hv → prod.	65.4%	63.0%	67.1%	63.2%
Dust uptake, Tg yr <sup>-1</sup>	37.1	0	73.0	0
Loss to nitrate, <sup>b</sup> Tg yr <sup>-1</sup>	36.9 (105.3–68.4)	46.0 (123.5–77.5)	168.7 (394.4–225.7)	176.1 (470.7–294.6)
Dry deposition, Tg yr <sup>-1</sup>	27.3	35.6	80.1	97.2
Wet deposition, Tg yr <sup>-1</sup>	41.5	52.9	117.3	139.4
Burden, Tg	1.30	1.78	2.16	2.98

<sup>a</sup>The numbers for reactions (R1)–(R25) are contributions to chemical production or loss from each reaction. Please see [http://www-as.harvard.edu/chemistry/trop/geos/doc/chem\\_mech/geoschem\\_mech.pdf](http://www-as.harvard.edu/chemistry/trop/geos/doc/chem_mech/geoschem_mech.pdf) for the formula of the species in these reactions and for the rate constants.

<sup>b</sup>The first number in the parentheses is the loss of gas-phase HNO<sub>3</sub> to nitrate formation, and the second number shows the release of gas-phase HNO<sub>3</sub> from nitrate, which are determined by aerosol thermodynamics.

Other points:

a) The comparison with ozone soundings does not really provide a good agreement (except for the general shape). Tropospheric O<sub>3</sub> is substantially deviating (factor of 2) from the observations which on the given scale. Therefore, it is misleading that the agreement is good, at least not below 12 km altitude.

Response:

Compared to O<sub>3</sub> in the UTLS, O<sub>3</sub> in the lower troposphere is more sensitive to anthropogenic activities (Bian et al., 2012); various local emissions can result in the discrepancies between the observed and simulated O<sub>3</sub> mixing ratios in the lower troposphere. Besides, the mismatch of the sampling year may also contribute to the discrepancies between the observations and model results. We have clarified this in Sec. 3.2: "The comparisons with multi-year observations show that the model can reproduce the vertical distributions of O<sub>3</sub> above 12 km in Kunming and Lhasa."

b) The authors do not discuss whether the S(VI) is in form of sulphate or bisulphate (both close the surface and in the UT) and how the ammonium is distributed between S(VI) and nitrate.

Are other cations available (K<sup>+</sup>, Mg<sup>+</sup>, Ca<sup>2+</sup>)? What are their concentrations in the model simulations?

Response:

Whether S(VI) is in the form of sulphate or bisulphate is decided by the thermodynamics of the  $\text{H}_2\text{SO}_4\text{-HNO}_3\text{-NH}_3$  aerosol system. The sulfate aerosols can be partly or totally neutralized by  $\text{NH}_3$  and form ammonium sulfate or ammonium bisulfate depending on  $\text{NH}_3$  concentrations. If excess  $\text{NH}_3$  is available beyond that required for sulfate neutralization to ammonium sulfate, nitrate aerosol can form; otherwise, and except for cloudy conditions,  $\text{HNO}_3$  remains in the gas phase (Seinfeld and Pandis, 2006). The  $\text{H}_2\text{SO}_4\text{-HNO}_3\text{-NH}_3$  aerosol system is simulated by ISORROPIA II thermodynamic equilibrium module (Fountoukis and Nenes, 2007) in the GEOS-Chem model (R. J. Park et al., 2004).

Figure C displays the latitude-altitude cross section of GR averaged over  $70\text{-}105^\circ\text{E}$  during June–August of year 2005. The positive GR ( $\text{TA} > 2\text{TS}$ ) values indicate that sulfate aerosol can be totally neutralized by  $\text{NH}_3$ , and S(VI) is in the form of sulfate. The negative GR ( $\text{TA} < 2\text{TS}$ ) values indicate that there is insufficient  $\text{NH}_3$  to neutralize the available sulfate, and sulfate may exist as bisulfate (Seinfeld and Pandis, 2006). Over the TP/SASM region, GR is generally positive both at the surface and in the UTLS, especially over  $20\text{-}40^\circ\text{N}$  where deep convection exits (Fig. 11), indicating that S(VI) is in form of sulfate and free ammonia is available to react with nitrate. We have added these discussions in Sec. 7.

The formation of nitrate on mineral dust aerosol is not considered in the publicly released versions of the GEOS-Chem model, so  $\text{K}^+$ ,  $\text{Mg}^{2+}$ , and  $\text{Ca}^{2+}$  are not available in the model.

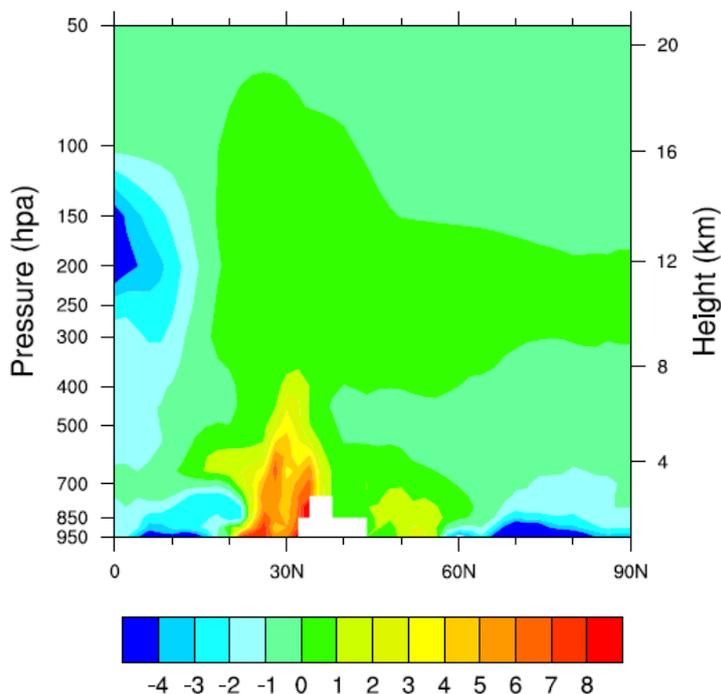


Figure C. The latitude-altitude cross section of GR averaged over  $70\text{-}105^\circ\text{E}$  during June–August of the year 2005.  $\text{GR} = \frac{\text{free ammonia}}{\text{total nitrate}} = \frac{\text{TA} - 2 \times \text{TS}}{\text{TN}}$  (Ansari and Pandis, 1998), where  $\text{TA} = \text{NH}_3 + \text{NH}_4^+$ ,  $\text{TS} = \text{SO}_4^{2-}$ , and  $\text{TN} = \text{HNO}_3 + \text{NO}_3^-$ .

c) Is there a reasonable correlation between enhanced nitrate and low

temperature together with high RH? The patterns of the two meteorological quantities are very smoothed out, such that this correlation (even though generally valid from a thermodynamically viewpoint) is not necessarily driving enhanced nitrate concentrations.

Response:

We agree with the reviewer that it's better to calculate the correlation coefficient between the enhanced nitrate and low temperature or high RH. However, large sample size is needed to obtain a stable correlation since the reliability of the correlation decreases with the sample size (<http://www.r-bloggers.com/at-what-sample-size-do-correlations-stabilize/>). To determine the effects of temperature and RH on summertime nitrate concentrations, at least decadal simulation is needed. For one-year simulation as described in the manuscript, it is difficult to quantify the effects of meteorological variables on nitrate concentrations by correlation coefficients or regression analysis.

Actually, the responses of nitrate concentrations to temperature and humidity have been analyzed by Dawson et al. (2007) using the Particulate Matter Comprehensive Air Quality Model with extensions (PMCAMx). The sensitivity test was performed by fixing all meteorological parameters but perturbing temperature or humidity in the simulation. Their sensitivity simulations showed that the increases in temperature led to increases in sulfate concentrations and decreases in nitrate concentrations. Compared to nitrate, sulfate concentrations showed smaller sensitivity to temperature changes (Dawson et al., 2007); as temperature increased, nitrate concentrations decreased by  $19\% \text{ K}^{-1}$  and  $17\% \text{ K}^{-1}$  in January and July respectively, while sulfate concentration increased by  $0.12\% \text{ K}^{-1}$  and  $1.3\% \text{ K}^{-1}$  in January and July, respectively. We have clarified this in the second paragraph of Sec. 6.1.

References:

- Ansari, A. S., and Pandis, S. N.: Response of Inorganic PM to Precursor Concentrations, *Environ. Sci. Technol.*, 32(18), 2706–2714, 1998.
- Bian, J., Yan, R., and Chen, H.: Tropospheric Pollutant Transport to the Stratosphere by Asian Summer Monsoon, *Chinese Journal of Atmospheric Sciences*, 35, 897–902, 2011.
- Bian, J., Pan, L. L., Paulik, L., Vömel, H., Chen, H., and Lü, D.: In situ water vapor and ozone measurements in Lhasa and Kunming during the Asian summer monsoon, *Geophys. Res. Lett.*, 39, L19808, doi:10.1029/2012GL052996, 2012.
- Brakebusch, M., Randall, C. E., Kinnison, D. E., Tilmes, S., Santee M. L., and Manney, G. L.: Evaluation of Whole Atmosphere Community Climate Model simulations of ozone during Arctic winter 2004–2005, *J. Geophys. Res. Atmos.*, 118, 2673–2688, doi:10.1002/jgrd.50226, 2013.
- Brühl, C., Lelieveld, J., Crutzen, P. J., and Tost, H.: The role of carbonyl sulphide as a source of stratospheric sulphate aerosol and its impact on climate, *Atmos. Chem. Phys.*, 12(3):1239-1253, 2012.
- Chen, H., Bian, J., and Lü, D.: Advances and prospects in the study of stratosphere-troposphere exchange, *Chinese J. Atmos. Sci.*, 30, 813–820, doi:10.1006-9895(2006)30:5<813:SDLCXP>2.0.TX;2-A, 2006.

- Chin, M. and Davis, D. D.: A reanalysis of carbonyl sulfide as a source of stratospheric background aerosol, *J. Geophys. Res.* 100, 8993–9005, 1995.
- Crutzen, P. J.: The possible importance of COS for the sulfate layer of stratosphere, *Geophys. Res. Lett.*, 3, 73–76, 1976.
- Crutzen, P. J. and Schmailzl, U.: Chemical budgets of the stratosphere, *Planet. Space Sci.* 31, 1009–1032, 1983.
- Dawson, J., Adams, P., and Pandis, S.: Sensitivity of PM<sub>2.5</sub> to climate in the Eastern US: a modeling case study, *Atmos. Chem. and phys.*, 7, 4295–4309, 2007.
- Eastham, S. D., Weisenstein, D. K., Barrett, S. R. H.: Development and evaluation of the unified tropospheric–stratospheric chemistry extension (UCX) for the global chemistry-transport model GEOS-Chem, *Atmos. Environ.*, 89(2):52–63, 2014.
- Fadnavis, S., Semeniuk, K., Pozzoli, L., Schultz, M., Ghude, S., Das, S., and Kakatkar, R.: Transport of aerosols into the UTLS and their impact on the Asian monsoon region as seen in a global model simulation, *Atmos. Chem. Phys.*, 13, 8771–8786, 2013.
- Feng, W., Chipperfield, M. P., Davies, S., Mann, G. W., Carslaw, K. S., Dhomse, S., Harvey, L., Randall, C., and Santee, M. L.: Modelling the effect of denitrification on polar ozone depletion for arctic winter 2004/2005. *Atmos. Chem. Phys.*, 11(13), 6559–6573, 2011.
- Fountoukis, C., and Nenes, A.: ISORROPIA II: a computationally efficient thermodynamic equilibrium model for  $K^+ - Ca^{2+} - Mg^{2+} - NH_4^+ - Na^+ - SO_4^{2-} - NO_3^- - Cl^- - H_2O$  aerosols, *Atmos. Chem. Phys.*, 7, 4639–4659, 2007.
- Gottelman, A., Kinnison, D. E., Dunkerton, T. J., and Brasseur, G. P.: Impact of monsoon circulations on the upper troposphere and lower stratosphere, *J. Geophys. Res.*, 109, D22101, doi:10.1029/2004JD004878, 2004.
- Hofmann, D. J.: Aircraft sulphur emissions, *Nature*, 349(6311):659–659, 1991.
- Jiang, H., Liao, H., Pye, H., Wu, S., Mickley, L. J., Seinfeld, J. H., and Zhang, X.: Projected effect of 2000-2050 changes in climate and emissions on aerosol levels in China and associated transboundary transport, *Atmos. Chem. Phys.*, 13, 7937–7960, 2013.
- Jin, J. J., Semeniuk, K., Beagley, S. R., Fomichev, V. I., Jonsson, A. I., McConnell, J. C., Urban, J., Murtagh, D., Manney, G. L., Boone, C. D., Bernath, P. F., Walker, K. A., Barret, B., Ricaud, P., and Dupuy, E.: Comparison of CMAM simulations of carbon monoxide (CO), nitrous oxide (N<sub>2</sub>O), and methane (CH<sub>4</sub>) with observations from Odin/SMR, ACE-FTS, and Aura/MLS, *Atmos. Chem. Phys.*, 9, 3233–3252, 2009.
- Kar, J., Bremer, H., Drummond, J. R., Rochon, Y. J., Jones, D., Nichitiu, F., Zou, J., Liu, J., Gille, J. C., and Edwards, D. P.: Evidence of vertical transport of carbon monoxide from Measurements of Pollution in the Troposphere (MOPITT), *Geophys. Res. Lett.*, 31, L23105, doi:10.1029/2004GL021128, 2004.
- Kjellström, E.: A three-dimensional global model study of carbonyl sulfide in the troposphere and the lower stratosphere, *J. Atmos. Chem.*, 29(2):151–177, 1998.
- Li, Q., Jiang, J. H., Wu, D. L., Read, W. G., Livesey, N. J., Waters, J. W., Zhang, Y., Wang, B., Filipiak, M. J., and Davis, C. P.: Convective outflow of South

- Asian pollution: A global CTM simulation compared with EOS MLS observations, *Geophys. Res. Lett.*, 32, L14826, doi:10.1029/2005GL022762, 2005.
- Liao, H., Seinfeld, J. H., Adams, P. J., and Mickley, L. J.: Global radiative forcing of coupled tropospheric ozone and aerosols in a unified general circulation model, *J. Geophys. Res.*, 109, D16207, doi:10.1029/2003JD004456, 2004.
- Liao, H., and Seinfeld, J. H.: Global impacts of gas-phase chemistry-aerosol interactions on direct radiative forcing by anthropogenic aerosols and ozone, *J. Geophys. Res.*, 110, D18208, doi:10.1029/2005JD005907, 2005.
- Liao, H., Zhang, Y., Chen, W.-T., Raes, F., and Seinfeld, J. H.: Effect of chemistry-aerosol-climate coupling on predictions of future climate and future levels of tropospheric ozone and aerosols, *J. Geophys. Res.*, 114, D10306, doi:10.1029/2008JD010984, 2009.
- Liu, H., Jacob, D. J., Bey, I., and Yantosca, R. M.: Constraints from <sup>210</sup>Pb and <sup>7</sup>Be on wet deposition and transport in a global three-dimensional chemical tracer model driven by assimilated meteorological fields, *J. Geophys. Res.*, 106, 12109–12128, 2001.
- Liu, J., Logan, J. A., Murray, L. T., Pumphrey, H. C., Schwartz, M. J., and Megretskaia, I. A.: Transport analysis and source attribution of seasonal and interannual variability of CO in the tropical upper troposphere and lower stratosphere. *Atmos. Chem. Phys.*, 13, 129–146, 2013.
- Liu, Y., Park, R. J., Jacob, D. J., Li, Q., Kilaru, V. and Sarnat, J. A.: Mapping annual mean ground-level PM<sub>2.5</sub> concentrations using Multiangle Imaging Spectroradiometer aerosol optical thickness over the contiguous United States, *J. Geophys. Res.*, 109, D22206, doi:10.1029/2004JD005025, 2004.
- Lou, S., Liao, H., and Zhu, B.: Impacts of aerosols on surface-layer ozone concentrations in China through heterogeneous reactions and changes in photolysis rates, *Atmos. Environ.*, 85, 123–138, 2014.
- Livesey, N. J., Read, W. G., Wagner, P. A., Froidevaux, L., Lambert, A., Manney, G. L., Pumphrey, H. C., Santee, M. L., Schwartz, M. J., Wang, S., Cofield, R. E., Cuddy, D. T., Fuller, R. A., Jarnot, R. F., Jiang, J. H., and Knosp, B. W.: Version 3.3 Level 2 data quality and description document, JPL D-33509, 2011.
- Maroulis, P. J., Torres, A. L., and Bandy, A. R.: Atmospheric concentrations of carbonyl sulfide in the southwestern and eastern United States, *Geophys. Res. Lett.* 4, 510–512, 1977.
- Miyazaki, K., Eskes, H. J., Sudo, K., Takigawa, M., Weele, M. V., and Boersma, K. F.: Simultaneous assimilation of satellite NO<sub>2</sub>, O<sub>3</sub>, CO, and HNO<sub>3</sub> data for the analysis of tropospheric chemical composition and emissions, *Atmos. Chem. Phys.*, 12, 9545–9579, doi:10.5194/acp-12-9545-2012, 2012.
- Park, M., Randel, W. J., Kinnison, D. E., Garcia, R. R., and Choi, W.: Seasonal variation of methane, water vapor, and nitrogen oxides near the tropopause: Satellite observations and model simulations, *J. Geophys. Res.*, 109, D03302, doi:10.1029/2003JD003706, 2004.
- Park, M., Randel, W. J., Gettelman, A., Massie, S. T., and Jiang, J. H.: Transport above the Asian summer monsoon anticyclone inferred from

- Aura Microwave Limb Sounder tracers, *J. Geophys. Res.*, 112, D16309, doi:10.1029/2006JD008294, 2007.
- Park, M., Randel, W. J., Emmons, L. K., Bernath, P. F., Walker, K. A., and Boone, C. D.: Chemical isolation in the Asian monsoon anticyclone observed in Atmospheric Chemistry Experiment (ACE–FTS) data, *Atmos. Chem. Phys.*, 8, 757–764, 2008.
- Park, M., Randel, W. J., Emmons, L. K., and Livesey, N. J.: Transport pathways of carbon monoxide in the Asian summer monsoon diagnosed from Model of Ozone and Related Tracers (MOZART), *J. Geophys. Res.*, 114, D08303, doi:10.1029/2008JD010621, 2009.
- Park, R. J., Jacob, D. J., Field, B. D., Yantosca, R. M., and Chin, M.: Natural and transboundary pollution influences on sulfate–nitrate–ammonium aerosols in the United States: Implications for policy, *J. Geophys. Res.*, 109, D15204, doi:10.1029/2003JD004473, 2004.
- Pye, H., Liao, H., Wu, S., Mickley, L. J., Jacob, D. J., Henze, D. K., and Seinfeld, J.: Effect of changes in climate and emissions on future sulfate–nitrate–ammonium aerosol levels in the United States, *J. Geophys. Res.*, 114, D01205, doi:10.1029/2008JD010701, 2009.
- Randel, W. J., and Park, M.: Deep convective influence on the Asian summer monsoon anticyclone and associated tracer variability observed with Atmospheric Infrared Sounder (AIRS), *J. Geophys. Res.*, 111, D12314, doi:10.1029/2005JD006490, 2006.
- Randel, W. J., Park, M., Emmons, L., Kinnison, D., Bernath, P., Walker, K. A., Boone, C., and Pumphrey, H.: Asian monsoon transport of pollution to the stratosphere, *Science*, 328, 611–613, 2010.
- Seinfeld, J. H., and Pandis, S. N.: Atmospheric chemistry and physics: from air pollution to climate change, second ed. John Wiley: A Wiley-Interscience Publication Press, 2006.
- Sturges, W. T., Penkett, S. A., Barnola, J. M., Chappellaz, J., Atlas, E., and Stroud, V.: A long-term record of carbonyl sulfide (COS) in two hemispheres from firn air measurements. *Geophys. Res. Lett.*, 28(21):4095–4098, 2001.
- Tai, A. P. K., Mickley, L. J., Jacob, D. J., Leibensperger, E. M., Zhang, L., and Fisher, J. A., and Pye, H. O. T.: Meteorological modes of variability for fine particulate matter (PM<sub>2.5</sub>) air quality in the united states: implications for PM<sub>2.5</sub> sensitivity to climate change, *Atmos. Chem. Phys.*, 12(6), 3131–3145, doi:10.5194/acp-12-3131-2012, 2012.
- Thomason, L. W., Kent, G. S., Trepte, C. R., and Poole, L. R.: A comparison of the stratospheric aerosol background periods of 1979 and 1989–1991, *J. Geophys. Res.* 102, 3611–3616, 1997.
- Weisenstein, D. K., Yue, G., Ko, M., Sze, N.-D., Rodriguez, J., and Scott, C.: A two-dimensional model of sulfur species and aerosols, *J. Geophys. Res.*, 102, 13019–13035, doi:10.1029/97JD00901, 1997.
- Yao, X., Chan, C. K., Fang, M., Cadle, S., Chan, T., Mulawa, P., He, K., and Ye, B.: The water-soluble ionic composition of PM<sub>2.5</sub> in Shanghai and Beijing, China, *Atmos. Environ.*, 36, 4223–4234, 2002.
- Zhang, L., Liao, H., and Li, J.: Impacts of Asian summer monsoon on seasonal and interannual variations of aerosols over eastern China, *J. Geophys. Res.*, 115, D00K05, doi:10.1029/2009JD012299, 2010.

## Responses to Editor

Comments to the Author:

Dear authors,

After the first revision your manuscript has been improved significantly. However, there is still a large room for further improvement, in particular, the scientific quality of this study should further enhanced, as required by the referees. Please study the referee's comments carefully and address the issues raised. In addition, I have three minor technical comments:

Line 204: "...hydrophilic OC and BC aerosols are assumed ...". Did you assume BC is 100% hydrophilic? If not, how did you treat this issue?

Line 339: "BD" = "Brewer-Dobson"? There seems no previous definition. It is not suggested to use this abbreviation.

Line 1426: change "datasets" to "data"

Sincerely,

Xiaobin Xu

Response:

We have addressed the issues suggested by the editor.

(1) Both BC and OC consist of hydrophilic and hydrophobic fractions in the model. It is assumed that 80% of BC and 50% of OC emitted from all primary sources are hydrophobic (Cooke et al., 1999; Chin et al., 2002; Chung and Seinfeld, 2002), which become hydrophilic with an e-folding time of 1.2 days following Cooke et al. (1999) and Chin et al. (2002). All secondary OC is assumed to be hydrophilic. Hydrophilic fractions of both BC and OC aerosols are assumed to be fully soluble.

(2) We have deleted the abbreviation of BD in the manuscript.

(3) Changed "datasets" to "data"..

References:

Chin, M., Ginoux, P., Kinne, S., Torres, O., Holben, B., Duncan, B. N., Martin, R. V., Logan, J. A., Higurashi, A., and Nakajima, T.: Tropospheric aerosol optical thickness from the GOCART model and comparisons with satellite and sunphotometer measurements, *J. Atmos. Sci.*, 59, 461–483, 2002.

Chung, S. H., and Seinfeld, J. H.: Global distribution and climate forcing of carbonaceous aerosols, *J. Geophys. Res.*, 107(D19), 4407, doi:10.1029/2001JD001397, 2002.

Cooke, W. F., Liousse, C., Cachier, H., and Feichter, J.: Construction of a 1°x1° fossil fuel emission data set for carbonaceous aerosol and implementation and radiative impact in the ECHAM-4 model, *J. Geophys. Res.*, 104, 22,137–22,162, 1999.

1     Summertime nitrate aerosol in the upper troposphere and lower stratosphere  
2         over the Tibetan Plateau and the South Asian summer monsoon region

3

4

5                     Yixuan Gu<sup>a,b</sup>, Hong Liao<sup>c,\*</sup>, and Jianchun Bian<sup>d</sup>

6

7     <sup>a</sup>State Key Laboratory of Atmospheric Boundary Layer Physics and  
8     Atmospheric Chemistry (LAPC), Institute of Atmospheric Physics, Chinese  
9     Academy of Sciences, Beijing, China.

10    <sup>b</sup>University of Chinese Academy of Sciences, Beijing, China

11    <sup>c</sup>School of Environmental Science and Engineering, Nanjing University of  
12    Information Science & Technology, Nanjing, China

13    <sup>d</sup>Key Laboratory of Middle Atmosphere and Global Environment Observation  
14    (LAGEO), Institute of Atmospheric Physics, Chinese Academy of Sciences,  
15    Beijing, China.

16

17

18

19    \*Corresponding author address:

20    Prof. Hong Liao

21    School of Environmental Science and Engineering

22    Nanjing University of Information Science & Technology

23    Nanjing 210044, China

24    E-mail: [hongliao@nuist.edu.cn](mailto:hongliao@nuist.edu.cn)

25

26 **Abstract**

27 We use the global three-dimensional Goddard Earth Observing System  
28 chemical transport model (GEOS-Chem) to examine the contribution of nitrate  
29 aerosol to aerosol concentrations in the upper troposphere and lower  
30 stratosphere (UTLS) over the Tibetan Plateau and the South Asian summer  
31 monsoon (TP/SASM) region during summertime of year 2005. Simulated  
32 surface-layer aerosol concentrations are compared with ground-based  
33 observations, and simulated aerosols in the UTLS are evaluated by using the  
34 Stratospheric Aerosol and Gas Experiment II satellite data. Simulations show  
35 elevated aerosol concentrations of sulfate, nitrate, ammonium, black carbon,  
36 organic carbon, and PM<sub>2.5</sub> (particles with diameter equal or less than 2.5 μm,  
37 defined as the sum of sulfate, nitrate, ammonium, black carbon, and organic  
38 carbon aerosols in this study) in the UTLS over the TP/SASM region  
39 throughout the summer. Nitrate aerosol is simulated to be of secondary  
40 importance near the surface but the most dominant aerosol species in the  
41 UTLS over the studied region. Averaged over summertime and over the  
42 TP/SASM region, C<sub>NIT</sub> (the ratio of nitrate concentration to PM<sub>2.5</sub> concentration)  
43 values are 5–35% at the surface, 25–50% at 200 hPa, and could exceed 60%  
44 at 100 hPa. The mechanisms for the accumulation of nitrate in the UTLS over  
45 the TP/SASM region include vertical transport and the gas-to-aerosol  
46 conversion of HNO<sub>3</sub> to form nitrate. The high relative humidity and low  
47 temperature associated with the deep convection over the TP/SASM region  
48 are favorable for the gas-to-aerosol conversion of HNO<sub>3</sub>.

## 49 **1 Introduction**

50 Aerosols in the upper troposphere and lower stratosphere (UTLS) have much  
51 longer residence times than those in the lower troposphere, influencing  
52 atmospheric chemistry and the Earth's climate with large spatial and temporal  
53 coverage (Rasch et al., 2008). Aerosols in the UTLS influence the  
54 concentrations of chemical species via changes in photolysis rates and  
55 heterogeneous reactions (Pitari et al., 2014). For example, heterogeneous  
56 reactions on sulfate aerosol can perturb the chemical partitioning in the lower  
57 stratosphere, leading to significant O<sub>3</sub> depletion through enhanced chlorine,  
58 bromine, and odd-hydrogen catalytic cycle (Zhao et al., 1997; Considine et al.,  
59 2001; Talukdar et al., 2012; Tang et al., 2014; Pitari et al., 2014). Aerosols in  
60 the UTLS also influence climate by altering properties of cirrus clouds via  
61 homogeneous or heterogeneous ice nucleation (Li et al., 2005; Liu et al., 2009;  
62 Yin et al., 2012; Fadnavis et al., 2013). Injection of aerosols into the UTLS has  
63 been reported to induce complex responses in circulation, temperature, and  
64 water vapor (Liu et al., 2009; Wu et al., 2011; Su et al., 2011; Fadnavis et al.,  
65 2013).

66 Aerosols over the Tibetan Plateau (TP) and the Asian summer monsoon  
67 region are especially important. The TP is surrounded by countries with large  
68 anthropogenic emissions (Li et al., 2005; Lau et al., 2006). Aerosols from India,  
69 Southeast Asia, and southern China can be transported to the TP by prevailing  
70 winds in the premonsoon and monsoon seasons (Lawrence and Lelieveld,  
71 2010; Xia et al., 2011). Observational and modeling studies have shown that  
72 persistent maxima of atmospheric constituents, such as water vapor  
73 (Gettelman et al., 2004; Randel and Park, 2006; Park et al., 2007), CO (Kar et

74 al., 2004; Li et al., 2005; Park et al., 2007, 2008, 2009), CH<sub>4</sub> (M. Park et al.,  
75 2004; Xiong et al., 2009), NO<sub>x</sub> (M. Park et al., 2004), HCN (Park et al., 2008;  
76 Randel et al., 2010), C<sub>2</sub>H<sub>6</sub> and C<sub>2</sub>H<sub>2</sub> (Park et al., 2008), exist in the UTLS  
77 above the TP and the South Asian summer monsoon (SASM) region because  
78 of the deep convection during boreal summer. Satellite observations  
79 suggested that the convection associated with the SASM is a vital pathway to  
80 transport air mass from the lower troposphere into the stratosphere (Chen et  
81 al., 2006; Randel and Park, 2006; Randel et al., 2010; Bian et al., 2011a). The  
82 heating associated with the persistent deep convection during summertime  
83 leads to the formation of the Tibetan anticyclone in the UTLS, which acts to  
84 isolate air within the anticyclone and traps the uplifted pollutants at that altitude  
85 (Park et al., 2007; Vernier et al., 2011; Bourgeois et al., 2012; Fadnavis et al.,  
86 2013; He et al., 2014). The stratosphere-troposphere exchange (STE) over the  
87 TP contributes largely to the global STE (Chen et al., 2006).

88 Previous studies have reported that aerosols exist in the UTLS over the  
89 TP/SASM region. Kim et al. (2003) carried out optical measurements with a  
90 ground-based lidar in Lhasa from August to October of 1999, and found an  
91 enhancement in aerosol concentration near the local tropopause with  
92 scattering ratio (SR, the ratio of aerosol plus molecular backscatter to  
93 molecular backscatter alone) of 1.1–1.2. Tobo et al. (2007) reported an  
94 enhancement of sub-micron aerosols (effective radius  $r = 0.15\text{--}0.6\ \mu\text{m}$ ) near  
95 the summertime tropopause (about 130 to 70 hPa), on the basis of in situ  
96 balloon measurements from an Optical Particle Counter at the same location in  
97 August of 1999. Vernier et al. (2009) examined satellite measurements from  
98 the Cloud-Aerosol Lidar with Orthogonal Polarization (CALIOP) onboard

99 Cloud-Aerosol Lidar and Infrared Pathfinder Satellite Observation (CALIPSO)  
100 and reported the presence of small depolarizing particles with high SR values  
101 (about 1.20 at 532 nm) at 16–17 km altitude over South Asia in July and  
102 August of 2007 and 2008. Bourgeois et al. (2012) found that an aerosol layer  
103 existed at 16–18 km altitude over the Asian continent and Indian Ocean  
104 (20°S–30°N, 5–105°E) on the basis of the CALIOP observations. Recently, He  
105 et al. (2014) examined the vertical profiles of aerosol extinction coefficients  
106 measured with a Micro Pulse Lidar at Naqu, a meteorological station located in  
107 the central part of the TP, and also showed a maximum in aerosol extinction  
108 coefficient ( $\sim 2.10^{-3} \text{ km}^{-1}$ ) in the UTLS (18–19 km) during the summer of 2011.

109 A number of previous studies have attempted to understand the chemical  
110 composition of aerosols in the UTLS. Froyd et al. (2009) measured aerosol  
111 composition with the National Oceanic and Atmospheric Administration (NOAA)  
112 single-particle mass spectrometer aboard the National Aeronautics and Space  
113 Administration (NASA) WB-57 high altitude aircraft platform, and reported that  
114 particles in the tropical tropopause layer were rich in nitrogen. Vernier et al.  
115 (2011) suggested that aerosol layer at the tropopause of Asia could be sulfur  
116 and/or organics, considering that Asian pollutants consisted of black carbon,  
117 organic carbon, SO<sub>2</sub>, and NO<sub>x</sub> (Park et al., 2009; Randel et al., 2010). Weigel  
118 et al. (2011) analyzed the volatility of aerosols obtained from in situ airborne  
119 measurements and reported that about 75–90 % of the particles in the tropical  
120 tropopause layer were volatile, but this study did not give any detailed  
121 analyses of chemical composition of aerosols. Bourgeois et al. (2012) showed,  
122 by using the ECHAM5.5-HAM2 model, that sulfate, water, and OC contributed,  
123 respectively, 53%, 29%, and 11% to aerosol extinction in the vicinity of the

124 tropical tropopause layer. The ECHAM5.5-HAM2 model used by Bourgeois et  
125 al. (2012) simulated all major aerosol species in the atmosphere except for  
126 nitrate.

127 Few previous studies have examined nitrate aerosol in the UTLS, although  
128 nitrate is expected to be important for the following reasons. First, emissions of  
129 precursors of nitrate, such as  $\text{NO}_x$  and  $\text{NH}_3$ , are high over India, Southeast  
130 Asia, and China (Streets et al., 2003; Datta et al., 2012; Huang et al., 2012).  
131 Second, simulated nitrate concentrations are high over those regions (Liao and  
132 Seinfeld, 2005; Mu and Liao, 2014; Lou et al., 2014). Third, measured  
133 concentrations of nitrate are comparable to or larger than those of sulfate at  
134 rural and urban sites in the SASM region. Shrestha et al. (2000) carried out  
135 measurements of aerosols at Phortse, Nepal, during September  
136 1996–November 1997, and showed that the average concentration of nitrate  
137 during the monsoon season (June–September) was  $0.34 \mu\text{g m}^{-3}$ , higher than  
138 that of sulfate ( $0.17 \mu\text{g m}^{-3}$ ). Decesari et al. (2010) reported, on the basis of  
139 measurements at the Nepal Climate Observatory–Pyramid from 2006 to 2008,  
140 that the concentrations of nitrate and sulfate were  $0.37 \mu\text{g m}^{-3}$  and  $0.50 \mu\text{g m}^{-3}$ ,  
141 respectively, during the monsoon season. Chatterjee et al. (2010) measured  
142 aerosols at a high altitude station in northeastern Himalayas during  
143 January–December 2005. They found that the average concentrations of  
144 fine-mode nitrate and sulfate were  $3.31 \pm 2.25 \mu\text{g m}^{-3}$  and  $3.80 \pm 2.9 \mu\text{g m}^{-3}$ ,  
145 respectively. At Lahore, an urban site in Pakistan, the observed daytime nitrate  
146 concentration of  $21.8 \mu\text{g m}^{-3}$  was also higher than sulfate concentration of  $12.6$   
147  $\mu\text{g m}^{-3}$  (Lodhi et al., 2009), as the observations were averaged over November  
148 2005 to March 2006. Fourth, the low temperatures in the UTLS would favor

149 nitrate formation (Seinfeld and Pandis, 2006). Therefore, it is of interest to take  
150 nitrate aerosol into consideration when we examine aerosols in the UTLS.

151 In this work we simulate nitrate aerosol and its contribution to aerosol  
152 concentrations in the UTLS over the TP (70–105°E, 25–40°N) and the SASM  
153 region (70–105°E, 10–25°N) by using the global chemical transport model  
154 GEOS-Chem driven by the assimilated meteorological fields. These regions of  
155 interest are shown in Fig. 1. Simulated surface-layer aerosol concentrations  
156 are compared with ground-based observations, and simulated aerosols in the  
157 UTLS are evaluated by using the Stratospheric Aerosol and Gas Experiment  
158 II (SAGE II) satellite data. Section 2 is a brief description of the GEOS-Chem  
159 model and numerical experiment. Section 3 presents the simulation and  
160 evaluation of distributions and concentrations of HNO<sub>3</sub> and O<sub>3</sub> to show model's  
161 capability in simulating the NO<sub>x</sub>-O<sub>3</sub>-HNO<sub>3</sub> cycle over the studied regions.  
162 Section 4 shows simulated aerosols and Section 5 presents the simulated  
163 contribution of nitrate to aerosol concentrations in the UTLS over the TP and  
164 the SASM region. Section 6 discusses the mechanisms for high concentrations  
165 of nitrate in the UTLS. Section 7 discusses the impacts of uncertainties in  
166 surface-layer aerosol concentrations on simulated nitrate in the UTLS.

167

## 168 **2 Model description and numerical experiment**

### 169 **2.1 GEOS-Chem model**

170 We simulate gas-phase species and aerosols using the global chemical  
171 transport model GEOS-Chem (version 9-01-03,  
172 <http://acmg.seas.harvard.edu/geos/index.html>) driven by the GEOS-5  
173 assimilated meteorological fields from the Goddard Earth Observing System of

174 the NASA Global Modeling and Assimilation Office. The version of the model  
175 used here has a horizontal resolution of 2° latitude by 2.5° longitude and 47  
176 vertical layers extending from the surface to 0.01 hPa. Over the TP and the  
177 SASM region, the model has about 34 layers in the troposphere and 12 layers  
178 in the stratosphere.

179 The GEOS-Chem model has a fully coupled treatment of tropospheric  
180 NO<sub>x</sub>-CO-hydrocarbon-aerosol chemistry and aerosols including sulfate (SO<sub>4</sub><sup>2-</sup>),  
181 nitrate (NO<sub>3</sub><sup>-</sup>), ammonium (NH<sub>4</sub><sup>+</sup>), organic carbon (OC), black carbon (BC) (R. J.  
182 Park et al., 2003; 2004; Pye et al., 2009), mineral dust (Fairlie et al., 2007), and  
183 sea salt (Alexander et al., 2005; Jaeglé et al., 2011). Anthropogenic aerosols  
184 are treated as bulk mass concentrations (particles of SO<sub>4</sub><sup>2-</sup>, NO<sub>3</sub><sup>-</sup>, NH<sub>4</sub><sup>+</sup>, BC,  
185 and OC are not size-resolved). Sea Salt mass is simulated for two size bins  
186 (0.1–0.5 and 0.5–8 μm) and mineral dust is simulated for four size bins  
187 (0.1–1.0, 1.0–1.8, 1.8–3.0, and 3.0–6.0 μm). Both BC and OC consist of  
188 hydrophilic and hydrophobic fractions in the model. It is assumed that 80% of  
189 BC and 50% of OC emitted from all primary sources are hydrophobic (Cooke  
190 et al., 1999; Chin et al., 2002; Chung and Seinfeld, 2002), which become  
191 hydrophilic with an e-folding time of 1.2 days following Cooke et al. (1999) and  
192 Chin et al. (2002). All secondary OC is assumed to be hydrophilic. Hydrophilic  
193 fractions of both BC and OC aerosols are assumed to be fully soluble.

194 The gas-aerosol partitioning of nitric acid and ammonium is calculated  
195 using the ISORROPIA II thermodynamic equilibrium module (Fountoukis and  
196 Nenes, 2007). In the version of the GEOS-Chem model used in this work, ions  
197 considered in ISORROPIA II include H<sup>+</sup>/Na<sup>+</sup>/NH<sub>4</sub><sup>+</sup>/Cl<sup>-</sup>/SO<sub>4</sub><sup>2-</sup>/HSO<sub>4</sub><sup>-</sup>/NO<sub>3</sub><sup>-</sup>/OH<sup>-</sup>. The  
198 two-way coupling between aerosols and gas phase chemistry provides

199 consistent chemical fields for aerosol simulation and aerosol mass for  
200 heterogeneous processes and calculations of gas-phase photolysis rates.  
201 Heterogeneous reactions include hydrolysis of  $\text{N}_2\text{O}_5$  (Evans and Jacob, 2005),  
202 irreversible absorption of  $\text{NO}_3$  and  $\text{NO}_2$  on wet aerosols (Jacob, 2000), and the  
203 uptake of  $\text{HO}_2$  by aerosols (Liao and Seinfeld, 2005; Thornton et al., 2008).  
204 [Aerosol species are treated as an external mixture in the calculation of aerosol](#)  
205 [optical properties.](#)

206 With respect to chemistry in the stratosphere, stratospheric  $\text{O}_3$   
207 concentrations are calculated using the linearized parameterization scheme  
208 (McLinden et al., 2000). The monthly mean production rates and loss  
209 frequencies of other stratospheric species (including long-lived species such  
210 as CFCs and  $\text{N}_2\text{O}$ ) use those from NASA Global Modeling Initiative (GMI)  
211 Combo simulations (Duncan et al., 2007; Considine et al., 2008; Murray et al.,  
212 2012).

213 Convective transport in GEOS-Chem mimics that in the parent GEOS  
214 general circulation model (GCM) (Hack, 1994; Zhang and McFarlane, 1995),  
215 which accounts for updraft, downdraft, and entrainment mass fluxes for deep  
216 and shallow convection (Wu et al., 2007). The aerosol wet deposition scheme  
217 in the GEOS-Chem follows that of Liu et al. (2001). For the scavenging of  
218 aerosols,  $\text{SO}_4^{2-}$ ,  $\text{NO}_3^-$ ,  $\text{NH}_4^+$ , and hydrophilic OC and hydrophilic BC aerosols  
219 are assumed to be fully soluble. Dry deposition follows the standard  
220 resistance-in-series model of Wesely (1989).

221 Global emissions of aerosols and their precursors in the GEOS-Chem  
222 follow R. J. Park et al. (2003, 2004), with anthropogenic emissions of  $\text{NO}_x$ , CO,  
223  $\text{SO}_2$ , and non-methane volatile organic compounds (NMVOC) in Asia

224 overwritten by David Streets' 2006 emission inventory  
225 (<http://mic.greenresource.cn/intex-b2006>). Emissions of NH<sub>3</sub> in Asia are taken  
226 from Streets et al. (2003). Since NH<sub>3</sub> emissions in China showed large  
227 uncertainties in previous studies (Streets et al., 2003; Kim et al., 2006; Y.  
228 Zhang et al., 2010; Huang et al., 2011, 2012), we use the most recent estimate  
229 of NH<sub>3</sub> emissions in China by Huang et al. (2012), which is 9.8 Tg yr<sup>-1</sup>, instead  
230 of 13.5 Tg yr<sup>-1</sup> from Streets et al. (2003). Table 1 summarizes the annual  
231 emissions of NO<sub>x</sub>, SO<sub>2</sub>, NH<sub>3</sub>, OC, and BC in Asia domain (60–155°E,  
232 10–55°N).

233 Natural NO<sub>x</sub> emissions from lightning are calculated using the scheme  
234 described by Sauvage et al. (2007) and Murray et al. (2012), and those from  
235 soil are simulated following Wang et al. (1998). Natural NH<sub>3</sub> emissions from  
236 soil, vegetation, and the oceans are taken from the Global Emissions Inventory  
237 Activity inventory (Bouwman et al., 1997). Biomass burning emissions are from  
238 the monthly Global Fire Emissions Database (GFED v3) driven by satellite  
239 observations of fire activity (van der Werf et al., 2010). Biogenic VOC (volatile  
240 organic compounds) emissions are calculated from the Model of Emissions of  
241 Gases and Aerosols from Nature (Guenther et al., 2006).

242 The monthly variations of emissions of SO<sub>2</sub> and NO<sub>x</sub> follow Wang et al.  
243 (2013) and those of BC and OC follow Lou et al. (2014). The monthly scaling  
244 factors for NH<sub>3</sub> emissions follow the global inventory compiled by Marcel  
245 Meinders and Lex Bouwman (Fisher et al., 2011). Monthly variations of  
246 emissions (anthropogenic plus natural emissions) of NO<sub>x</sub>, SO<sub>2</sub>, NH<sub>3</sub>, OC, and  
247 BC over Asia are displayed in Fig. 2. The emissions of NH<sub>3</sub> are the highest in  
248 June as a result of the agriculture practice and high temperatures (Wang et al.,

249 2013).

## 250 **2.2 Numerical experiment**

251 To examine the contribution of nitrate to aerosol concentrations in the UTLS  
252 over the TP/SASM region, we simulate aerosol concentrations by using the  
253 emissions of and meteorological fields of year 2005. Year 2005 is chosen so  
254 that we can use the observational datasets for this year from SAGE II and MLS,  
255 as described in Sects. 3 and 4. Following Rasch et al. (2008), we perform a  
256 10-year spin-up run to generate the initial conditions (to allow the stratospheric  
257 species to reach quasi-steady state conditions). We would consider that the  
258 tropospheric simulation can be representative of year 2005 but stratosphere  
259 simulation should represent a multi-year average, because the production  
260 rates and loss frequencies in the stratosphere are the averages over years of  
261 2004–2010 ([http://wiki.seas.harvard.edu/geos-chem/index.php/Stratospheric\\_chemistry](http://wiki.seas.harvard.edu/geos-chem/index.php/Stratospheric_chemistry)).  
262 chemistry).

263

## 264 **3 Simulated concentrations of HNO<sub>3</sub> and O<sub>3</sub> and model evaluation**

265 Nitrate aerosol forms when nitric acid (HNO<sub>3</sub>) reacts with alkaline gases (for  
266 example, ammonia) in the atmosphere (Seinfeld and Pandis, 2006). HNO<sub>3</sub>, as  
267 the important precursor of nitrate, is the major oxidation product of nitrogen  
268 oxides (NO<sub>x</sub> = NO+NO<sub>2</sub>) (Seinfeld and Pandis, 2006). To show the model's  
269 capability in simulating the NO<sub>x</sub>-O<sub>3</sub>-HNO<sub>3</sub> cycle over the studied regions, we  
270 present and evaluate the simulated HNO<sub>3</sub> and O<sub>3</sub> in this section.

271 Simulated mixing ratios of HNO<sub>3</sub> and O<sub>3</sub> in the UTLS are evaluated by  
272 using datasets from the limb viewing satellite instrument of Microwave Limb  
273 Sounder (MLS, version 3.3, level 2,

274 ftp://acdisc.gsfc.nasa.gov/data/s4pa///Aura\_MLS\_Level2/). The MLS datasets  
275 provide valuable information on atmospheric compositions in the UTLS  
276 (Waters et al., 2006). For HNO<sub>3</sub>, the MLS provides datasets for 215 to 1.5 hPa,  
277 with a vertical resolution of 3–4 km and a horizontal resolution of 400–500 km.  
278 Since further evaluations are needed for datasets at altitudes with pressures  
279 higher than 215 hPa (Livesey et al., 2011), we use only datasets for pressures  
280 lower than that. For O<sub>3</sub>, the MLS provides datasets for 261 to 0.02 hPa, with a  
281 vertical resolution of 2.5–3 km and a horizontal resolution of 300–400 km in the  
282 UTLS (Santee et al., 2007; Livesey et al., 2011). The uncertainties of the MLS  
283 HNO<sub>3</sub> and O<sub>3</sub> datasets in the UTLS are about ±0.5–1 ppbv and 0.02–0.04  
284 ppmv, respectively (Livesey et al., 2011).

### 285 **3.1 HNO<sub>3</sub>**

286 Figure 3(a) shows the simulated global distribution of HNO<sub>3</sub> concentrations  
287 averaged over June-August of 2005. Concentrations of HNO<sub>3</sub> exceed 1 ppbv  
288 over the industrialized areas such as Europe, North America, central and  
289 eastern Asia, and over biomass burning regions in the tropics, in agreement  
290 with the distributions and magnitudes reported in Liao et al. (2003). Over South  
291 Asia, simulated HNO<sub>3</sub> concentrations are high (0.3–1 ppbv) in the northern  
292 Indian subcontinent, because the emissions of NO<sub>x</sub> and NH<sub>3</sub> are high in this  
293 region (Streets et al., 2003; Zhang et al., 2009; Datta et al., 2012).

294 Figures 4(a)-4(b) show the simulated HNO<sub>3</sub> concentrations in the UTLS  
295 averaged over June-August of 2005. Since the tropopause is located at  
296 70–150 hPa (12–15 km) over the TP/SASM region (Li et al., 2005; Bian et al.,  
297 2011b; Fadnavis et al., 2014), we choose the vertical layers of 200 hPa and  
298 100 hPa to represent the UTLS. At both 200 hPa and 100 hPa, the highest

299 HNO<sub>3</sub> concentrations are simulated to occur in the high latitude regions in the  
300 Northern Hemisphere (NH) (Fig. 4(a) and Fig. 4(b)). Simulated HNO<sub>3</sub>  
301 concentrations at 100 hPa are low over the region of 40–100°E and 10–30°N,  
302 which is part of the anticyclone region defined in Fig. 1. Figure 4(c) shows the  
303 latitude-altitude cross section of simulated seasonal mean HNO<sub>3</sub> mixing ratios  
304 averaged over 70–105°E. In boreal summer, the highest HNO<sub>3</sub> mixing ratios  
305 are simulated to occur at 30 hPa over the Polar Regions in both hemispheres.  
306 Over high latitudes, HNO<sub>3</sub> concentrations in the Southern Hemisphere (SH)  
307 are simulated to be higher than those in the NH.

308 To evaluate the simulated HNO<sub>3</sub>, Figures 4(d)-4(f) show HNO<sub>3</sub>  
309 concentrations in the UTLS from MLS that are averaged over June-August of  
310 2005. At 200 and 100 hPa altitudes, the observed HNO<sub>3</sub> mixing ratios are high  
311 in the high latitudes in the NH, which are captured by the GEOS-Chem model.  
312 The observed HNO<sub>3</sub> at 100 hPa exhibits low values of less than 400 pptv over  
313 30–100°E and 10–30°N in the Asian monsoon anticyclone region (Fig. 4(e)). At  
314 100 hPa, the observed HNO<sub>3</sub> mixing ratio averaged over the TP/SASM region  
315 (70–105°E, 10–40°N) is 301.3 pptv, which is lower than the simulated value of  
316 349.1 pptv. The difference between the simulated and observed HNO<sub>3</sub> mixing  
317 ratio lies within the confidence range of ±500–1000 pptv of the MLS  
318 instruments (Livesey et al., 2011). Considering all the grid cells with MLS  
319 HNO<sub>3</sub> data available, the simulated seasonal mean HNO<sub>3</sub> concentrations show  
320 normalized mean bias (NMB) of +15.9% at 100 hPa over the TP/SASM region  
321 in summer of year 2005. The observed pattern of the HNO<sub>3</sub> vertical distribution  
322 (Fig. 4(f)) is also captured by the GEOS-Chem model (Fig. 4(c)). The  
323 distributions of HNO<sub>3</sub> in the UTLS are associated with the Brewer-Dobson

324 circulation proposed by Brewer (1949) and Dobson (1956), traveling upwards  
325 across the tropopause to the stratosphere at the equator and downwards to  
326 the troposphere near the Polar region.

### 327 **3.2 O<sub>3</sub>**

328 Figure 3(b) shows the global distribution of simulated summertime  
329 surface-layer O<sub>3</sub> concentrations. Simulated O<sub>3</sub> concentrations are in a range of  
330 40–70 ppbv over Europe, North America, China, and the biomass burning  
331 region of South Africa. Our model results agree closely with the simulated  
332 distributions and magnitudes reported in Mickley et al. (1999), Collins et al.,  
333 (2000), Liao et al. (2003), Wu et al., (2008), Zeng et al. (2008), and Fadnavis et  
334 al. (2014). Fadnavis et al. (2014) also presented aircraft measurements over  
335 India in September of 2010 during the Cloud Aerosol Interaction and  
336 Precipitation Enhancement Experiment (CAIPEEX). Our simulated O<sub>3</sub>  
337 concentrations of 30–40 ppbv over India agree with the CAIPEEX  
338 measurements.

339 Figures 5(a)-5(b) show the simulated O<sub>3</sub> concentrations in the UTLS  
340 averaged over June-August of 2005. The distributions of O<sub>3</sub> concentrations in  
341 the UTLS are similar to those of HNO<sub>3</sub>, with elevated values in the high  
342 latitudes of the NH. Relatively low O<sub>3</sub> mixing ratios of less than 200 ppbv are  
343 simulated at 100 hPa over 10–30°N, 20–110°E, within the anticyclone region  
344 defined in Fig. 1. Our simulated distributions and magnitudes of O<sub>3</sub> agree with  
345 those reported in Bian et al. (2011b), which examined the summertime  
346 distributions of O<sub>3</sub> in the UTLS during 2005–2009 by using the MLS version 2.2  
347 level 2 products (Livesey et al., 2008). Because the background O<sub>3</sub>  
348 concentrations are generally high in the UTLS and the stratosphere, the low O<sub>3</sub>

349 concentrations in the UTLS over the TP/SASM region are caused by the deep  
350 convection that transports O<sub>3</sub>-poor air upward (Fu et al., 2006; Randel and  
351 Park, 2006; Park et al., 2007; Bian et al., 2011b). Figure 5(c) displays the  
352 latitude-altitude cross section of seasonal mean O<sub>3</sub> mixing ratios averaged  
353 over 70–105°E. As a result of the Brewer-Dobson circulation, O<sub>3</sub>  
354 concentrations in the UTLS are lower over the tropics than in the Polar  
355 Regions, even though the maximum O<sub>3</sub> concentrations are located around 10  
356 hPa over the tropics (Brewer, 1949). Our simulated O<sub>3</sub> concentrations in the  
357 UTLS agree well with the measurements from MLS (Fig. 5(d)-5(f)). At 100 hPa,  
358 simulated and MLS observed O<sub>3</sub> mixing ratios averaged over the TP/SASM  
359 region (70–105°E, 10–40°N) are 190.6 and 145.1 ppbv, respectively.  
360 Compared to MLS observations, simulated O<sub>3</sub> concentrations at 100 hPa have  
361 a NMB of +31.4% over the TP/SASM region in summer of 2005. Our simulated  
362 global STE of O<sub>3</sub> is 420 Tg yr<sup>-1</sup>, which is within the range reported in previous  
363 studies (475±120 Tg yr<sup>-1</sup> in McLinden et al. (2000), 420 Tg yr<sup>-1</sup> in Škerlak et al.  
364 (2014), 556±154 Tg yr<sup>-1</sup> in Stevenson et al. (2006), and 550±140 Tg yr<sup>-1</sup> in  
365 Solomon et al. (2007)).

366 In addition to the comparisons against MLS products, the simulated O<sub>3</sub>  
367 profiles are compared with balloon-borne sonde measurements in Fig. 6. The  
368 measurements were carried out at Kunming (KM, 102.7°E, 25.0°N) in August  
369 of 2009 and 2012, and at Lhasa (LH, 91.1°E, 29.7°N) in August of 2010 and  
370 2013. The uncertainties of the observed O<sub>3</sub> mixing ratios were estimated to be  
371 within 5–10% (Bian et al. 2012). [The comparisons with multi-year observations](#)  
372 [show that the model can reproduce the vertical distributions of O<sub>3</sub> above 12 km](#)  
373 [in Kunming and Lhasa](#). At 100 hPa, the simulated monthly mean O<sub>3</sub> mixing

374 ratio in KM is 112.6 ppbv, and the observed value is 124.2 ppbv in 2009 and  
375 113.5 ppbv in 2012. In LH, the simulated monthly O<sub>3</sub> mixing ratio at 100 hPa is  
376 152.6 ppbv, and the observed O<sub>3</sub> mixing ratio at that altitude is 142.4 ppbv in  
377 2010 and 167.9 ppbv in 2013. The magnitudes of O<sub>3</sub> mixing ratios from these  
378 balloon-borne sonde measurements support those from MLS; O<sub>3</sub> mixing ratios  
379 in the UTLS are less than 200 ppbv over the TP/SASM region.

380

## 381 **4 Simulated aerosols and model evaluation**

### 382 **4.1 Simulated aerosols**

383 Figure 7 (a) shows the simulated surface-layer concentrations of SO<sub>4</sub><sup>2-</sup>, NO<sub>3</sub><sup>-</sup>,  
384 NH<sub>4</sub><sup>+</sup>, OC, BC, and PM<sub>2.5</sub> (the sum of the mass of SO<sub>4</sub><sup>2-</sup>, NO<sub>3</sub><sup>-</sup>, NH<sub>4</sub><sup>+</sup>, BC, and  
385 OC aerosols) averaged over June-August of year 2005. As expected,  
386 simulated aerosol concentrations are high over polluted regions such as India  
387 and eastern China as a result of the high anthropogenic emissions of aerosol  
388 precursors and aerosols (Streets et al., 2003; Huang et al., 2012). Over the  
389 TP/SASM region (70–105°E, 10–40°N), the average concentrations of SO<sub>4</sub><sup>2-</sup>,  
390 NO<sub>3</sub><sup>-</sup>, NH<sub>4</sub><sup>+</sup>, BC, and OC are 1.70, 0.94, 0.85, 0.30, and 0.94 μg m<sup>-3</sup>,  
391 respectively. NO<sub>3</sub><sup>-</sup> is simulated to be of secondary importance at the surface  
392 over the region of our interest. The simulated distributions and magnitudes of  
393 these aerosol species are similar to those reported in Wang et al. (2013) and  
394 Mu and Liao (2014).

395 Figures 7(b) and 7(c) also show the simulated concentrations of SO<sub>4</sub><sup>2-</sup>,  
396 NO<sub>3</sub><sup>-</sup>, NH<sub>4</sub><sup>+</sup>, OC, BC, and PM<sub>2.5</sub> in the UTLS. Elevated concentrations of SO<sub>4</sub><sup>2-</sup>,  
397 NO<sub>3</sub><sup>-</sup>, NH<sub>4</sub><sup>+</sup>, OC, BC and PM<sub>2.5</sub> are simulated over the TP and Plateau south  
398 slope at 200 hPa altitude, and extend from eastern Mediterranean to western

399 China at 100 hPa. The simulated enhanced concentrations of  $\text{SO}_4^{2-}$ , OC, and  
400 BC at 100 hPa over the anticyclone region (20–120°E, 10–40°N) agree with  
401 previous observational and modeling studies (Lelieveld et al., 2001; Li et al.,  
402 2005; Fadnavis et al., 2013). Li et al. (2005) reported elevated CO  
403 concentrations in the upper troposphere over the TP, on the basis of both MLS  
404 measurements and the GEOS-Chem simulation for September 2004.  
405 Fadnavis et al. (2013) also simulated maximum concentrations of  $\text{SO}_4^{2-}$ , OC,  
406 BC, and mineral dust aerosols in the UTLS during the Asian summer monsoon  
407 season owing to convective uplifting of the boundary layer pollutants. With  
408  $\text{NO}_3^-$  aerosol accounted for in our simulation,  $\text{NO}_3^-$  is simulated to be the most  
409 dominant aerosol species in the UTLS over the TP/SASM region, followed  
410 by  $\text{SO}_4^{2-}$ ,  $\text{NH}_4^+$ , OC, and BC. At 100 hPa, the averaged concentrations of  $\text{SO}_4^{2-}$ ,  
411  $\text{NO}_3^-$ ,  $\text{NH}_4^+$ , OC, and BC over the TP/SASM region (70–105°E, 10–40°N)  
412 region are 0.026, 0.069, 0.014, 0.011, and 0.002  $\mu\text{g m}^{-3}$ , respectively.

#### 413 **4.2 Comparisons of simulated aerosol concentrations with in-situ** 414 **observations**

415 The simulated aerosol concentrations in East Asia in the GEOS-Chem model  
416 have been evaluated in previous studies (L. Zhang et al., 2010; Fu et al., 2012;  
417 Jeong and Park, 2013; Jiang et al., 2013; Wang et al., 2013; Lou et al., 2014).  
418 Here we are focused on the evaluation of aerosols in the South Asian  
419 monsoon region. For lack of publicly accessible in situ measurements of  
420 summertime aerosols in South Asia monsoon area, we compiled monthly or  
421 seasonal mean measured concentrations of each aerosol species based on  
422 measurements reported in the literature (see Table S1 in the Supplementary  
423 Material). These measurements were carried out over years of 1992–2010.

424 The locations of sites with measurements available are shown in Fig. 8(a).  
425 Most sites are located in the upwind directions of the TP, with pollutants that  
426 can be transported to the UTLS during the South Asian summer monsoon  
427 season. The observed  $PM_{10}$  concentrations listed in Table S1 are multiplied by  
428 0.6 to convert to  $PM_{2.5}$  for model evaluation, following the suggestions in  
429 Zhang et al. (2002) and Chatterjee et al. (2010).

430 Figures 8(b)–8(f) show the scatterplots of simulated versus observed  
431 seasonal mean aerosol concentrations. Compared with measurements,  
432 simulated  $SO_4^{2-}$ ,  $NO_3^-$ ,  $NH_4^+$ , OC and BC have NMBs of  $-17.0\%$ ,  $+38.8\%$ ,  
433  $+42.0\%$ ,  $-69.7\%$  and  $-41.0\%$ , respectively, as the concentrations of all  
434 seasons are considered. The correlations between model results and  
435 observations have  $R$  values of 0.49–0.85 for all aerosol species, indicating that  
436 the model is capable of capturing the spatial distributions and seasonal  
437 variations of each aerosol species in the South Asian monsoon region despite  
438 the biases in concentrations. If we consider simulated and measured  
439 concentrations for JJA alone, the simulated concentrations of  $SO_4^{2-}$ ,  $NO_3^-$ ,  
440  $NH_4^+$ , OC and BC exhibit seasonal NMBs of  $-14.7\%$ ,  $+51.5\%$ ,  $+74.9\%$ ,  $-57.2\%$   
441 and  $-32.2\%$ , respectively, and the values of  $R$  are in the range of 0.24–0.85.  
442 Note that the measurements of  $NO_3^-$  and  $NH_4^+$  are quite limited in terms of the  
443 number of samples, and the discrepancies between model results and  
444 measurements may also arise from the mismatch of the model year 2005 with  
445 the years of 1992–2010 with observations available.

### 446 **4.3 Comparisons of simulated aerosol extinction coefficients with SAGE** 447 **II datasets**

448 Satellite datasets from the Stratospheric Aerosol and Gas Experiment II

449 (SAGE II, [https://eosweb.larc.nasa.gov/project/sage2/sage2\\_v620\\_table](https://eosweb.larc.nasa.gov/project/sage2/sage2_v620_table)) are  
450 used to evaluate the simulated aerosol extinction in the UTLS. The SAGE II  
451 instrument was launched in October 1984 aboard the Earth Radiation Budget  
452 Satellite (ERBS) and terminated on 8 September 2005 (McCormick et al. 1987;  
453 Chu et al. 1989). The datasets used here are aerosol extinction coefficients at  
454 525 nm from the version 6.20 SAGE retrievals, covering from 0.5 to 40 km with  
455 a vertical resolution of 0.5 km. Many validation studies have been conducted  
456 on the SAGE II aerosol data (Russell and McCormick, 1989; Oberbeck et al.,  
457 1989; Wang et al., 1989), which indicated that extinction coefficients have  
458 uncertainties of 20–30%. The extinction coefficients of aerosols in the  
459 GEOS-Chem model are calculated using aerosol mass concentration,  
460 extinction efficiency, effective radius, particle mass density, and the assumed  
461 aerosol size distribution (Drury et al., 2010). The hygroscopic growth of each  
462 aerosol species with relative humidity is accounted for, using the hygroscopic  
463 growth factors listed in Martin et al. (2003).

464 Figure 9(a) presents the simulated monthly mean distribution of aerosol  
465 extinction coefficients at 100 hPa for July of 2005. At 100 hPa, the simulated  
466 aerosol extinction coefficients are relatively high over the anticyclone region,  
467 where anthropogenic aerosol species (Fig. 7) and natural aerosols such as  
468 mineral dust and sea salt contribute to aerosol extinction coefficients in  
469 summer. Note that the contributions of sulfate, nitrate, ammonium, OC, sea  
470 salt, and mineral dust are all considered when we calculate aerosol extinction  
471 coefficients. Aerosol extinction coefficients are simulated to be  $1.2\text{--}2\times 10^{-3}$   
472  $\text{km}^{-1}$  at 100 hPa over the Asian continent and Indian Ocean ( $20^{\circ}\text{S}\text{--}30^{\circ}\text{N}$ ,  
473  $30^{\circ}\text{--}105^{\circ}\text{E}$ ). These values agree closely with aerosol extinction coefficients

474 measured at Naqu during August of 2011 for the same altitude, the maximum  
475 of which was  $2.4 \times 10^{-3} \text{ km}^{-1}$  (He et al., 2014). Vernier et al. (2011) also  
476 identified this Asian aerosol layer with high SR at 100 hPa by observations of  
477 CALIPSO for JJA of 2006–2008.

478 Figure 9(b) displays the monthly mean vertical profiles of aerosol extinction  
479 coefficients averaged over the Asian monsoon anticyclone region ( $20\text{--}120^\circ\text{E}$   
480  $10\text{--}40^\circ\text{N}$ ) (Fig. 1) for July of 2005. The SAGE II datasets are available for July  
481 only in 2005. The profiles from SAGE II and the GEOS-Chem simulation are all  
482 shown. The vertical distributions of aerosol extinction coefficients “with nitrate”  
483 and “without nitrate” are both from the baseline run with full chemistry. The  
484 vertical distribution of aerosol extinction coefficient “with nitrate” (or “without  
485 nitrate”) indicates that the contribution of nitrate aerosol to aerosol extinction is  
486 (or is not) accounted for. Accounting for all aerosol species, the GEOS-Chem  
487 model reproduces well the aerosol extinction coefficients above 10 km, but the  
488 discrepancies are rather large in altitudes less than 10 km. Note that the  
489 uncertainties in satellite datasets increase as the altitude decreases  
490 (Vanhellemont et al., 2008; Kulkarni and Ramachandran, 2015), and the  
491 missing data in the lower troposphere along the satellite trajectories over the  
492 region of our interest also contribute to the discrepancies

493 Comparisons of profiles of aerosol extinction coefficients with and without  
494 nitrate aerosol indicate that the profiles show small differences in altitudes less  
495 than 6 km but large discrepancies from 6 km to the tropopause. With nitrate  
496 aerosol accounted for, the simulated aerosol extinction coefficients agree  
497 closely with SAGE II datasets in the UTLS (averaged over 14–16 km, the  
498 simulated value is  $8.6 \times 10^{-4} \text{ km}^{-1}$  while the observed value is  $8.0 \times 10^{-4} \text{ km}^{-1}$ ).

499 Without nitrate aerosol, the simulated aerosol extinction coefficient at 14–16  
500 km altitude is  $1.5 \times 10^{-4} \text{ km}^{-1}$ , which underestimates the aerosol extinction  
501 coefficient by 82.6% compared to that calculated with all the aerosol species.  
502 These comparisons of extinction coefficients with and without nitrate aerosol  
503 suggest that nitrate aerosol plays an important role in aerosol extinction in the  
504 UTLS over the region of our interest.

505

## 506 **5 Contribution of nitrate to aerosol concentrations in the UTLS**

507 Since nitrate aerosol is simulated to be the most abundant aerosol species in  
508 the UTLS over the TP/SASM region, we analyze the contribution of nitrate to  
509  $\text{PM}_{2.5}$  concentration ( $C_{\text{NIT}} = \text{nitrate concentration} / \text{PM}_{2.5} \text{ concentration}$ ) in this  
510 section. Figure 10 shows the simulated seasonal mean distributions of  $C_{\text{NIT}}$  for  
511 June–August of year 2005. At the surface layer (Fig. 10(a)), simulated high  $C_{\text{NIT}}$   
512 values are located over the areas with high nitrate concentrations (India and  
513 eastern China) as well as the oceans where  $\text{NO}_3^-$  also forms on sea salt and  
514 mineral dust particles (Arimoto et al., 1996; Nakamura et al., 2005; George and  
515 Nair, 2008). Over the TP/SASM region, the  $C_{\text{NIT}}$  values in JJA are 5–35% at the  
516 surface, 25–50% at 200 hPa (Fig. 10(b)), and could exceed 60% at 100 hPa  
517 (Fig. 10(c)). The latitude–altitude cross section of  $C_{\text{NIT}}$  (Fig. 10(d)) shows that  
518  $C_{\text{NIT}}$  over 20–40°N increases with altitude and reaches maximum values  
519 around the extratropical tropopause.

520 Table 2 lists the mean concentrations of  $\text{SO}_4^{2-}$ ,  $\text{NO}_3^-$ ,  $\text{NH}_4^+$ , BC and OC, and  
521 their contributions to  $\text{PM}_{2.5}$  during summertime of 2005 over the TP/SASM, TP,  
522 and SASM regions. Over the TP/SASM region,  $\text{SO}_4^{2-}$ ,  $\text{NO}_3^-$ ,  $\text{NH}_4^+$ , BC and OC  
523 are simulated to contribute 35.9%, 19.8%, 18.1%, 6.4%, and 19.8%,

524 respectively, to  $PM_{2.5}$  mass concentration at the surface layer. The  
525 contributions increase significantly in the UTLS. The largest  $C_{NIT}$  is simulated  
526 in the SASM region at 100 hPa, where  $NO_3^-$  accounts for 60.5% of  $PM_{2.5}$  mass  
527 concentration. The high  $C_{NIT}$  values indicate that  $NO_3^-$  plays an important role  
528 in the aerosol layer in the UTLS over the TP/SASM region.

529       Considering the large uncertainties in simulated sea salt (Jaeglé et al.,  
530 2011) and mineral dust (Fairlie et al., 2007) aerosols, we tend to be focused on  
531 anthropogenic aerosol species ( $SO_4^{2-}$ ,  $NO_3^-$ ,  $NH_4^+$ , BC, and OC) in this work. In  
532 our model, concentrations of sea salt (or mineral dust) are simulated to be  
533  $1.0\text{--}1.7\text{ ng m}^{-3}$  (or  $5.0\text{--}7.0\text{ ng m}^{-3}$ ) over the studied region in the summer of  
534 2005, which contribute less than 1.2% (or 5.0%) to total aerosol mass at 100  
535 hPa. Therefore the consideration of sea salt and mineral dust can slightly  
536 reduce  $C_{NIT}$  values, but  $C_{NIT}$  values at 100 hPa are still as high as 45-65% over  
537 the TP/SASM region in summer.

538

## 539 **6 Mechanisms for high nitrate concentrations in the UTLS**

### 540 **6.1 Upward transport of nitrate from the lower troposphere**

541 The intense convective transport of chemical species into the UTLS over the  
542 TP/SASM region during summertime has been widely discussed in previous  
543 studies (Randel et al., 2010; Bian et al., 2011a; Fadnavis et al., 2013, 2014;  
544 Qie et al., 2014; He et al., 2014). Since nitrate aerosol is simulated to be of  
545 secondary abundant aerosol species in the surface layer over the TP/SASM  
546 region (Fig. 7), the vertical mass transport through the deep convection in this  
547 region contributes to the accumulation of  $NO_3^-$  in the UTLS. Figure 11 shows  
548 the latitude-altitude cross sections of simulated concentrations of  $SO_4^{2-}$  and

549  $\text{NO}_3^-$  averaged over 70–105°E in June-August of 2005, together with the  
550 wind vectors obtained from the European Centre for Medium-Range Weather  
551 Forecasts (ECMWF) ERA-Interim Reanalysis data. Note that the assimilated  
552 GEOS-5 meteorological fields do not have vertical winds  
553 ([http://wiki.seas.harvard.edu/geos-chem/index.php/List\\_of\\_GEOS-5\\_met\\_fields](http://wiki.seas.harvard.edu/geos-chem/index.php/List_of_GEOS-5_met_fields)  
554 s), so we use the ECMWF reanalysis wind fields to do the analysis here. High  
555 values of aerosol concentrations are found on the south slope of the  
556 Himalayas, where the deep convection exists. Although both  $\text{SO}_4^{2-}$  and  $\text{NO}_3^-$   
557 are transported upward to the extratropical tropopause, the details of the  
558 vertical distributions are different. At altitudes higher than 8 km, the  
559 concentrations of  $\text{NO}_3^-$  do not decrease with altitude as quickly as those of  
560  $\text{SO}_4^{2-}$ , and the concentrations of  $\text{NO}_3^-$  over 10–40°N are higher than those of  
561  $\text{SO}_4^{2-}$ .

562 The chemical mechanisms for the formation of  $\text{SO}_4^{2-}$ ,  $\text{NO}_3^-$ , and  $\text{NH}_4^+$   
563 aerosols in the GEOS-Chem model were described in R. J. Park et al. (2004),  
564 which are comprehensive and have been used extensively in previous studies  
565 to simulate these three aerosol species (R. J. Park et al., 2004; Pye et al.,  
566 2009; L. Zhang et al., 2010; Zhu et al., 2012; Jiang et al., 2013; Lou et al.,  
567 2014). Sulfate aerosol forms from gas-phase oxidation of  $\text{SO}_2$  by OH and from  
568 in-cloud oxidation of  $\text{SO}_2$  by  $\text{O}_3$  and  $\text{H}_2\text{O}_2$ . Nitrate forms from the partitioning of  
569  $\text{HNO}_3$  between gas and aerosol phases, which is calculated by the  
570 ISORROPIA II thermodynamic equilibrium module (Fountoukis and Nenes,  
571 2007) in the GEOS-Chem model. Major reactions for the production and loss  
572 of  $\text{HNO}_3$  were listed in Liao and Seinfeld (2005).  $\text{HNO}_3$  is produced by the  
573 reaction of  $\text{NO}_2$  with OH during daytime and by hydrolysis of  $\text{N}_2\text{O}_5$  on aerosol

574 surfaces at night. The chemical mechanisms for  $\text{SO}_4^{2-}$  and  $\text{NO}_3^-$  have  
575 different sensitivity to meteorological conditions. During the vertical transport,  
576 temperature decreases, which reduces the gas-phase oxidation of  $\text{SO}_2$  (Yao et  
577 al., 2002; Seinfeld and Pandis 2006) but promotes the formation of  $\text{NO}_3^-$  by  
578 shifting gas-particle equilibria (Dawson et al., 2007; Liao et al., 2009). Dawson  
579 et al. (2007) examined the sensitivities of sulfate and nitrate concentrations to  
580 temperature by using the Particulate Matter Comprehensive Air Quality Model  
581 with extensions (PMCAMx). The sensitivity test was performed by fixing all  
582 meteorological parameters but perturbing temperature. Their sensitivity  
583 simulations showed that the increases in temperature led to increases in  
584 sulfate concentrations and decreases in nitrate concentrations. Compared to  
585 nitrate, sulfate concentrations showed smaller sensitivity to temperature  
586 changes (Dawson et al., 2007); as temperature increased, nitrate  
587 concentrations decreased by  $19\% \text{ K}^{-1}$  and  $17\% \text{ K}^{-1}$  in January and July  
588 respectively, while sulfate concentration increased by  $0.12\% \text{ K}^{-1}$  and  $1.3\% \text{ K}^{-1}$   
589 in January and July, respectively. Therefore the different chemical mechanisms  
590 for  $\text{SO}_4^{2-}$  and  $\text{NO}_3^-$  formation contribute to the differences in their vertical  
591 distributions.

## 592 **6.2 The gas-to-aerosol conversion of $\text{HNO}_3$ to form nitrate**

593 As mentioned above, the formation of gas-phase  $\text{HNO}_3$  and the partitioning of  
594  $\text{HNO}_3$  between gas and aerosol phases are the two major chemical processes  
595 that influence  $\text{NO}_3^-$  concentrations. We have evaluated the ability of the  
596 GEOS-Chem model to simulate gas-phase  $\text{HNO}_3$  in Section 3.1 (by  
597 comparisons of our model results with MLS observations and concentrations  
598 from previous modeling studies), so we quantify here  $\text{NO}_3^-$  formation from

599 gas-to-aerosol conversion of  $\text{HNO}_3$  based on the ISORROPIA II  
600 thermodynamic equilibrium module (Fountoukis and Nenes, 2007). The  
601 gas-to-aerosol conversion of  $\text{HNO}_3$  to form  $\text{NO}_3^-$  is very sensitive to relative  
602 humidity (RH) and temperature (Fountoukis and Nenes 2007; Dawson et al.,  
603 2007). Low temperature and high RH are favorable for  $\text{NO}_3^-$  formation. Figure  
604 12 shows the seasonal mean horizontal distributions of RH and temperature at  
605 100 hPa and the latitude-altitude cross sections of these two parameters  
606 averaged over 70–105°E. RH exhibits high values in the TP/SASM region,  
607 which are consistent with the high  $\text{H}_2\text{O}$  mixing ratios in this area reported in  
608 Gettelman et al. (2004), M. Park et al. (2004), and Fu et al. (2006). At 100 hPa,  
609 the locations with high RH of exceeding 45% correspond well with those with  
610 high  $\text{C}_{\text{NIT}}$  values (Fig. 10(c)). The latitude-altitude cross section of RH (Fig.  
611 12(c)) shows that RH has high values over the places with intense upward  
612 transport (Fig. 11). For temperature, as Fig. 12(b) and 12(d) show, summertime  
613 temperatures are cold (190–200 K) at 100 hPa in the TP/SASM region,  
614 consistent with the distribution and magnitude reported for August, 2011, in He  
615 et al. (2014) on the basis of the NCEP Reanalysis data. The low temperatures  
616 over the TP/SASM region are associated with the adiabatic expansion of  
617 ascending air mass of the deep convections (Yanai et al., 1992; Park et al.,  
618 2007; He et al., 2014).

619 Because of the favorable conditions of RH and temperature, the  
620 gas-to-aerosol conversion of  $\text{HNO}_3$  to form nitrate can occur during the upward  
621 transport and in the UTLS. Figure 13 shows the mass budget for nitrate  
622 aerosol within the selected box of (70–105°E, 10–40°N, 8–16 km) to see the  
623 role of nitrate formation over the TP/SASM region. The horizontal mass fluxes

624 have a net negative value of  $0.10 \text{ Tg season}^{-1}$ , reducing nitrate aerosol in the  
625 selected box. The vertical transport and the gas-to-aerosol conversion of  
626  $\text{HNO}_3$  increase nitrate mass in the selected box, with values of  $0.09 \text{ Tg}$   
627  $\text{season}^{-1}$  and  $0.11 \text{ Tg season}^{-1}$ , respectively, indicating that the gas-to-aerosol  
628 conversion plays an important role in the enhancement of nitrate in the UTLS  
629 over the TP/SASM region. Although relatively high RH exists near the  
630 tropopause of the TP/SASM region, the air near the tropopause is still dryer  
631 compared to that in the lower altitudes. Model results show that the  
632 gas-to-aerosol partition of  $\text{HNO}_3$  decreases with altitude over 8–16 km,  
633 indicating that the gas to aerosol conversion contributes to nitrate  
634 accumulation in the UTLS mainly during the process of upward transport.

635 Previous studies have also reported that nitric acid trihydrates (NAT,  
636  $\text{HNO}_3 \cdot (\text{H}_2\text{O})_3$ ) could form in the polar and tropical stratosphere at low  
637 temperatures through two mechanisms: (1) the homogeneous nucleation out  
638 of supercooled ternary solutions, and (2) the heterogeneous formation on ice  
639 particles (Hofmann et al., 1989; Carslaw et al., 1998; Voigt et al., 2000; Popp et  
640 al., 2006; Kirner et al., 2011). A typical NAT condensation temperature is  
641 approximate 193 K (Kirner et al., 2011). As shown in Fig. 12, the temperatures  
642 around 100 hPa over the TP/SASM region are in the range of 190–200 K,  
643 which are low enough to produce some NAT particles. However, balloon-borne  
644 measurements of depolarization ratio and backscattering ratio of aerosols at  
645 Lhasa during August-October of 1999 by Kim et al. (2003) and Tobo et al.  
646 (2007) suggested that coarse and aspherical particles such as NAT are scarce  
647 in the UTLS of the TP/SASM.

648

649 **7 Sensitivities of simulated nitrate in the UTLS to anthropogenic NO<sub>x</sub>,**  
650 **NH<sub>3</sub>, and SO<sub>2</sub> emissions in Asia**

651 Since simulated SO<sub>4</sub><sup>2-</sup>, NO<sub>3</sub><sup>-</sup> and NH<sub>4</sub><sup>+</sup> concentrations have, respectively,  
652 NMBs of -17.0%, +38.8%, and +42.0% on an annual mean basis and of  
653 -14.7%, +51.5%, and +74.9% in summer (Section 4.2), we perform four  
654 sensitivity simulations to examine the impacts of uncertainties in surface-layer  
655 aerosol concentrations on simulated nitrate in the UTLS. In the first three  
656 cases, anthropogenic emissions of NO<sub>x</sub>, NH<sub>3</sub>, and SO<sub>2</sub> in Asia are changed by  
657 -50%, -50%, and +20%, respectively, relative to those in our standard  
658 simulation. In the last case, anthropogenic emissions of all these three species  
659 are changed simultaneously, with NO<sub>x</sub> reduced by 50%, NH<sub>3</sub> reduced by 50%,  
660 and SO<sub>2</sub> increased by 20% in Asia relative to the standard case. The purpose  
661 of these sensitivity studies is to reduce NMBs of simulated surface-layer  
662 concentrations of SO<sub>4</sub><sup>2-</sup>, NO<sub>3</sub><sup>-</sup> and NH<sub>4</sub><sup>+</sup> and see whether NO<sub>3</sub><sup>-</sup> is still the  
663 most dominant aerosol species in the UTLS. Model results from these  
664 sensitivity studies for summer of 2005 are presented in Table 3.

665 As anthropogenic emissions of SO<sub>2</sub> in Asia are increased by 20%, the  
666 NMB of simulated surface-layer SO<sub>4</sub><sup>2-</sup> concentrations is -4.4%, which is an  
667 improvement compared to the NMB of -14.7% in the standard simulation.  
668 However, the increases in SO<sub>2</sub> emissions lead to larger NMBs of surface-layer  
669 NO<sub>3</sub><sup>-</sup> and NH<sub>4</sub><sup>+</sup> because of the increased formation of ammonium sulfate or  
670 ammonium bisulfate. The percentage contributions of SO<sub>4</sub><sup>2-</sup> to total aerosol  
671 mass in the UTLS increase slightly by 2.7% at 200 hPa and by 1.6% at 100  
672 hPa, and nitrate in the UTLS also shows small sensitivity to the change in SO<sub>2</sub>  
673 emissions.

674 With anthropogenic emissions of  $\text{NO}_x$  in Asia reduced by 50%, the NMB of  
675 simulated surface-layer  $\text{NO}_3^-$  concentrations changes from +51.5% in the  
676 standard simulation to -11.7% in this sensitivity run. The contribution of each  
677 of  $\text{SO}_4^{2-}$ ,  $\text{NO}_3^-$  and  $\text{NH}_4^+$  aerosols to total aerosol mass in the UTLS is not  
678 sensitive to this reduction in  $\text{NO}_x$  emissions at the surface; the percentage  
679 contribution obtained from this sensitivity run is very close to the value  
680 obtained in the standard simulation (Table 3). Similarly, in the sensitivity study  
681 with  $\text{NH}_3$  emissions reduced by 50% in Asia, simulated surface-layer  
682 concentrations of  $\text{NO}_3^-$  and  $\text{NH}_4^+$  are improved in terms of the values of NMBs,  
683 but the improvement in simulated aerosol concentrations at the surface-layer  
684 does not influence our conclusion of high nitrate aerosol concentration in the  
685 UTLS.

686 As shown in Table 3, for the surface layer, simulated nitrate concentration  
687 over the TP/SASM region decreases by 46.8% with a 50% reduction in  
688 anthropogenic  $\text{NO}_x$  emissions in Asia, and it decreases by 22.3% when  
689 anthropogenic  $\text{NH}_3$  emissions are reduced by the same percentage, indicating  
690 that surface-layer nitrate aerosol is more sensitive to anthropogenic emissions  
691 of  $\text{NO}_x$  than to those of  $\text{NH}_3$ . Relative to the baseline simulation, simulated  
692 nitrate concentrations at 200 hPa and 100 hPa decrease, respectively, by 49.0%  
693 and 17.7% with a 50% reduction in  $\text{NH}_3$  emissions, whereas only by 2.1% and  
694 1.3% with a 50% reduction in  $\text{NO}_x$  emissions. Over the studied region, the role  
695 of  $\text{NH}_3$  in the sulfate-nitrate-ammonium aerosol system can be quantified by  
696 the gas ratio of  $\text{GR} = \frac{\text{free ammonia}}{\text{total nitrate}} = \frac{\text{TA} - 2 \times \text{TS}}{\text{TN}}$  (Ansari and Pandis, 1998), where  
697  $\text{TA} = \text{NH}_3 + \text{NH}_4^+$ ,  $\text{TS} = \text{SO}_4^{2-}$ , and  $\text{TN} = \text{HNO}_3 + \text{NO}_3^-$ . Over the TP/SASM  
698 region, GR is generally positive both at the surface and in the UTLS, especially

699 over 20–40°N where deep convection exits (Fig. 11), indicating that S(VI) is in  
700 from of sulfate and free ammonia is available to react with nitrate (Seinfeld and  
701 Pandis 2006). However, GR is generally less than 1.0 above 400 hPa in  
702 summer over the TP/SASM region, which indicates nitrate concentrations are  
703 most sensitive to changes in NH<sub>3</sub> and explains the small sensitivity of nitrate  
704 aerosol to NO<sub>x</sub> emissions in the UTLS.

705 In the sensitivity study with emissions of NO<sub>x</sub>, NH<sub>3</sub>, and SO<sub>2</sub> in Asia  
706 changed simultaneously, simulated surface-layer concentrations of SO<sub>4</sub><sup>2-</sup>, NO<sub>3</sub><sup>-</sup>  
707 and NH<sub>4</sub><sup>+</sup> have NMBs of -8.3%, -27.0% and +55.4%, respectively, which are  
708 all improved compared to those in the standard simulation. Even though nitrate  
709 aerosol is now underestimated at the surface, it still accounts for 53.3% of the  
710 PM<sub>2.5</sub> concentration at 100 hPa over the TP/SASM region in summer.

711 It should be noted that the concentrations of OC and BC are also  
712 underestimated, with NMBs of -57.2% and -32.2%, respectively, in summer  
713 (Section 4.2). We have done a simple calculation with the concentrations of  
714 OC and BC in the UTLS multiplied by 2.3 and 1.5, respectively, and nitrate is  
715 still the most dominant aerosol species in summertime in the UTLS over the  
716 TP/SASM region (not shown in Table 3). Therefore the uncertainties in surface  
717 aerosol concentrations do not compromise the conclusion of this study.

718

## 719 **8 Conclusions**

720 In this work we simulate nitrate aerosol and its contribution to aerosol  
721 concentrations in the UTLS over the TP/SASM region (70–105°E, 10–40°N)  
722 for summertime of year 2005, using the global chemical transport model  
723 GEOS-Chem driven by the assimilated meteorological fields.

724 Simulated HNO<sub>3</sub> and O<sub>3</sub> are evaluated to show the model's ability to  
725 simulate the NO<sub>x</sub>-O<sub>3</sub>-HNO<sub>3</sub> cycle over the studied region. In the UTLS, both  
726 the horizontal and vertical distributions of simulated HNO<sub>3</sub> and O<sub>3</sub> agree well  
727 with the MLS observations. At 100 hPa, simulated seasonal mean HNO<sub>3</sub> and  
728 O<sub>3</sub> mixing ratios show NMBs of +15.9% and +31.4%, respectively, over the  
729 TP/SASM region (70–105°E, 10–40°N) in summer of year 2005, and the model  
730 biases lie within the confidence range of the MLS instruments. Both simulated  
731 and observed O<sub>3</sub> concentrations show relatively low values of less than 200  
732 ppbv at 100 hPa over the TP/SASM region.

733 Averaged over the TP/SASM region, the surface-layer concentrations of  
734 SO<sub>4</sub><sup>2-</sup>, NO<sub>3</sub><sup>-</sup>, NH<sub>4</sub><sup>+</sup>, BC, and OC are simulated to be 1.70, 0.94, 0.85, 0.30, and  
735 0.94 μg m<sup>-3</sup>, respectively. Nitrate aerosol is simulated to be of secondary  
736 importance near the surface over the region of our interest. Comparisons of  
737 simulated aerosol concentrations with ground-based observations show that  
738 simulated summertime concentrations of SO<sub>4</sub><sup>2-</sup>, NO<sub>3</sub><sup>-</sup>, NH<sub>4</sub><sup>+</sup>, OC and BC have  
739 NMB of -14.7%, +51.5%, +74.9%, -57.2% and -32.2%, respectively. Note that  
740 the measurements of NO<sub>3</sub><sup>-</sup> and NH<sub>4</sub><sup>+</sup> are quite limited in terms of the number  
741 of samples.

742 Model results show elevated concentrations of SO<sub>4</sub><sup>2-</sup>, NO<sub>3</sub><sup>-</sup>, NH<sub>4</sub><sup>+</sup>, OC, BC  
743 and PM<sub>2.5</sub> in the UTLS over the TP/SASM region throughout the summer. NO<sub>3</sub><sup>-</sup>  
744 is simulated to be the most dominant aerosol species in the UTLS of the  
745 TP/SASM region. Accounting for NO<sub>3</sub><sup>-</sup> aerosol, the GEOS-Chem model  
746 reproduces well the magnitude of aerosol extinctions above 10 km, as model  
747 results are compared with the SAGE II measurements. The discrepancies  
748 between the simulated and observed aerosol extinction coefficient are within 8%

749 in the UTLS (averaged over 14–16 km). Simulated vertical profiles of aerosol  
750 extinction coefficients with and without nitrate aerosol show large  
751 discrepancies from 6 km to tropopause, indicating the important role of nitrate  
752 in aerosol layer in the UTLS over the TP/SASM region.

753 The contribution of  $\text{NO}_3^-$  to aerosols in the TP/SASM region is quantified  
754 by  $C_{\text{NIT}}$  (the ratio of nitrate concentration to  $\text{PM}_{2.5}$  concentration). Over the  
755 TP/SASM region, the  $C_{\text{NIT}}$  values in summer are 5–35% at the surface, 25–  
756 50% at 200 hPa, and could exceed 60% at 100 hPa. The mechanisms for the  
757 accumulation of nitrate in the UTLS over the TP/SASM region include vertical  
758 transport and the gas-to-aerosol conversion of  $\text{HNO}_3$  to form nitrate. Such  
759 gas-to-aerosol conversion occurs during the upward transport and in the UTLS.  
760 The high relative humidity and low temperature associated with the deep  
761 convection over the TP/SASM region are favorable for nitrate formation.

762 Results from the present study indicate that nitrate is an important aerosol  
763 species in the UTLS over the ASM/TP region. Considering the scarce  
764 measurements of nitrate in the UTLS and the model uncertainties, more  
765 observational and modeling studies are needed to further explore the aerosol  
766 composition in the Asian tropopause aerosol layer. Further simulations of  
767 nitrate aerosol in the UTLS also need to account for NAT formation at low  
768 temperatures (Kirner et al., 2011) and the roles of natural aerosols, including  
769 the transport of mineral dust and sea salt to the UTLS as well as nitrate  
770 formation on these natural particles (Ma et al., 2003).

771

772

773 *Acknowledgments.* This work was supported by the National Basic Research

774 Program of China (973 program, Grant No. 2014CB441202), the Strategic  
775 Priority Research Program of the Chinese Academy of Sciences (Grant No.  
776 XDA05100503), and the National Natural Science Foundation of China under  
777 grants 41021004, 41475137, and 91544219. We gratefully acknowledge  
778 NASA, USA, for providing the MLS and SAGE II data on their website.

779

## 780 **References**

- 781 [Ansari, A. S., and Pandis, S. N.: Response of Inorganic PM to Precursor](#)  
782 [Concentrations, \*Environ. Sci. Technol.\*, 32\(18\), 2706–2714, 1998.](#)
- 783 [Adhikary, B., Carmichael, G. R., Tang, Y., Leung, L. R., Qian, Y., Schauer, J. J.,](#)  
784 [Stone, E. A., Ramanathan, V., and Ramana, M. V.: Characterization of the](#)  
785 [seasonal cycle of south Asian aerosols: A regional-scale modeling](#)  
786 [analysis, \*J. Geophys. Res.\*, 112, D22S22, doi:10.1029/2006JD008143,](#)  
787 [2007.](#)
- 788 [Alexander, B., Park, R. J., Jacob, D. J., Li, Q., Yantosca, R. M., Savarino, J.,](#)  
789 [Lee, C., and Thiemens, M.: Sulfate formation in sea-salt aerosols:](#)  
790 [Constraints from oxygen isotopes, \*J. Geophys. Res.\*, 110, D10307,](#)  
791 [doi:10.1029/2004JD005659, 2005.](#)
- 792 [Arimoto, R., Duce, R., Savoie, D., Prospero, J., Talbot, R., Cullen, J., Tomza,](#)  
793 [U., Lewis, N., and Ray, B.: Relationships among aerosol constituents from](#)  
794 [Asia and the North Pacific during PEM–West A, \*J. Geophys. Res.\*, 101,](#)  
795 [2011–2023, 1996.](#)
- 796 [Babu, S. S. and Moorthy, K. K.: Aerosol black carbon over a tropical coastal](#)  
797 [station in India, \*Geophys. Res. Lett.\*, 29, 2098,](#)  
798 [doi:10.1029/2002GL015662, 2002.](#)
- 799 [Bano, T., Singh, S., Gupta, N., Soni, K., Tanwar, R., Nath, S., Arya, B., and](#)  
800 [Gera, B.: Variation in aerosol black carbon concentration and its emission](#)  
801 [estimates at the mega-city Delhi, \*Int. J. Remote Sens.\*, 32, 6749–6764,](#)  
802 [2011.](#)
- 803 [Bian, J., Yan, R., and Chen, H.: Tropospheric Pollutant Transport to the](#)  
804 [Stratosphere by Asian Summer Monsoon, \*Chinese Journal of\*](#)  
805 [Atmospheric Sciences, 35, 897–902, 2011a.](#)
- 806 [Bian, J., Yan, R., Chen, H., Lü, D., and MASSIE, S. T.: Formation of the](#)  
807 [Summertime Ozone Valley over the Tibetan Plateau: The Asian Summer](#)  
808 [Monsoon and Air Column Variations, \*Adv. Atmos. Sci.\*, 28, 1318–1325,](#)  
809 [2011b.](#)
- 810 [Bian, J., Pan, L. L., Paulik, L., Vömel, H., Chen, H., and Lü, D.: In situ water](#)  
811 [vapor and ozone measurements in Lhasa and Kunming during the Asian](#)  
812 [summer monsoon, \*Geophys. Res. Lett.\*, 39, L19808,](#)  
813 [doi:10.1029/2012GL052996, 2012.](#)
- 814 [Bourgeois, Q., Bey, I., and Stier, P.: A permanent aerosol layer at the tropical](#)  
815 [tropopause layer driven by the intertropical convergence zone, \*Atmos.\*](#)  
816 [Chem. Phys. Discuss.](#), 12, 2863–2889, 2012.

817 Bouwman, A., Lee, D., Asman, W., Dentener, F., Van Der Hoek, K., and Olivier,  
818 J.: A global high-resolution emission inventory for ammonia, *Global*  
819 *Biogeochem. Cy.*, 11, 561-587, 1997.

820 Brewer, A. W.: Evidence for a world circulation provided by the measurements  
821 of helium and water vapour distribution in the stratosphere, *Q. J. Roy.*  
822 *Meteor. Soc.*, 75, 351-363, 1949.

823 Carrico, C. M., Bergin, M. H., Shrestha, A. B., Dibb, J. E., Gomes, L., and  
824 Harris, J. M.: The importance of carbon and mineral dust to seasonal  
825 aerosol properties in the Nepal Himalaya, *Atmos. Environ.*, 37, 2811–2824,  
826 2003.

827 Carslaw, K., Wirth, M., Tsiaras, A., Luo, B., Dörnbrack, A., Leutbecher, M.,  
828 Volkert, H., Renger, W., Bacmeister, J., and Peter, T.: Particle  
829 microphysics and chemistry in remotely observed mountain polar  
830 stratospheric clouds, *J. Geophys. Res.*, 103, 5785–5796, 1998.

831 Chatterjee, A., Adak, A., Singh, A. K., Srivastava, M. K., Ghosh, S. K., Tiwari,  
832 S., Devara, P. C., and Raha, S.: Aerosol chemistry over a high altitude  
833 station at northeastern Himalayas, India, *PloS one*, 5, e11122,  
834 doi:10.1371/journal.pone.0011122, 2010.

835 Chatterjee, A., Ghosh, S. K., Adak, A., Singh, A. K., Devara, P. C., and Raha,  
836 S.: Effect of Dust and Anthropogenic Aerosols on Columnar Aerosol  
837 Optical Properties over Darjeeling (2200 m asl), Eastern Himalayas, India,  
838 *PloS one*, 7, e40286, doi:10.1371/journal.pone.0040286, 2012.

839 Chen, H., Bian, J., and Lü, D.: Advances and prospects in the study of  
840 stratosphere-troposphere exchange, *Chinese J. Atmos. Sci.*, 30, 813–820,  
841 doi:1006-9895(2006)30:5<813:SDLCXP>2.0.TX;2-A, 2006.

842 Chin, M., Ginoux, P., Kinne, S., Torres, O., Holben, B., Duncan, B. N., Martin,  
843 R. V., Logan, J. A., Higurashi, A., and Nakajima, T.: Tropospheric aerosol  
844 optical thickness from the GOCART model and comparisons with satellite  
845 and sunphotometer measurements, *J. Atmos. Sci.*, 59, 461–483, 2002.

846 Chowdhury, Z., Zheng, M., Schauer, J. J., Sheesley, R. J., Salmon, L. G., Cass,  
847 G. R., and Russell, A. G.: Speciation of ambient fine organic carbon  
848 particles and source apportionment of PM<sub>2.5</sub> in Indian cities, *J. Geophys.*  
849 *Res.*, 112, D15303, doi:10.1029/2007JD008386, 2007.

850 Chu, W., McCormick, M., Lenoble, J., Brogniez, C., and Pruvost, P.: SAGE II  
851 inversion algorithm, *J. Geophys. Res.*, 94, 8339–8351, 1989.

852 Chung, S. H., and Seinfeld, J. H.: Global distribution and climate forcing of  
853 carbonaceous aerosols, *J. Geophys. Res.*, 107(D19), 4407,  
854 doi:10.1029/2001JD001397, 2002.

855 Collins, W. J., Stevenson, D. S., Johnson, C. E., and Derwent, R. G.: The  
856 European regional ozone distribution and its links with the global scale for  
857 the years 1992 and 2015, *Atmos. Environ.*, 34, 255–267, 2000.

858 Considine, D. B., Rosenfield, J. E., and Fleming, E. L.: An interactive model  
859 study of the influence of the Mount Pinatubo aerosol on stratospheric  
860 methane and water trends, *J. Geophys. Res.*, 106, 27711-27727,  
861 doi:10.1029/2001jd000331, 2001.

862 Considine, D. B., Logan, J. A., and Olsen, M. A.: Evaluation of  
863 near-tropopause ozone distributions in the Global Modeling Initiative  
864 combined stratosphere/troposphere model with ozonesonde data, *Atmos.*  
865 *Chem. Phys.*, 8, 2365–2385, 2008.

866 Cooke, W. F., Liousse, C., Cachier, H., and Feichter, J.: Construction of a 1°x1°

867 fossil fuel emission data set for carbonaceous aerosol and implementation  
868 and radiative impact in the ECHAM-4 model, *J. Geophys. Res.*, 104,  
869 22,137–22,162, 1999.

870 Datta, A., Sharma, S., Harit, R., Kumar, V., Mandal, T., and Pathak, H.:  
871 Ammonia emission from subtropical crop land area in India, *Asia-Pac. J.*  
872 *Atmos. Sci.*, 48, 275–281, 2012.

873 Dawson, J., Adams, P., and Pandis, S.: Sensitivity of PM<sub>2.5</sub> to climate in the  
874 Eastern US: a modeling case study, *Atmos. Chem. and phys.*, 7,  
875 4295–4309, 2007.

876 Decesari, S., Facchini, M., Carbone, C., Giulianelli, L., Rinaldi, M., Finessi, E.,  
877 Fuzzi, S., Marinoni, A., Cristofanelli, P., and Duchi, R.: Chemical  
878 composition of PM<sub>10</sub> and PM<sub>1</sub> at the highaltitude Himalayan station Nepal  
879 Climate Observatory-Pyramid (NCO-P)(5079 m asl), *Atmos. Chem. Phys.*,  
880 10, 4583–4596, 2010.

881 Dobson, G. M. B.: Origin and distribution of the polyatomic molecules in the  
882 atmosphere, *Proceedings of the Royal Society of London. Series A,*  
883 *Mathematical and Physical Sciences*, 187–193, 1956.

884 Drury, E., Jacob, D. J., Spurr, R. J., Wang, J., Shinozuka, Y., Anderson, B. E.,  
885 Clarke, A. D., Dibb, J., McNaughton, C., and Weber, R.: Synthesis of  
886 satellite (MODIS), aircraft (ICARTT), and surface (IMPROVE, EPA–AQS,  
887 AERONET) aerosol observations over eastern North America to improve  
888 MODIS aerosol retrievals and constrain surface aerosol concentrations  
889 and sources, *J. Geophys. Res.*, 115, D14204, doi:10.1029/2009JD012629,  
890 2010.

891 Duncan, B., Strahan, S., Yoshida, Y., Steenrod, S., and Livesey, N.: Model  
892 study of the cross-tropopause transport of biomass burning pollution,  
893 *Atmos. Chem. Phys.*, 7, 3713–3736, 2007.

894 Dutkiewicz, V. A., Alvi, S., Ghauri, B. M., Choudhary, M. I., and Husain, L.:  
895 Black carbon aerosols in urban air in South Asia, *Atmos. Environ.*, 43,  
896 1737–1744, 2009.

897 Evans, M., and Jacob, D. J.: Impact of new laboratory studies of N<sub>2</sub>O<sub>5</sub>  
898 hydrolysis on global model budgets of tropospheric nitrogen oxides, ozone,  
899 and OH, *Geophys. Res. Lett.*, 32, 10 L09813, doi:10.1029/2005GL022469,  
900 2005.

901 Fadnavis, S., Semeniuk, K., Pozzoli, L., Schultz, M., Ghude, S., Das, S., and  
902 Kakatkar, R.: Transport of aerosols into the UTLS and their impact on the  
903 Asian monsoon region as seen in a global model simulation, *Atmos. Chem.*  
904 *Phys.*, 13, 8771–8786, 2013.

905 Fadnavis, S., Semeniuk, K., Schultz, M., Mahajan, A., Pozzoli, L., Sonbawane,  
906 S., and Kiefer, M.: Transport pathways of peroxyacetyl nitrate in the upper  
907 troposphere and lower stratosphere from different monsoon systems  
908 during the summer monsoon season, *Atmos. Chem. Phys. Discuss.*, 14,  
909 20159–20195, 2014.

910 Fairlie, T. D., Jacob, D. J., and Park, R. J.: The impact of transpacific transport  
911 of mineral dust in the United States, *Atmos. Environ.*, 41, 1251–1266,  
912 2007.

913 Fisher, J. A., Jacob, D. J., Wang, Q., Bahreini, R., Carouge, C. C., Cubison, M.  
914 J., Dibb, J. E., Diehl, T., Jimenez, J. L., and Leibensperger, E. M.: Sources,  
915 distribution, and acidity of sulfate–ammonium aerosol in the Arctic in  
916 winter–spring, *Atmos. Environ.*, 45, 7301–7318, 2011.

917 Fountoukis, C., and Nenes, A.: ISORROPIA II: a computationally efficient  
918 thermodynamic equilibrium model for  
919  $K^+$ - $Ca^{2+}$ - $Mg^{2+}$ - $NH_4^+$ - $Na^+$ - $SO_4^{2-}$ - $NO_3^-$ - $Cl^-$ - $H_2O$  aerosols, *Atmos. Chem.*  
920 *Phys.*, 7, 4639–4659, 2007.

921 Froyd, K., Murphy, D., Sanford, T., Thomson, D., Wilson, J., Pfister, L., and Lait,  
922 L.: Aerosol composition of the tropical upper troposphere, *Atmos. Chem.*  
923 *Phys.*, 9, 4363–4385, 2009.

924 Fu, R., Hu, Y., Wright, J. S., Jiang, J. H., Dickinson, R. E., Chen, M., Filipiak,  
925 M., Read, W. G., Waters, J. W., and Wu, D. L.: Short circuit of water vapor  
926 and polluted air to the global stratosphere by convective transport over the  
927 Tibetan Plateau, *P. Natl. A. Sci.*, 103, 5664–5669, 2006.

928 Fu, T. -M., Cao, J., Zhang, X., Lee, S., Zhang, Q., Han, Y., Qu, W., Han, Z.,  
929 Zhang, R., and Wang, Y.: Carbonaceous aerosols in China: top-down  
930 constraints on primary sources and estimation of secondary contribution,  
931 *Atmos. Chem. Phys.*, 12, 2725–2746, 2012.

932 Ganguly, D., Jayaraman, A., and Gadhavi, H.: Physical and optical properties  
933 of aerosols over an urban location in western India: Seasonal variabilities,  
934 *J. Geophys. Res.*, 111, D24206, doi:10.1029/2006JD007392, 2006.

935 George, S. K., and Nair, P. R.: Aerosol mass loading over the marine  
936 environment of Arabian Sea during ICARB: Sea-salt and non-sea-salt  
937 components, *J. Earth Syst. Sci.*, 117, 333–344, 2008.

938 George, S. K., Nair, P. R., Parameswaran, K., Jacob, S., and Abraham, A.:  
939 Seasonal trends in chemical composition of aerosols at a tropical coastal  
940 site of India, *J. Geophys. Res.*, 113, D16209, doi:10.1029/2007JD009507,  
941 2008.

942 Gettelman, A., Kinnison, D. E., Dunkerton, T. J., and Brasseur, G. P.: Impact of  
943 monsoon circulations on the upper troposphere and lower stratosphere, *J.*  
944 *Geophys. Res.*, 109, D22101, doi:10.1029/2004JD004878, 2004.

945 Guenther, A., Karl, T., Harley, P., Wiedinmyer, C., Palmer, P., and Geron, C.:  
946 Estimates of global terrestrial isoprene emissions using MEGAN (Model of  
947 Emissions of Gases and Aerosols from Nature), *Atmos. Chem. Phys.*  
948 *Discuss.*, 6, 107–173, 2006.

949 Hack, J. J.: Parameterization of moist convection in the National Center for  
950 Atmospheric Research community climate model (CCM2), *J. Geophys.*  
951 *Res.*, 99, 5551–5568, doi:10.1029/93jd03478, 1994.

952 He, Q., Li, C., Ma, J., Wang, H., Yan, X., Liang, Z., and Qi, G.: Enhancement of  
953 aerosols in UTLS over the Tibetan Plateau induced by deep convection  
954 during the Asian summer monsoon, *Atmos. Chem. Phys. Discuss.*, 14,  
955 3169–3191, 10.5194/acpd-14-3169-2014, 2014.

956 Hegde, P., Sudheer, A., Sarin, M., and Manjunatha, B.: Chemical  
957 characteristics of atmospheric aerosols over southwest coast of India,  
958 *Atmos. Environ.*, 41, 7751–7766, 2007.

959 Hofmann, D., Rosen, J., Harder, J., and Hereford, J.: Balloon-borne  
960 measurements of aerosol, condensation nuclei, and cloud particles in the  
961 stratosphere at McMurdo Station, Antarctica, during the spring of 1987, *J.*  
962 *Geophys. Res.*, 94, 11253–11269, doi:10.1029/JD094iD09p11253, 1989.

963 Huang, C., Chen, C. H., Li, L., Cheng, Z., Wang, H. L., Huang, H. Y., Streets, D.  
964 G., and Wang, Y. J.: Emission inventory of anthropogenic air pollutants  
965 and VOC species in the Yangtze River Delta region, China, *Atmos. Chem.*  
966 *Phys.*, 11, 4105–4120, 2011.

967 Huang, X., Song, Y., Li, M., Li, J., Huo, Q., Cai, X., Zhu, T., Hu, M., and Zhang,  
968 H.: A high-resolution ammonia emission inventory in China, *Global*  
969 *Biogeochem. Cy.*, 26, GB1030, doi:10.1029/2011GB004161, 2012.

970 Husain, L., Dutkiewicz, V. A., Khan, A., and Ghauri, B. M.: Characterization of  
971 carbonaceous aerosols in urban air, *Atmos. Environ.*, 41, 6872–6883,  
972 2007.

973 Jacob, D. J.: Heterogeneous chemistry and tropospheric ozone, *Atmos.*  
974 *Environ.*, 34, 2131-2159, 2000.

975 Jaeglé, L., Quinn, P., Bates, T., Alexander, B., and Lin, J.-T.: Global distribution  
976 of sea salt aerosols: new constraints from in situ and remote sensing  
977 observations, *Atmos. Chem. Phys.*, 11, 3137–3157, 2011.

978 Jayaraman, A., Gadhavi, H., Ganguly, D., Misra, A., Ramachandran, S., and  
979 Rajesh, T.: Spatial variations in aerosol characteristics and regional  
980 radiative forcing over India: Measurements and modeling of 2004 road  
981 campaign experiment, *Atmos. Environ.*, 40, 6504–6515, 2006.

982 Jeong, J. I., and Park, R. J.: Effects of the meteorological variability on regional  
983 air quality in East Asia, *Atmos. Environ.*, 69, 46–55, 2013.

984 Jiang, H., Liao, H., Pye, H., Wu, S., Mickley, L. J., Seinfeld, J. H., and Zhang,  
985 X.: Projected effect of 2000-2050 changes in climate and emissions on  
986 aerosol levels in China and associated transboundary transport, *Atmos.*  
987 *Chem. Phys.*, 13, 7937–7960, 2013.

988 Kar, J., Bremer, H., Drummond, J. R., Rochon, Y. J., Jones, D., Nichitiu, F., Zou,  
989 J., Liu, J., Gille, J. C., and Edwards, D. P.: Evidence of vertical transport of  
990 carbon monoxide from Measurements of Pollution in the Troposphere  
991 (MOPITT), *Geophys. Res. Lett.*, 31, L23105, doi:10.1029/2004GL021128,  
992 2004.

993 Kim, J., Song, C. H., Ghim, Y., Won, J., Yoon, S., Carmichael, G., and Woo, J.  
994 H.: An investigation on NH<sub>3</sub> emissions and particulate NH<sub>4</sub><sup>+</sup> – NO<sub>3</sub><sup>-</sup>  
995 formation in East Asia, *Atmos. Environ.*, 40, 2139–2150, 2006.

996 Kim, Y.- S., Shibata, T., Iwasaka, Y., Shi, G., Zhou, X., Tamura, K., and Ohashi,  
997 T.: Enhancement of aerosols near the cold tropopause in summer over  
998 Tibetan Plateau: lidar and balloonborne measurements in 1999 at Lhasa,  
999 Tibet, China, in: *Lidar Remote Sensing for Industry and Environment*  
1000 *Monitoring III*, edited by: Singh U. N., Itabe, T., and Liu, Z., *Proceedings of*  
1001 *SPIE*, Hangzhou, China, 4893, 496–503, 2003.

1002 Kirner, O., Ruhnke, R., Buchholz-Dietsch, J., Jöckel, P., Brühl, C., and Steil, B.:  
1003 Simulation of polar stratospheric clouds in the chemistry-climate-model  
1004 EMAC via the submodel PSC, *Geoscientific Model Development*, 4,  
1005 169–182, 2011.

1006 Kulkarni, P., and Ramachandran, S.: Comparison of aerosol extinction  
1007 between lidar and SAGE II over Gadanki, a tropical station in India, *Ann.*  
1008 *Geophys.*, 2015, 351–362,

1009 Kulshrestha, U., Saxena, A., Kumar, N., Kumari, K., and Srivastava, S.:  
1010 Chemical composition and association of size-differentiated aerosols at a  
1011 suburban site in a semi-arid tract of India, *J. Atmos. Chem.*, 29, 109–118,  
1012 1998.

1013 Latha, K. M., and Badarinath, K.: Seasonal variations of black carbon aerosols  
1014 and total aerosol mass concentrations over urban environment in India,  
1015 *Atmos. Environ.*, 39, 4129–4141, 2005.

1016 Lau, K. M., Kim, M. K., and Kim, K. M.: Asian summer monsoon anomalies

1017 induced by aerosol direct forcing: the role of the Tibetan Plateau, *Clim.*  
 1018 *Dyn.*, 26, 855–864, doi:10.1007/s00382-006-0114-z, 2006.  
 1019 Lawrence, M. G., and Lelieveld, J.: Atmospheric pollutant outflow from  
 1020 southern Asia: a review, *Atmos. Chem. Phys.*, 10, 11017-11096,  
 1021 doi:10.5194/acp-10-11017-2010, 2010.  
 1022 Lelieveld, J., Crutzen, P. J., Ramanathan, V., Andreae, M. O., Brenninkmeijer,  
 1023 C. A. M., Campos, T., Cass, G. R., Dickerson, R. R., Fischer, H., de Gouw,  
 1024 J. A., Hansel, A., Jefferson, A., Kley, D., de Laat, A. T. J., Lal, S., Lawrence,  
 1025 M. G., Lobert, J. M., Mayol-Bracero, O. L., Mitra, A. P., Novakov, T.,  
 1026 Oltmans, S. J., Prather, K. A., Reiner, T., Rodhe, H., Scheeren, H. A.,  
 1027 Sikka, D., and Williams, J.: The Indian Ocean Experiment: Widespread air  
 1028 pollution from South and Southeast Asia, *Science*, 291, 1031–1036,  
 1029 doi:10.1126/science.1057103, 2001.  
 1030 Leon, J.-F., Chazette, P., Dulac, F., Pelon, J., Flamant, C., Bonazzola, M.,  
 1031 Foret, G., Alfaro, S., Cachier, H., and Cautenet, S.: Large-scale advection  
 1032 of continental aerosols during INDOEX, *J. Geophys. Res.*, 106,  
 1033 28427–28428, 28439, 2001.  
 1034 Li, Q., Jiang, J. H., Wu, D. L., Read, W. G., Livesey, N. J., Waters, J. W., Zhang,  
 1035 Y., Wang, B., Filipiak, M. J., and Davis, C. P.: Convective outflow of South  
 1036 Asian pollution: A global CTM simulation compared with EOS MLS  
 1037 observations, *Geophys. Res. Lett.*, 32, L14826,  
 1038 doi:10.1029/2005GL022762, 2005.  
 1039 Liao, H., Adams, P. J., Chung, S. H., Seinfeld, J. H., Mickley, L. J., and Jacob,  
 1040 D. J.: Interactions between tropospheric chemistry and aerosols in a  
 1041 unified general circulation model, *J. Geophys. Res.*, 108, 4001,  
 1042 doi:10.1029/2001JD001260, 2003.  
 1043 Liao, H., and Seinfeld, J. H.: Global impacts of gas-phase chemistry-aerosol  
 1044 interactions on direct radiative forcing by anthropogenic aerosols and  
 1045 ozone, *J. Geophys. Res.*, 110, D18208, doi:10.1029/2005JD005907,  
 1046 2005.  
 1047 Liao, H., Zhang, Y., Chen, W.-T., Raes, F., and Seinfeld, J. H.: Effect of  
 1048 chemistry-aerosol-climate coupling on predictions of future climate and  
 1049 future levels of tropospheric ozone and aerosols, *J. Geophys. Res.*, 114,  
 1050 D10306, doi:10.1029/2008JD010984, 2009.  
 1051 Liu, H., Jacob, D. J., Bey, I., and Yantosca, R. M.: Constraints from <sup>210</sup>Pb and  
 1052 <sup>7</sup>Be on wet deposition and transport in a global three-dimensional  
 1053 chemical tracer model driven by assimilated meteorological fields, *J.*  
 1054 *Geophys. Res.*, 106, 12109–12128, 2001.  
 1055 Liu, X., Penner, J. E., and Wang, M.: Influence of anthropogenic sulfate and  
 1056 black carbon on upper tropospheric clouds in the NCAR CAM3 model  
 1057 coupled to the IMPACT global aerosol model, *J. Geophys. Res.*, 114,  
 1058 D03204, doi:10.1029/2008JD010492, 2009.  
 1059 Livesey, N. J., Filipiak, M. J., Froidevaux, L., Read, W. G., Lambert, A., Santee,  
 1060 M. L., Jiang, J. H., Pumphrey, H. C., Waters, J. W., and Cofield, R. E.:  
 1061 Validation of Aura Microwave Limb Sounder O<sub>3</sub> and CO observations in  
 1062 the upper troposphere and lower stratosphere, *J. Geophys. Res.*, 113,  
 1063 D15S02, doi:10.1029/2007JD008805, 2008.  
 1064 Livesey, N. J., Read, W. G., Wagner, P. A., Froidevaux, L., Lambert, A.,  
 1065 Manney, G. L., Pumphrey, H. C., Santee, M. L., Schwartz, M. J., Wang, S.,  
 1066 Cofield, R. E., Cuddy, D. T., Fuller, R. A., Jarnot, R. F., Jiang, J. H., and

1067 Knosp, B. W.: Version 3.3 Level 2 data quality and description document,  
1068 JPL D-33509, 2011.

1069 Lodhi, A., Ghauri, B., Khan, M. R., Rahman, S., and Shafique, S.: Particulate  
1070 matter (PM<sub>2.5</sub>) concentration and source apportionment in Lahore, J.  
1071 Brazil. Chem. Soc., 20, 1811–1820, 2009.

1072 Lou, S., Liao, H., and Zhu, B.: Impacts of aerosols on surface-layer ozone  
1073 concentrations in China through heterogeneous reactions and changes in  
1074 photolysis rates, Atmos. Environ., 85, 123–138, 2014.

1075 Ma, J., Tang, J., Li, S.-M., and Jacobson, M. Z.: Size distributions of ionic  
1076 aerosols measured at Waliguan Observatory: Implication for nitrate  
1077 gas-to-particle transfer processes in the free troposphere, J. Geophys.  
1078 Res., 108, 4541, doi:10.1029/2002jd003356, 2003.

1079 Martin, R. V., Jacob, D. J., Yantosca, R. M., Chin, M., and Ginoux, P.: Global  
1080 and regional decreases in tropospheric oxidants from photochemical  
1081 effects of aerosols, J. Geophys. Res., 108, 4097,  
1082 doi:10.1029/2002JD002622, 2003.

1083 McCormick, M. P.: SAGE II: an overview, Adv. Space Res., 7, 219-226, 1987.

1084 McLinden, C., Olsen, S., Hannegan, B., Wild, O., Prather, M., and Sundet, J.:  
1085 Stratospheric ozone in 3-D models: A simple chemistry and the  
1086 cross-tropopause flux, J. Geophys. Res., 105, 14653–14665,  
1087 doi:10.1029/2000JD900124, 2000.

1088 Mickley, L. J., Murti, P., Jacob, D. J., Logan, J. A., Koch, D., and Rind, D.:  
1089 Radiative forcing from tropospheric ozone calculated with a unified  
1090 chemistry-climate model, J. Geophys. Res., 104, 30153-30172, 1999.

1091 Ming, J., Zhang, D., Kang, S., and Tian, W.: Aerosol and fresh snow chemistry  
1092 in the East Rongbuk Glacier on the northern slope of Mt. Qomolangma  
1093 (Everest), J. Geophys. Res., 112, D15307, doi:10.1029/2007JD008618,  
1094 2007.

1095 Momin, G. A., Rao, P. S. P., Safai, P. D., Ali, K., Naik, M. S., and Pillai, A. G.:  
1096 Atmospheric aerosol characteristic studies at Pune and  
1097 Thiruvananthapuram during INDOEX programme–1998, Curr. Sci., 76,  
1098 985-989, 1999.

1099 Mu, Q., and Liao, H.: Simulation of the interannual variations of aerosols in  
1100 China: role of variations in meteorological parameters, Atmos. Chem.  
1101 Phys., 14, 9597–9612, 2014.

1102 Murray, L. T., Jacob, D. J., Logan, J. A., Hudman, R. C., and Koshak, W. J.:  
1103 Optimized regional and interannual variability of lightning in a global  
1104 chemical transport model constrained by LIS/OTD satellite data, J.  
1105 Geophys. Res., 117, D20307, doi:10.1029/2012JD017934, 2012.

1106 Nair, P. R., George, S. K., Sunilkumar, S., Parameswaran, K., Jacob, S., and  
1107 Abraham, A.: Chemical composition of aerosols over peninsular India  
1108 during winter, Atmos. Environ., 40, 6477–6493, 2006.

1109 Nair, V. S., Solmon, F., Giorgi, F., Mariotti, L., Babu, S. S., and Moorthy, K. K.:  
1110 Simulation of South Asian aerosols for regional climate studies, J.  
1111 Geophys. Res., 117, D04209, doi:10.1029/2011JD016711, 2012.

1112 Nakamura, T., Matsumoto, K., and Uematsu, M.: Chemical characteristics of  
1113 aerosols transported from Asia to the East China Sea: an evaluation of  
1114 anthropogenic combined nitrogen deposition in autumn, Atmos. Environ.,  
1115 39, 1749–1758, 2005.

1116 Oberbeck, V. R., Livingston, J. M., Russell, P. B., Pueschel, R. F., Rosen, J. N.,

1117 Osborn, M. T., Kritz, M. A., Snetsinger, K. G., and Ferry, G. V.: SAGE II  
1118 aerosol validation: Selected altitude measurements, including particle  
1119 micrometeorological measurements, *J. Geophys. Res.*, 94, 8367–8380,  
1120 doi:10.1029/JD094iD06p08367, 1989.

1121 Pant, P., Hegde, P., Dumka, U., Sagar, R., Satheesh, S., Moorthy, K. K., Saha,  
1122 A., and Srivastava, M.: Aerosol characteristics at a high-altitude location in  
1123 central Himalayas: Optical properties and radiative forcing, *J. Geophys.  
1124 Res.*, 111, D17206, doi:10.1029/2005JD006768, 2006.

1125 Park, M., Randel, W. J., Kinnison, D. E., Garcia, R. R., and Choi, W.: Seasonal  
1126 variation of methane, water vapor, and nitrogen oxides near the  
1127 tropopause: Satellite observations and model simulations, *J. Geophys.  
1128 Res.*, 109, D03302, doi:10.1029/2003JD003706, 2004.

1129 Park, M., Randel, W. J., Gettelman, A., Massie, S. T., and Jiang, J. H.:  
1130 Transport above the Asian summer monsoon anticyclone inferred from  
1131 Aura Microwave Limb Sounder tracers, *J. Geophys. Res.*, 112, D16309,  
1132 doi:10.1029/2006JD008294, 2007.

1133 Park, M., Randel, W. J., Emmons, L. K., Bernath, P. F., Walker, K. A., and  
1134 Boone, C. D.: Chemical isolation in the Asian monsoon anticyclone  
1135 observed in Atmospheric Chemistry Experiment (ACE–FTS) data, *Atmos.  
1136 Chem. Phys.*, 8, 757–764, 2008.

1137 Park, M., Randel, W. J., Emmons, L. K., and Livesey, N. J.: Transport  
1138 pathways of carbon monoxide in the Asian summer monsoon diagnosed  
1139 from Model of Ozone and Related Tracers (MOZART), *J. Geophys. Res.*,  
1140 114, D08303, doi:10.1029/2008JD010621, 2009.

1141 Park, R. J., Jacob, D. J., Chin, M., and Martin, R. V.: Sources of carbonaceous  
1142 aerosols over the United States and implications for natural visibility, *J.  
1143 Geophys. Res.*, 108, 4355, doi:10.1029/2002JD003190, 2003.

1144 Park, R. J., Jacob, D. J., Field, B. D., Yantosca, R. M., and Chin, M.: Natural  
1145 and transboundary pollution influences on sulfate–nitrate–ammonium  
1146 aerosols in the United States: Implications for policy, *J. Geophys. Res.*,  
1147 109, D15204, doi:10.1029/2003JD004473, 2004.

1148 Pitari, G., Aquila, V., Kravitz, B., Robock, A., Watanabe, S., Cionni, I., Luca, N.  
1149 D., Genova, G. D., Mancini, E., and Tilmes, S.: Stratospheric ozone  
1150 response to sulfate geoengineering: Results from the Geoengineering  
1151 Model Intercomparison Project (GeoMIP), *J. Geophys. Res.*, 119,  
1152 2629–2653, doi: 10.1002/2013JD020566, 2014.

1153 Popp, P., Marcy, T., Jensen, E., Kärcher, B., Fahey, D., Gao, R., Thompson, T.,  
1154 Rosenlof, K., Richard, E., and Herman, R.: The observation of nitric  
1155 acid-containing particles in the tropical lower stratosphere, *Atmos. Chem.  
1156 Phys.*, 6, 601–611, 2006.

1157 Pye, H., Liao, H., Wu, S., Mickley, L. J., Jacob, D. J., Henze, D. K., and  
1158 Seinfeld, J.: Effect of changes in climate and emissions on future  
1159 sulfate–nitrate–ammonium aerosol levels in the United States, *J. Geophys.  
1160 Res.*, 114, D01205, doi:10.1029/2008JD010701, 2009.

1161 Qie, X., Wu, X., Yuan, T., Bian, J., and Lü, D.: Comprehensive Pattern of Deep  
1162 Convective Systems over the Tibetan Plateau–South Asian Monsoon  
1163 Region Based on TRMM Data, *J. Clim.*, 27, 6612–6626, 2014.

1164 Ram, K., Sarin, M., and Hegde, P.: Atmospheric abundances of primary and  
1165 secondary carbonaceous species at two high-altitude sites in India:  
1166 Sources and temporal variability, *Atmos. Environ.*, 42, 6785–6796, 2008.

- 1167 Ramanathan, V., Li, F., Ramana, M., Praveen, P., Kim, D., Corrigan, C.,  
 1168 Nguyen, H., Stone, E. A., Schauer, J. J., and Carmichael, G.: Atmospheric  
 1169 brown clouds: Hemispherical and regional variations in long-range  
 1170 transport, absorption, and radiative forcing, *J. Geophys. Res.*, 112,  
 1171 D22S21, doi:10.1029/2006JD008124, 2007.
- 1172 Randel, W. J., and Park, M.: Deep convective influence on the Asian summer  
 1173 monsoon anticyclone and associated tracer variability observed with  
 1174 Atmospheric Infrared Sounder (AIRS), *J. Geophys. Res.*, 111, D12314,  
 1175 doi:10.1029/2005JD006490, 2006.
- 1176 Randel, W. J., Park, M., Emmons, L., Kinnison, D., Bernath, P., Walker, K. A.,  
 1177 Boone, C., and Pumphrey, H.: Asian monsoon transport of pollution to the  
 1178 stratosphere, *Science*, 328, 611–613, 2010.
- 1179 Rasch, P. J., Tilmes, S., Turco, R. P., Robock, A., Oman, L., Chen, C. C.,  
 1180 Stenchikov, G. L., and Garcia, R. R.: An overview of geoengineering of  
 1181 climate using stratospheric sulphate aerosols, *Philos. Trans. R. Soc.*  
 1182 *A-Math. Phys. Eng. Sci.*, 366, 4007-4037, doi:10.1098/rsta.2008.0131,  
 1183 2008.
- 1184 Rastogi, N., and Sarin, M.: Long-term characterization of ionic species in  
 1185 aerosols from urban and high-altitude sites in western India: Role of  
 1186 mineral dust and anthropogenic sources, *Atmos. Environ.*, 39, 5541–5554,  
 1187 2005.
- 1188 Rastogi, N., and Sarin, M.: Quantitative chemical composition and  
 1189 characteristics of aerosols over western India: one-year record of  
 1190 temporal variability, *Atmos. Environ.*, 43, 3481–3488, 2009.
- 1191 Rengarajan, R., Sarin, M., and Sudheer, A.: Carbonaceous and inorganic  
 1192 species in atmospheric aerosols during wintertime over urban and  
 1193 high-altitude sites in North India, *J. Geophys. Res.*, 112, D21307,  
 1194 doi:10.1029/2006JD008150, 2007.
- 1195 Russell, P. B., and McCormick, M. P.: SAGE II aerosol data validation and initial  
 1196 data use: An introduction and overview, *J. Geophys. Res.*, 94, 8335–8338,  
 1197 1989.
- 1198 Safai, P., Kewat, S., Praveen, P., Rao, P., Momin, G., Ali, K., and Devara, P.:  
 1199 Seasonal variation of black carbon aerosols over a tropical urban city of  
 1200 Pune, India, *Atmos. Environ.*, 41, 2699–2709, 2007.
- 1201 Salam, A., Bauer, H., Kassin, K., Mohammad Ullah, S., and Puxbaum, H.:  
 1202 Aerosol chemical characteristics of a mega-city in Southeast Asia  
 1203 (Dhaka–Bangladesh), *Atmos. Environ.*, 37, 2517–2528, 2003.
- 1204 Santee, M., Lambert, A., Read, W., Livesey, N., Cofield, R., Cuddy, D., Daffer,  
 1205 W., Drouin, B., Froidevaux, L., and Fuller, R.: Validation of the Aura  
 1206 Microwave Limb Sounder HNO<sub>3</sub> measurements, *J. Geophys. Res.*, 112,  
 1207 D24S40, doi:10.1029/2007JD008721, 2007.
- 1208 Sauvage, B., Martin, R., Donkelaar, A. v., Liu, X., Chance, K., Jaeglé, L.,  
 1209 Palmer, P., Wu, S., and Fu, T.-M.: Remote sensed and in situ constraints  
 1210 on processes affecting tropical tropospheric ozone, *Atmos. Chem. Phys.*,  
 1211 7, 815–838, 2007.
- 1212 Seinfeld, J. H., and Pandis, S. N.: Atmospheric chemistry and physics: from air  
 1213 pollution to climate change, second ed. John Wiley: A Wiley-Interscience  
 1214 Publication Press, 2006.
- 1215 Sharma, R. K., Bhattarai, B., Sapkota, B., Gewali, M., and Kjeldstad, B.: Black  
 1216 carbon aerosols variation in Kathmandu valley, Nepal, *Atmos. Environ.*, 63,

1217 282–288, doi:10.1016/j.atmosenv.2012.09.023, 2012.

1218 Shrestha, A. B., Wake, C. P., Dibb, J. E., Mayewski, P. A., Whitlow, S. I.,  
1219 Carmichael, G. R., and Ferm, M.: Seasonal variations in aerosol  
1220 concentrations and compositions in the Nepal Himalaya, *Atmos. Environ.*,  
1221 34, 3349–3363, 10.1016/s1352-2310(99)00366-0, 2000.

1222 Škerlak, B., Sprenger, M., and Wernli, H.: A global climatology of  
1223 stratosphere-troposphere exchange using the ERA-Interim data set from  
1224 1979 to 2011, *Atmos. Chem. Phys.*, 14, 913–937, 2014.

1225 Stevenson, D. S., Dentener, F. J., Schultz, M. G., Ellingsen, K., Van Noije, T. P.  
1226 C., Wild, O., Zeng, G., Amann, M., Atherton, C. S., and Bell, N.:  
1227 Multimodel ensemble simulations of present-day and near-future  
1228 tropospheric ozone, *J. Geophys. Res.*, 111, D08301,  
1229 doi:10.1029/2005JD006338, 2006.

1230 Streets, D. G., Bond, T. C., Carmichael, G. R., Fernandes, S. D., Fu, Q., He, D.,  
1231 Klimont, Z., Nelson, S. M., Tsai, N. Y., and Wang, M. Q.: An inventory of  
1232 gaseous and primary aerosol emissions in Asia in the year 2000, *J.*  
1233 *Geophys. Res.*, 108, GTE 30–31, 2003.

1234 Su, H., Jiang, J. H., Lu, X. H., Penner, J. E., Read, W. G., Massie, S.,  
1235 Schoeberl, M. R., Colarco, P., Livesey, N. J., and Santee, M. L.: Observed  
1236 Increase of TTL Temperature and Water Vapor in Polluted Clouds over  
1237 Asia, *J. Clim.*, 24, 2728–2736, 10.1175/2010jcli3749.1, 2011.

1238 Sudheer, A., and Sarin, M.: Carbonaceous aerosols in MABL of Bay of Bengal:  
1239 Influence of continental outflow, *Atmos. Environ.*, 42, 4089–4100, 2008.

1240 Talukdar, R. K., Burkholder, J. B., Roberts, J. M., Portmann, R. W., and  
1241 Ravishankara, A.: Heterogeneous Interaction of N<sub>2</sub>O<sub>5</sub> with HCl Doped  
1242 H<sub>2</sub>SO<sub>4</sub> under Stratospheric Conditions: ClNO<sub>2</sub> and Cl<sub>2</sub> Yields, *J. Phys.*  
1243 *Chem. A.*, 116, 6003–6014, 2012.

1244 Tang, M., Telford, P., Pope, F., Rkiouak, L., Abraham, N., Archibald, A.,  
1245 Braesicke, P., Pyle, J., McGregor, J., and Watson, I.: Heterogeneous  
1246 reaction of N<sub>2</sub>O<sub>5</sub> with airborne TiO<sub>2</sub> particles and its implication for  
1247 stratospheric particle injection, *Atmos. Chem. Phys.*, 14, 6035–6048,  
1248 2014.

1249 Tare, V., Tripathi, S., Chinnam, N., Srivastava, A., Dey, S., Manar, M.,  
1250 Kanawade, V. P., Agarwal, A., Kishore, S., and Lal, R.: Measurements of  
1251 atmospheric parameters during Indian Space Research Organization  
1252 Geosphere Biosphere Program Land Campaign II at a typical location in  
1253 the Ganga Basin: 2. chemical properties, *J. Geophys. Res.*, 111, D23210,  
1254 doi:10.1029/2006JD007279, 2006.

1255 Thornton, J. A., Jaeglé, L., and McNeill, V. F.: Assessing known pathways for  
1256 HO<sub>2</sub> loss in aqueous atmospheric aerosols: Regional and global impacts  
1257 on tropospheric oxidants, *J. Geophys. Res.*, 113, D05303,  
1258 doi:10.1029/2007JD009236, 2008.

1259 Tobo, Y., Zhang, D., Iwasaka, Y., and Shi, G.: On the mixture of aerosols and  
1260 ice clouds over the Tibetan Plateau: Results of a balloon flight in the  
1261 summer of 1999, *Geophys. Res. Lett.*, 34, L23801,  
1262 doi:10.1029/2007GL031132, 2007.

1263 Tripathi, S., Dey, S., Tare, V., and Satheesh, S.: Aerosol black carbon radiative  
1264 forcing at an industrial city in northern India, *Geophys. Res. Lett.*, 32,  
1265 L08802, doi:10.1029/2005GL022515, 2005.

1266 van der Werf, G. R., Randerson, J. T., Giglio, L., Collatz, G. J., Mu, M.,

1267 Kasibhatla, P. S., Morton, D. C., DeFries, R. S., Jin, Y., and van Leeuwen,  
 1268 T. T.: Global fire emissions and the contribution of deforestation, savanna,  
 1269 forest, agricultural, and peat fires (1997–2009), *Atmos. Chem. Phys.*, 10,  
 1270 11707–11735, 2010.

1271 Vanhellefont, F., Tetard, C., Bourassa, A., Fromm, M., Dodion, J., Fussen, D.,  
 1272 Brogniez, C., Degenstein, D., Gilbert, K., and Turnbull, D.: Aerosol  
 1273 extinction profiles at 525 nm and 1020 nm derived from ACE imager data:  
 1274 comparisons with GOMOS, SAGE II, SAGE III, POAM III, and OSIRIS,  
 1275 *Atmos. Chem. Phys.*, 8, 2027–2037, 2008.

1276 Venkataraman, C., Reddy, C. K., Josson, S., and Reddy, M. S.: Aerosol size  
 1277 and chemical characteristics at Mumbai, India, during the INDOEX-IFP  
 1278 (1999), *Atmos. Environ.*, 36, 1979–1991, 2002.

1279 Verma, S., Boucher, O., Reddy, M., Upadhyaya, H., Van, P., Binkowski, F., and  
 1280 Sharma, O.: Tropospheric distribution of sulphate aerosols mass and  
 1281 number concentration during INDOEX-IFP and its transport over the  
 1282 Indian Ocean: a GCM study, *Atmos. Chem. Phys.*, 12, 6185–6196, 2012.

1283 Vernier, J.-P., Pommereau, J.-P., Garnier, A., Pelon, J., Larsen, N., Nielsen, J.,  
 1284 Christensen, T., Cairo, F., Thomason, L., and Leblanc, T.: Tropical  
 1285 stratospheric aerosol layer from CALIPSO lidar observations, *J. Geophys.*  
 1286 *Res.*, 114, D00H10, doi:10.1029/2009JD011946, 2009.

1287 Vernier, J. P., Thomason, L., and Kar, J.: CALIPSO detection of an Asian  
 1288 tropopause aerosol layer, *Geophys. Res. Lett.*, 38, L07804,  
 1289 doi:10.1029/2010GL046614, 2011.

1290 Voigt, C., Schreiner, J., Kohlmann, A., Zink, P., Mauersberger, K., Larsen, N.,  
 1291 Deshler, T., Kröger, C., Rosen, J., and Adriani, A.: Nitric acid trihydrate  
 1292 (NAT) in polar stratospheric clouds, *Science*, 290, 1756–1758, 2000.

1293 Wang, P., McCormick, M., McMaster, L., Chu, W., Swissler, T., Osborn, M.,  
 1294 Russell, P., Oberbeck, V., Livingston, J., and Rosen, J.: SAGE II aerosol  
 1295 data validation based on retrieved aerosol model size distribution from  
 1296 SAGE II aerosol measurements, *J. Geophys. Res.*, 94, 8381–8393,  
 1297 doi:10.1029/JD094iD06p08381, 1989.

1298 Wang, Y., Logan, J. A., and Jacob, D. J.: Global simulation of tropospheric  
 1299 O<sub>3</sub>–NO<sub>x</sub>–hydrocarbon chemistry: 2. Model evaluation and global ozone  
 1300 budget, *J. Geophys. Res.*, 103, 10727–10755, 1998.

1301 Wang, Y., Zhang, Q., He, K., Zhang, Q., and Chai, L.:  
 1302 Sulfate-nitrate-ammonium aerosols over China: response to 2000–2015  
 1303 emission changes of sulfur dioxide, nitrogen oxides, and ammonia, *Atmos.*  
 1304 *Chem. Phys.*, 13, 2635–2652, 2013.

1305 Waters, J. W., Froidevaux, L., Harwood, R. S., Jarnot, R. F., Pickett, H. M.,  
 1306 Read, W. G., Siegel, P. H., Cofield, R. E., Filipiak, M. J., and Flower, D.:  
 1307 The earth observing system microwave limb sounder (EOS MLS) on the  
 1308 Aura satellite, *IEEE T. Geosci. Remote.*, 44, 1075–1092, 2006.

1309 Weigel, R., Borrmann, S., Kazil, J., Minikin, A., Stohl, A., Wilson, J., Reeves, J.,  
 1310 Kunkel, D., De Reus, M., and Frey, W.: In situ observations of new particle  
 1311 formation in the tropical upper troposphere: the role of clouds and the  
 1312 nucleation mechanism, *Atmos. Chem. Phys. Discuss.*, 11, 2011.

1313 Wesely, M.: Parameterization of surface resistances to gaseous dry deposition  
 1314 in regional-scale numerical models, *Atmos. Environ.*, 23, 1293–1304,  
 1315 1989.

1316 Wu, L. T., Su, H., and Jiang, J. H.: Regional simulations of deep convection

1317 and biomass burning over South America: 2. Biomass burning aerosol  
1318 effects on clouds and precipitation, *J. Geophys. Res.*, 116,  
1319 doi:10.1029/2011jd016106, 2011.

1320 Wu, S., Mickley, L. J., Jacob, D. J., Logan, J. A., Yantosca, R. M., and Rind, D.:  
1321 Why are there large differences between models in global budgets of  
1322 tropospheric ozone? *J. Geophys. Res.*, 112, D05302,  
1323 doi:10.1029/2006JD007801, 2007.

1324 Wu, S., Mickley, L. J., Jacob, D. J., Rind, D., and Streets, D. G.: Effects of  
1325 2000–2050 changes in climate and emissions on global tropospheric  
1326 ozone and the policy–relevant background surface ozone in the United  
1327 States, *J. Geophys. Res.*, 113, D18312, doi:10.1029/2007JD009639,  
1328 2008.

1329 Xia, X., Zong, X., Cong, Z., Chen, H., Kang, S., and Wang, P.: Baseline  
1330 continental aerosol over the central Tibetan plateau and a case study of  
1331 aerosol transport from South Asia, *Atmos. Environ.*, 45, 7370–7378, 2011.

1332 Xiong, X., Houweling, S., Wei, J., Maddy, E., Sun, F., and Barnet, C.: Methane  
1333 plume over south Asia during the monsoon season: satellite observation  
1334 and model simulation, *Atmos. Chem. Phys.*, 9, 783–794, 2009.

1335 Yanai, M., Li, C., and Song, Z.: Seasonal heating of the Tibetan Plateau and its  
1336 effects on the evolution of the Asian summer monsoon, *J. Meteorol. Soc.*  
1337 *Jan.*, 70, 319–351, 1992.

1338 Yao, X., Chan, C. K., Fang, M., Cadle, S., Chan, T., Mulawa, P., He, K., and Ye,  
1339 B.: The water-soluble ionic composition of PM<sub>2.5</sub> in Shanghai and Beijing,  
1340 China, *Atmos. Environ.*, 36, 4223–4234, 2002.

1341 Yin, Y., Chen, Q., Jin, L., Chen, B., Zhu, S., and Zhang, X.: The effects of deep  
1342 convection on the concentration and size distribution of aerosol particles  
1343 within the upper troposphere: A case study, *J. Geophys. Res.*, 117,  
1344 D22202, doi:10.1029/2012JD017827, 2012.

1345 Zeng, G., Pyle, J., and Young, P.: Impact of climate change on tropospheric  
1346 ozone and its global budgets, *Atmos. Chem. Phys.*, 8, 369–387, 2008.

1347 Zhang, G. J., and McFarlane, N. A.: Sensitivity of climate simulations to the  
1348 parameterization of cumulus convection in the Canadian Climate Centre  
1349 general circulation model, *Atmos.-Ocean*, 33, 407–446, 1995.

1350 Zhang, L., Liao, H., and Li, J.: Impacts of Asian summer monsoon on seasonal  
1351 and interannual variations of aerosols over eastern China, *J. Geophys.*  
1352 *Res.*, 115, D00K05, doi:10.1029/2009JD012299, 2010.

1353 Zhang, N., Cao, J., Ho, K., and He, Y.: Chemical characterization of aerosol  
1354 collected at Mt. Yulong in wintertime on the southeastern Tibetan Plateau,  
1355 *Atmos. Res.*, 107, 76, 2012.

1356 Zhang, Q., Streets, D. G., Carmichael, G. R., He, K., Huo, H., Kannari, A.,  
1357 Klimont, Z., Park, I., Reddy, S., and Fu, J.: Asian emissions in 2006 for the  
1358 NASA INTEX-B mission, *Atmos. Chem. Phys.*, 9, 5131–5153, 2009.

1359 Zhang, X., Cao, J., Li, L., Arimoto, R., Cheng, Y., Huebert, B., and Wang, D.:  
1360 Characterization of atmospheric aerosol over Xian in the south margin of  
1361 the Loess Plateau, China, *Atmos. Environ.*, 36, 4189–4199, 2002.

1362 Zhang, Y., Dore, A., Ma, L., Liu, X., Ma, W., Cape, J., and Zhang, F.:  
1363 Agricultural ammonia emissions inventory and spatial distribution in the  
1364 North China Plain, *Environ. Pollut.*, 158, 490–501, 2010.

1365 Zhao, X., Turco, R. P., Kao, C. Y. J., and Elliott, S.: Aerosol-induced chemical  
1366 perturbations of stratospheric ozone: Three-dimensional simulations and

1367 analysis of mechanisms, *J. Geophys. Res.*, 102, 3617–3637,  
1368 doi:10.1029/96jd03406, 1997.  
1369 Zhu, J., Liao, H., and Li, J.: Increases in aerosol concentrations over  
1370 eastern China due to the decadal-scale weakening of the East Asian  
1371 summer monsoon, *Geophys. Res. Lett.*, 39, L09809,  
1372 doi:10.1029/2012GL051428, 2012.

1373  
1374

Table 1. Summary of Annual Emissions of Aerosols and Aerosol Precursors in Asia (60°E-155°E, 10°N-55°N)

Species	Global	Asia
<b>NO<sub>x</sub> (Tg N yr<sup>-1</sup>)</b>		
Aircraft	0.5	0.08
Anthropogenic	28.6	9.96
Biomass burning	4.7	0.27
Fertilizer	0.7	0.31
Lightning	5.9	0.87
Soil	5.9	0.96
Total	46.3	12.45
<b>SO<sub>2</sub> (Tg S yr<sup>-1</sup>)</b>		
Aircraft	0.1	0.01
Anthropogenic	52.6	23.46
Biomass burning	1.2	0.07
Volcanoes	4.4	1.04
No_eruption	8.9	1.78
Ship	7.4	0.94
Total	74.6	27.30
<b>NH<sub>3</sub> (Tg N yr<sup>-1</sup>)</b>		
Anthropogenic	34.9	17.83
Natural	14.2	2.01
Biomass burning	3.5	0.21
Biofuel	1.6	0.71
Total	54.2	20.76
<b>OC (Tg C yr<sup>-1</sup>)</b>		
Anthropogenic	3.1	1.42
Biomass burning	18.7	1.10
Biofuel	6.3	3.28
Biogenic	9.7	1.22
Total	37.8	7.02
<b>BC (Tg C yr<sup>-1</sup>)</b>		
Anthropogenic	3.0	1.43
Biomass burning	2.2	0.12
Biofuel	1.6	0.86
Total	6.8	2.41

1375  
 1376  
 1377  
 1378

Table 2. Simulated seasonal mean concentrations of aerosols and their contributions to PM<sub>2.5</sub> (in percentages in parentheses) during summertime (June-August) of 2005 for the TP/SASM, TP, and SASM regions. The unit is  $\mu\text{g m}^{-3}$  for concentrations at the surface, and  $10^{-2} \mu\text{g m}^{-3}$  for concentrations at 200 hPa and 100 hPa.

	PM <sub>2.5</sub>	SO <sub>4</sub> <sup>2-</sup>	NO <sub>3</sub> <sup>-</sup>	NH <sub>4</sub> <sup>+</sup>	OC	BC
TP/SASM						
Surface	4.73	1.70(35.9%)	0.94(19.8%)	0.85(18.1%)	0.94(19.8%)	0.30(6.4%)
200 hPa	16.19	3.27(20.2%)	7.57(46.8%)	2.67(16.5%)	2.22(13.7%)	0.44(2.7%)
100 hPa	12.14	2.60(21.4%)	6.90(56.8%)	1.43(11.8%)	1.05(8.6%)	0.16(1.3%)
TP						
Surface	5.44	2.12(39.0%)	1.05(19.3%)	1.08(19.9%)	0.88(16.1%)	0.31(5.7%)
200 hPa	19.80	4.16(21.0%)	9.43(47.6%)	3.25(16.4%)	2.49(12.6%)	0.47(2.4%)
100 hPa	10.58	2.60(24.6%)	5.51(52.0%)	1.35(12.7%)	0.99(9.4%)	0.14(1.3%)
SASM						
Surface	4.02	1.28(31.8%)	0.83(20.5%)	0.63(15.6%)	1.00(24.8%)	0.29(7.2%)
200 hPa	12.57	2.38(18.9%)	5.72(45.5%)	2.10(16.7%)	1.95(15.5%)	0.41(3.3%)
100 hPa	13.71	2.60(19.0%)	8.30(60.5%)	1.52(11.1%)	1.11(8.1%)	0.18(1.3%)

1379 Table 3. Sensitivity simulations to examine the impacts of uncertainties in surface-layer aerosol concentrations on simulated  $\text{NO}_3^-$   
 1380 in the UTLS. “Conc” and “Ctr” denote, respectively, simulated seasonal mean concentrations of  $\text{SO}_4^{2-}$ ,  $\text{NO}_3^-$ ,  $\text{NH}_4^+$ , OC, BC and  
 1381 their contributions to  $\text{PM}_{2.5}$  (in percentages) during summertime (June-August) of 2005. The mass concentrations are averaged  
 1382 over the TP/SASM region, with unit of  $\mu\text{g m}^{-3}$  at the surface layer and of  $10^{-2} \mu\text{g m}^{-3}$  at 200 hPa and 100 hPa. Also shown are the  
 1383 NMBs, as the simulated surface-layer concentrations are compared with measurements described in Section 4.2.

Species	Baseline Case			$\text{SO}_2$ (+20%)			$\text{NO}_x$ (-50%)			$\text{NH}_3$ (-50%)			All Change		
	Conc.	Ctri.	NMB	Conc.	Ctri.	NMB	Conc.	Ctri.	NMB	Conc.	Ctri.	NMB	Conc.	Ctri.	NMB
Surface															
$\text{SO}_4^{2-}$	1.70	35.9%	-14.7%	1.92	38.1%	-4.4%	1.58	39.5%	-18.1%	1.70	38.1%	-14.7%	1.78	43.2%	-8.3%
$\text{NO}_3^-$	0.94	19.8%	+51.5%	0.94	18.7%	+53.5%	0.50	12.5%	-11.7%	0.73	16.4%	+24.1%	0.39	9.5%	-27.0%
$\text{NH}_4^+$	0.85	18.1%	+74.9%	0.94	18.6%	+93.8%	0.68	17.1%	+44.1%	0.78	17.6%	+64.6%	0.71	17.3%	+55.4%
OC	0.94	19.8%	-57.2%	0.94	18.6%	-57.2%	0.94	23.4%	-57.2%	0.94	21.0%	-57.2%	0.94	22.7%	-57.2%
BC	0.30	6.4%	-32.2%	0.30	6.0%	-32.2%	0.30	7.5%	-32.2%	0.30	6.8%	-32.2%	0.30	7.3%	-32.2%
200 hPa															
$\text{SO}_4^{2-}$	3.27	20.2%		3.67	22.9%		3.31	20.6%		3.29	29.1%		3.74	33.7%	
$\text{NO}_3^-$	7.57	46.8%		7.05	43.9%		7.41	46.0%		3.86	34.2%		3.19	28.7%	
$\text{NH}_4^+$	2.67	16.5%		2.67	16.6%		2.71	16.8%		1.49	13.2%		1.50	13.5%	
OC	2.22	13.7%		2.22	13.8%		2.22	13.8%		2.22	19.7%		2.22	20.0%	
BC	0.44	2.7%		0.44	2.7%		0.44	2.7%		0.44	3.9%		0.44	4.0%	
100 hPa															
$\text{SO}_4^{2-}$	2.60	21.4%		2.80	23.0%		2.66	21.9%		2.60	25.2%		2.87	27.2%	
$\text{NO}_3^-$	6.90	56.8%		6.72	55.3%		6.81	56.1%		5.68	55.0%		5.62	53.3%	
$\text{NH}_4^+$	1.43	11.8%		1.43	11.7%		1.45	12.0%		0.84	8.1%		0.84	8.0%	
OC	1.05	8.6%		1.05	8.6%		1.05	8.7%		1.05	10.2%		1.05	10.0%	
BC	0.16	1.3%		0.16	1.3%		0.16	1.3%		0.16	1.6%		0.16	1.5%	

1384 **Figure Captions**

1385

1386 **Figure. 1.** Regions examined in this study: the Tibetan Plateau region (TP,  
1387 70–105°E, 25–40°N), the SASM region (SASM, 70–105°E, 10–25°N), and the  
1388 anticyclone region of (20–120°E, 10–40°N).

1389

1390 **Figure. 2.** Monthly variations in emissions of  $\text{NO}_x$  ( $\text{Tg N month}^{-1}$ ),  $\text{SO}_2$  ( $\text{Tg S}$   
1391  $\text{month}^{-1}$ ),  $\text{NH}_3$  ( $\text{Tg N month}^{-1}$ ), OC ( $\text{Tg C month}^{-1}$ ), and BC ( $\text{Tg C month}^{-1}$ )  
1392 over Asia. Values shown are the total emissions (anthropogenic plus natural  
1393 emissions listed in Table 1).

1394

1395 **Figure. 3.** Simulated global distributions of surface-layer  $\text{HNO}_3$  (pptv) and  $\text{O}_3$   
1396 (ppbv) averaged over June-August, 2005.

1397

1398 **Figure. 4.** Comparisons of simulated  $\text{HNO}_3$  concentrations (pptv) with  
1399 observations (pptv) from MLS. (a) and (b) are simulated concentrations at 200  
1400 hPa and 100 hPa, respectively. (c) is the latitude-altitude cross section of  
1401 simulated  $\text{HNO}_3$  concentrations averaged over 70–105°E. (d)-(f) are the same  
1402 as (a)-(c), except that (d)-(f) are observations from MLS. The white areas in (d)  
1403 and (f) have no datasets available from MLS. All the datasets are averaged  
1404 over June-August of 2005.

1405

1406 **Figure. 5.** Comparisons of simulated  $\text{O}_3$  concentrations (ppbv) with  
1407 observations (ppbv) from MLS. (a) and (b) are simulated concentrations at 200  
1408 hPa and 100 hPa, respectively. (c) is the latitude-altitude cross section of  
1409 simulated  $\text{O}_3$  concentrations averaged over 70–105°E. (d)-(f) are the same as  
1410 (a)-(c), except that (d)-(f) are observations from MLS. All the datasets are  
1411 averaged over June-August of 2005.

1412

1413 **Figure. 6.** The simulated and observed vertical profiles of monthly mean  $\text{O}_3$   
1414 mixing ratios at (a) Kunming and (b) Lhasa in August. The model results are  
1415 from the simulation of year 2005. The observations in Kunming were  
1416 conducted during August 7–13 (11 profiles of  $\text{O}_3$  collected) in 2009 and during  
1417 August 12–31 in 2012 (daily observations). The observations in Lhasa were  
1418 conducted during August 22–28 in 2010 (12 profiles of  $\text{O}_3$  collected) and  
1419 during August 4–26 in 2013 (daily observations).

1420

1421 **Figure. 7.** Simulated seasonal mean concentrations ( $\mu\text{g m}^{-3}$ ) of sulfate, nitrate,  
1422 ammonium, organic carbon, black carbon, and  $\text{PM}_{2.5}$  at (a) the surface layer, (b)  
1423 200 hPa, and (c) 100 hPa, during summer (June-August) of year 2005. Note  
1424 that color bars are different for concentrations at the surface, 200 hPa, and 100  
1425 hPa.

1426

1427 **Figure. 8.** (a) Locations with measured aerosol concentrations from previous  
1428 studies. Also shown are surface winds during summertime. (b)–(f) show the  
1429 comparisons of simulated seasonal mean concentrations of sulfate, nitrate,  
1430 ammonium, OC, and BC with measured values, respectively. Also shown in  
1431 (b)–(f) are the 1:1 line (dashed), linear fit (solid line and equation), correlation  
1432 coefficient between simulated and measured concentrations (R), and

1433 normalized mean bias (NMB) (defined as  $NMB = \frac{\sum_{i=1}^n (P_i - O_i)}{\sum_{i=1}^n O_i} \times 100\%$ , where  $P_i$   
1434 and  $O_i$  are predicted and observed concentrations at station  $i$  for each aerosol  
1435 species).

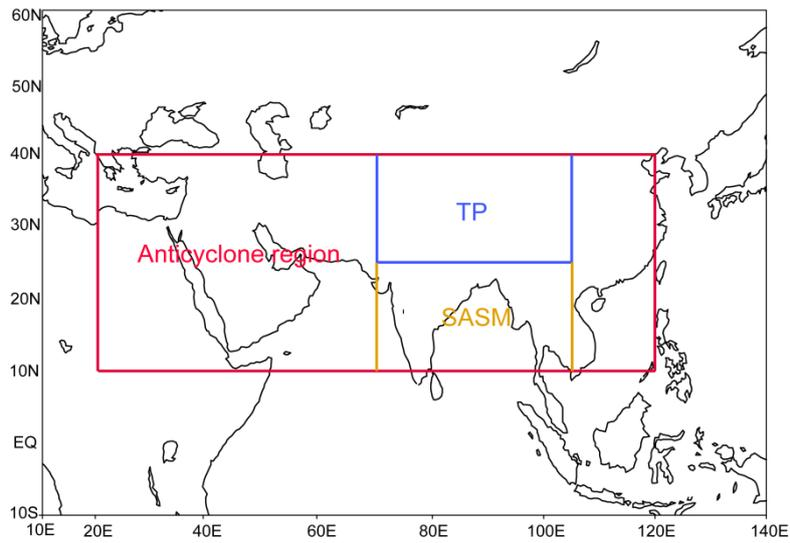
1436  
1437 **Figure. 9.** (a) Monthly mean distribution of aerosol extinction coefficients ( $\text{km}^{-1}$ )  
1438 at 100 hPa for July of 2005. (b) Monthly mean vertical distributions of aerosol  
1439 extinction coefficients (at 525 nm for SAGE II and 550 nm for GEOS-Chem)  
1440 ( $\text{km}^{-1}$ ) averaged over the Asian monsoon anticyclone region ( $20\text{--}120^\circ\text{E}$ ,  
1441  $10\text{--}40^\circ\text{N}$ ) for July of 2005. The horizontal dashed line represents the  
1442 tropopause averaged over the Asian monsoon anticyclone region simulated by  
1443 the GEOS-Chem model.

1444  
1445 **Figure. 10.** Simulated contributions of nitrate to  $\text{PM}_{2.5}$  ( $C_{\text{NIT}} = [\text{NIT}] / [\text{PM}_{2.5}]$   
1446  $\times 100\%$ ) averaged over summer (June-August) of year 2005 at (a)  
1447 surface-layer, (b) 200 hPa, and (c) 100 hPa. (d) The latitude-altitude cross  
1448 section of simulated  $C_{\text{NIT}}$  (%) averaged over  $70\text{--}105^\circ\text{E}$ .

1449  
1450 **Figure. 11.** Latitude-altitude cross sections of simulated concentrations (color  
1451 shades,  $\mu\text{g m}^{-3}$ ) of  $\text{SO}_4^{2-}$  and  $\text{NO}_3^-$  averaged over  $70\text{--}105^\circ\text{E}$  in June-August  
1452 of 2005, together with the wind vectors obtained from the European Centre for  
1453 Medium-Range Weather Forecasts (ECMWF) ERA-Interim Reanalysis data.  
1454 The black line is the tropopause simulated by the GEOS-Chem model.

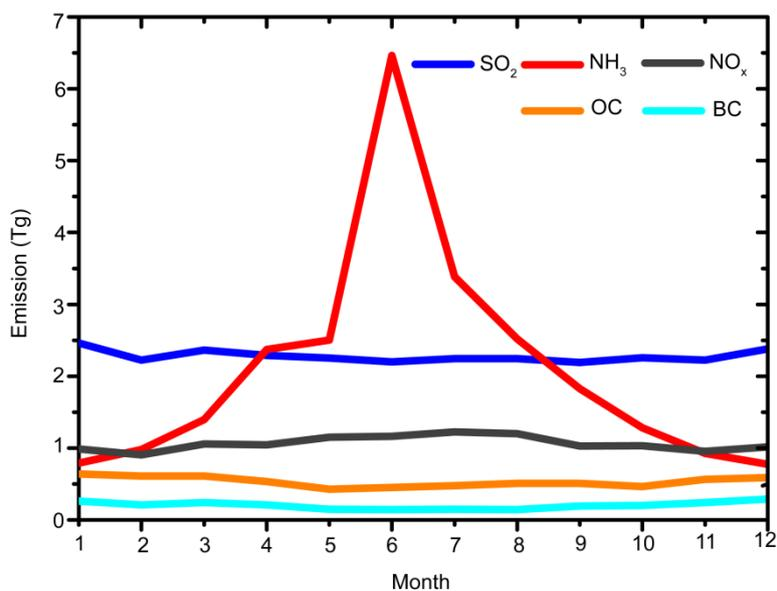
1455  
1456 **Figure. 12.** (a)-(b) Distributions of RH (%) and temperature (K) at 100 hPa.  
1457 (c)-(d) The latitude-altitude cross sections of RH (%) and temperature (K)  
1458 averaged over  $70\text{--}105^\circ\text{E}$ . RH and temperature are from the GEOS5  
1459 assimilated meteorological fields, and all the values are the averages over  
1460 June-August of year 2005.

1461  
1462 **Figure. 13.** Mass budget for nitrate aerosol within the selected box of  
1463 ( $70\text{--}105^\circ\text{E}$ ,  $10\text{--}40^\circ\text{N}$ ,  $8\text{--}16$  km). E/W transport indicates net mass flux through  
1464 the east and west lateral boundaries, N/S transport indicates net mass flux  
1465 through the north and south lateral boundaries, and upward transport is the net  
1466 mass flux through the top and bottom sides of the box. The mass flux is  
1467 positive if it increases nitrate mass within the box. Unit of fluxes is  $\text{Tg season}^{-1}$ .  
1468 All the values are the averages over June-August of 2005.



1469  
1470  
1471  
1472  
1473

**Figure. 1.** Regions examined in this study: the Tibetan Plateau region (TP, 70–105°E, 25–40°N), the SASM region (SASM, 70–105°E, 10–25°N), and the anticyclone region of (20–120°E, 10–40°N).



1474

1475

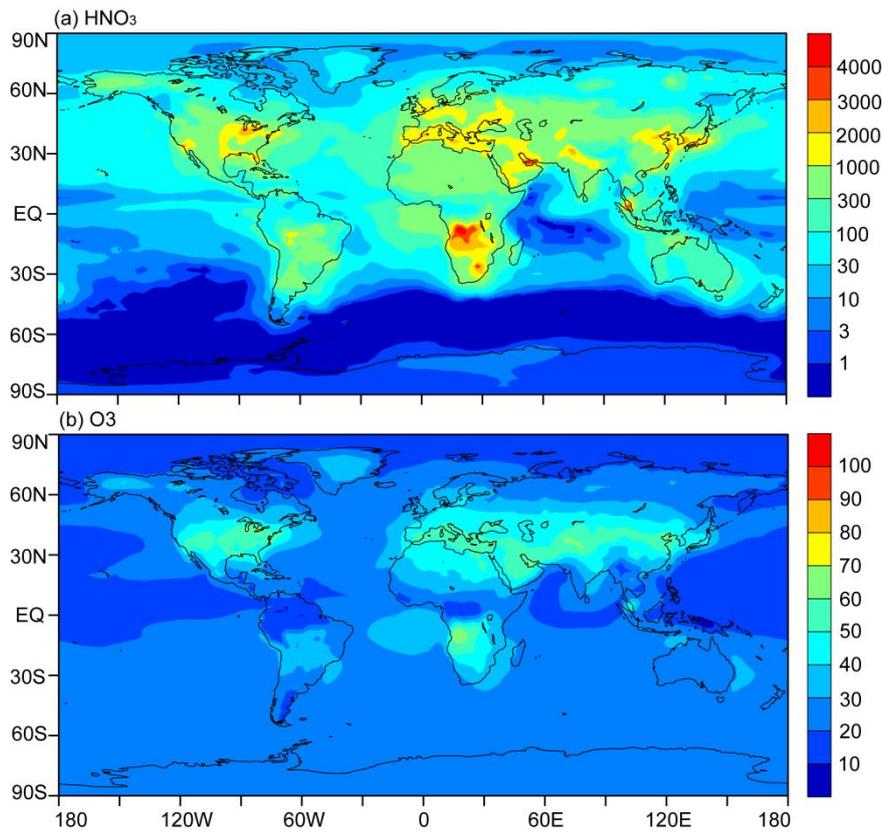
1476

1477

1478

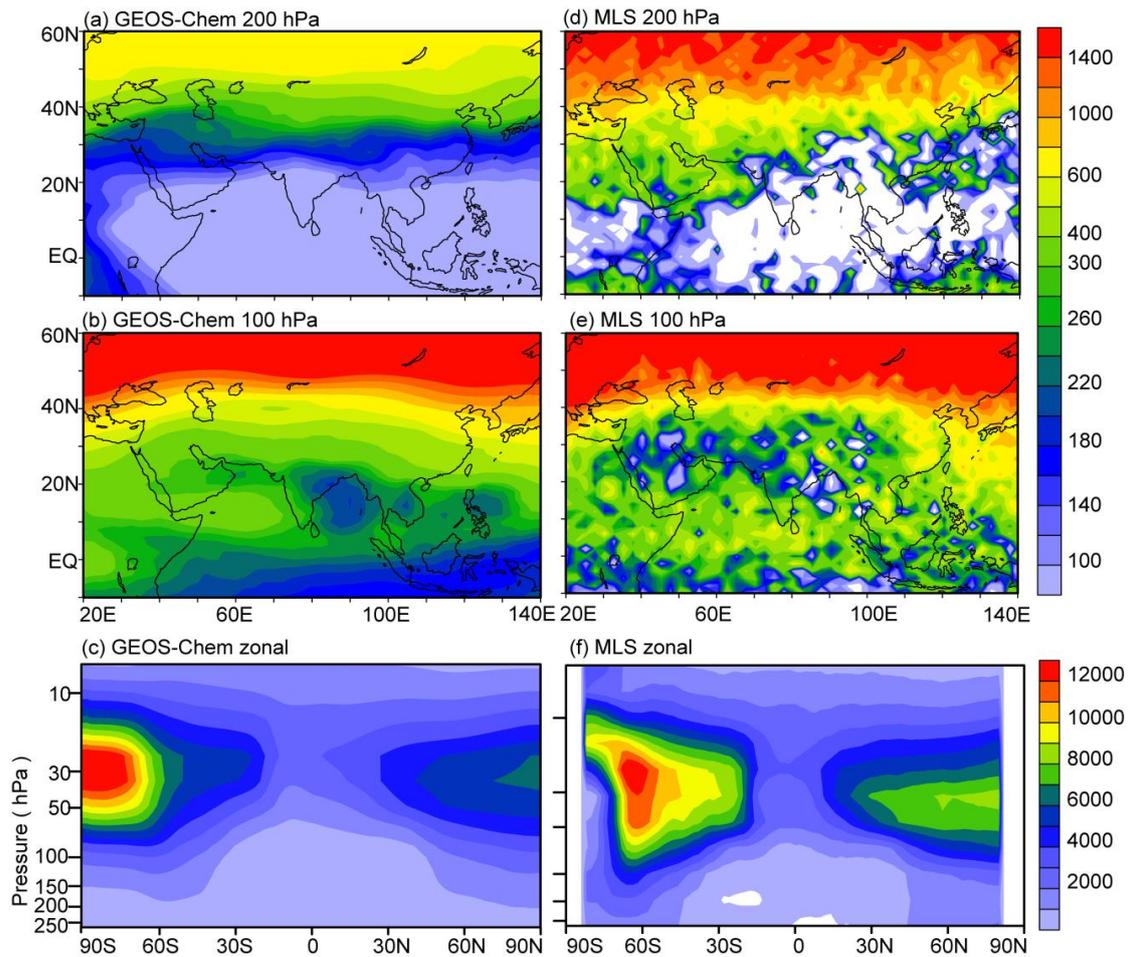
1479

**Figure. 2.** Monthly variations in emissions of NO<sub>x</sub> (Tg N month<sup>-1</sup>), SO<sub>2</sub> (Tg S month<sup>-1</sup>), NH<sub>3</sub> (Tg N month<sup>-1</sup>), OC (Tg C month<sup>-1</sup>), and BC (Tg C month<sup>-1</sup>) over Asia. Values shown are the total emissions (anthropogenic plus natural emissions listed in Table 1).



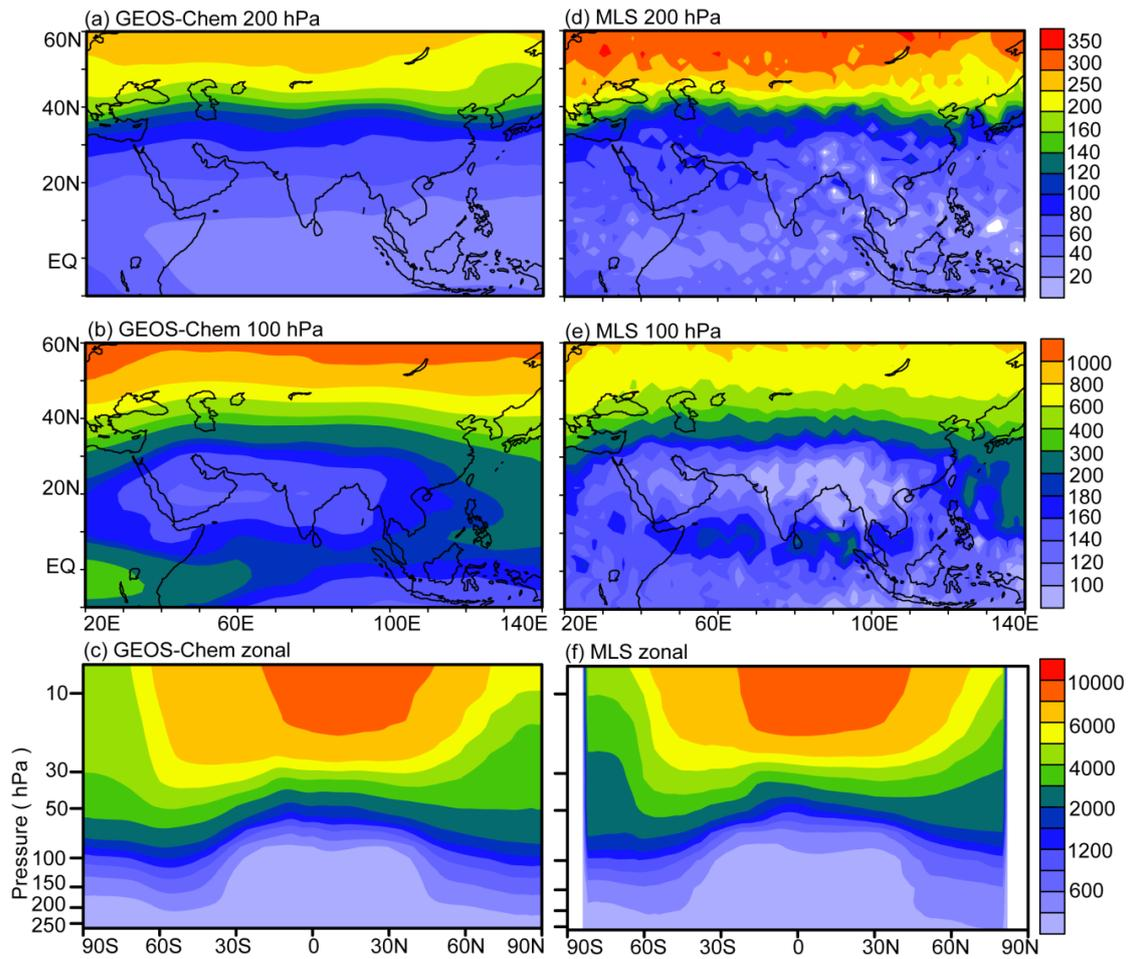
1480  
 1481  
 1482  
 1483

**Figure. 3.** Simulated global distributions of surface-layer HNO<sub>3</sub> (pptv) and O<sub>3</sub> (ppbv) averaged over June-August, 2005.



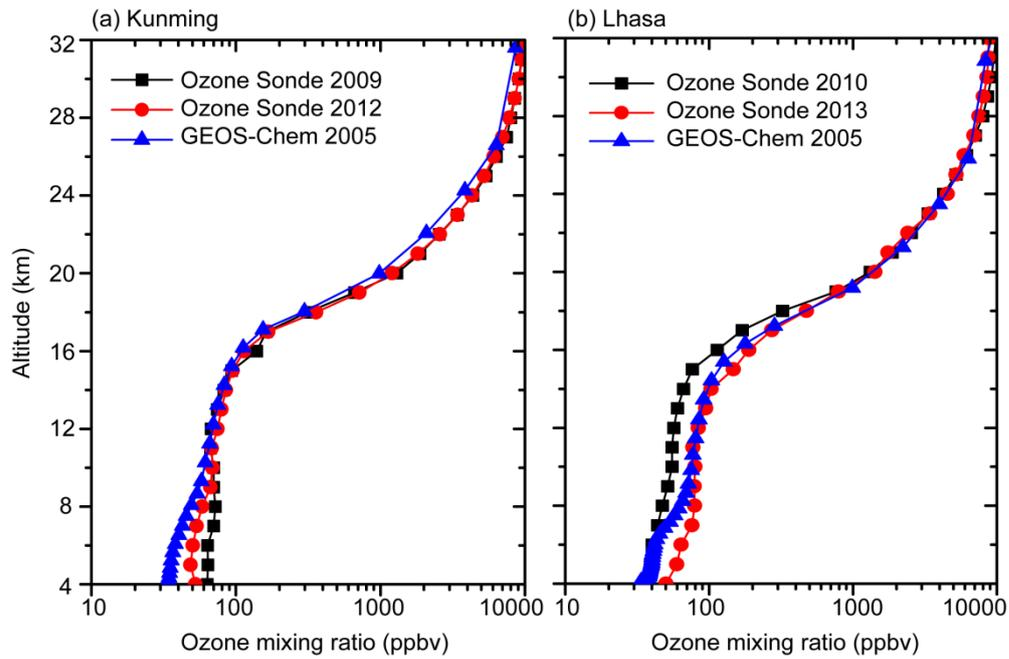
1484  
 1485  
 1486  
 1487  
 1488  
 1489  
 1490  
 1491  
 1492

**Figure. 4.** Comparisons of simulated  $\text{HNO}_3$  concentrations (pptv) with observations (pptv) from MLS. (a) and (b) are simulated concentrations at 200 hPa and 100 hPa, respectively. (c) is the latitude-altitude cross section of simulated  $\text{HNO}_3$  concentrations averaged over  $70\text{--}105^\circ\text{E}$ . (d)-(f) are the same as (a)-(c), except that (d)-(f) are observations from MLS. The white areas in (d) and (f) have no data available from MLS. All the datasets are averaged over June-August of 2005.



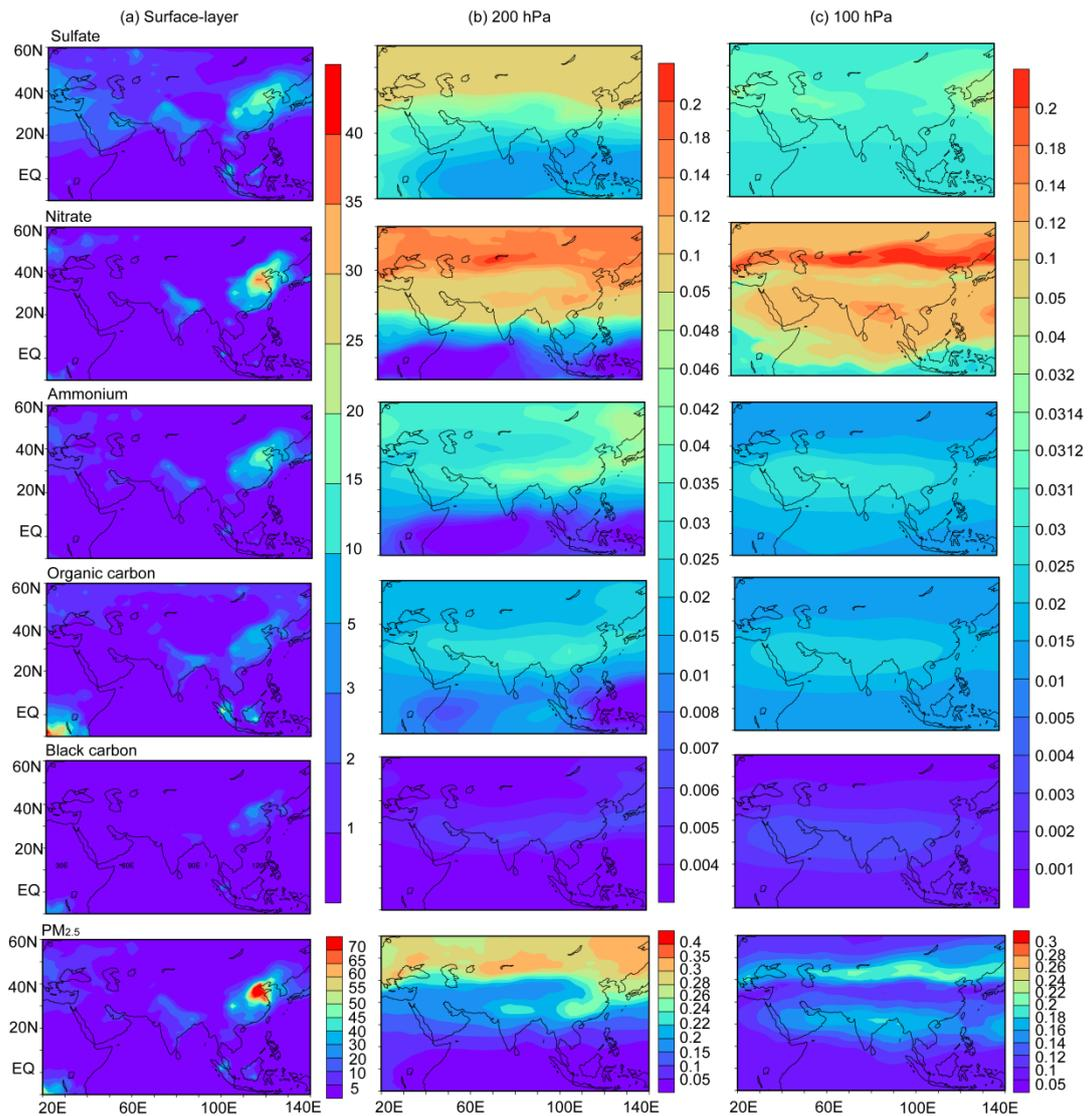
1493  
 1494  
 1495  
 1496  
 1497  
 1498  
 1499  
 1500

**Figure. 5.** Comparisons of simulated O<sub>3</sub> concentrations (ppbv) with observations (ppbv) from MLS. (a) and (b) are simulated concentrations at 200 hPa and 100 hPa, respectively. (c) is the latitude-altitude cross section of simulated O<sub>3</sub> concentrations averaged over 70–105°E. (d)-(f) are the same as (a)-(c), except that (d)-(f) are observations from MLS. All the datasets are averaged over June-August of 2005.



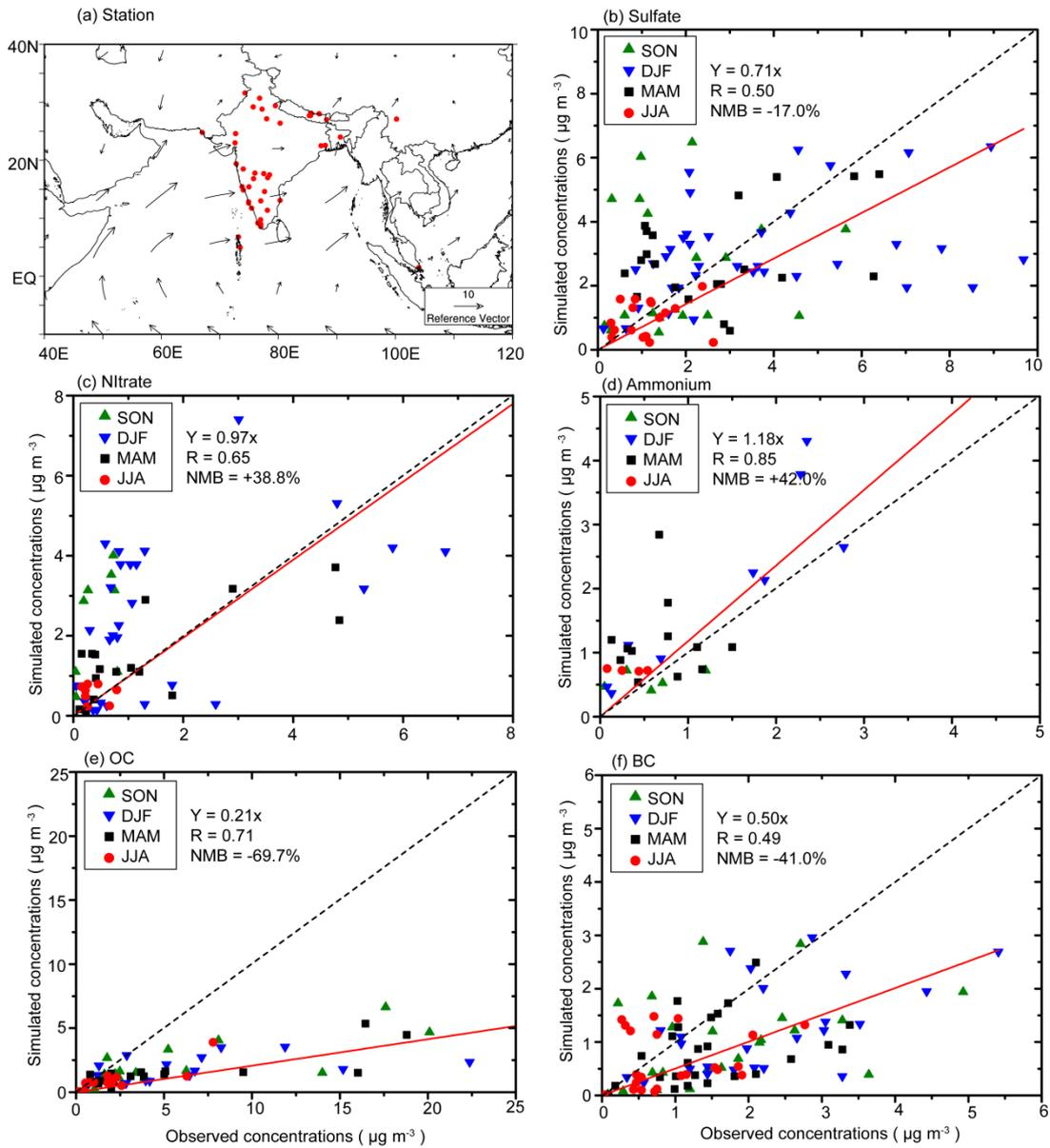
1501  
 1502  
 1503  
 1504  
 1505  
 1506  
 1507  
 1508  
 1509

Figure 6. The simulated and observed vertical profiles of monthly mean  $O_3$  mixing ratios at (a) Kunming and (b) Lhasa in August. The model results are from the simulation of year 2005. The observations in Kunming were conducted during August 7–13 (11 profiles of  $O_3$  collected) in 2009 and during August 12–31 in 2012 (daily observations). The observations in Lhasa were conducted during August 22–28 in 2010 (12 profiles of  $O_3$  collected) and during August 4–26 in 2013 (daily observations).



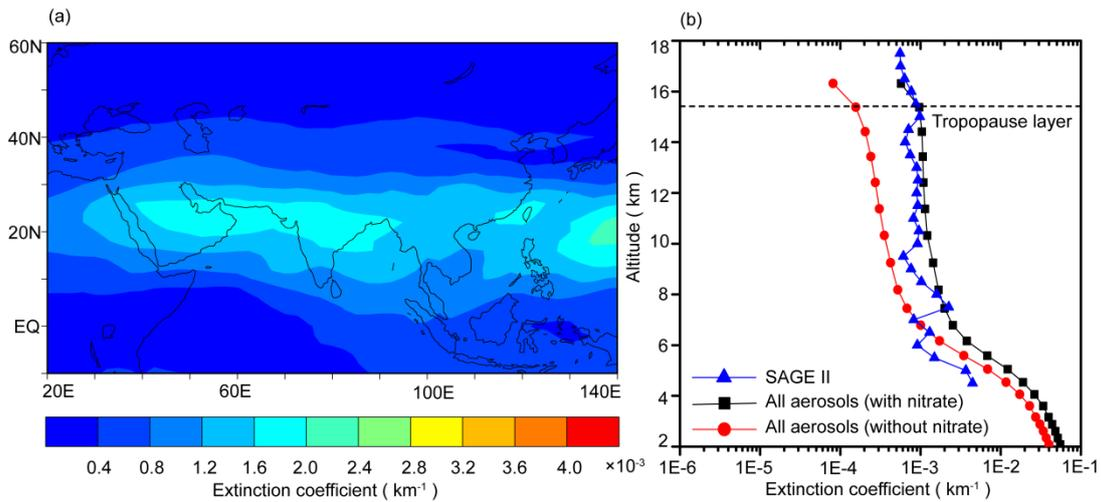
1510  
1511

1512 **Figure. 7.** Simulated seasonal mean concentrations ( $\mu\text{g m}^{-3}$ ) of sulfate, nitrate,  
 1513 ammonium, organic carbon, black carbon, and  $\text{PM}_{2.5}$  at (a) the surface layer, (b)  
 1514 200 hPa, and (c) 100 hPa, during summer (June-August) of year 2005. Note  
 1515 that color bars are different for concentrations at the surface, 200 hPa, and  
 1516 100 hPa.



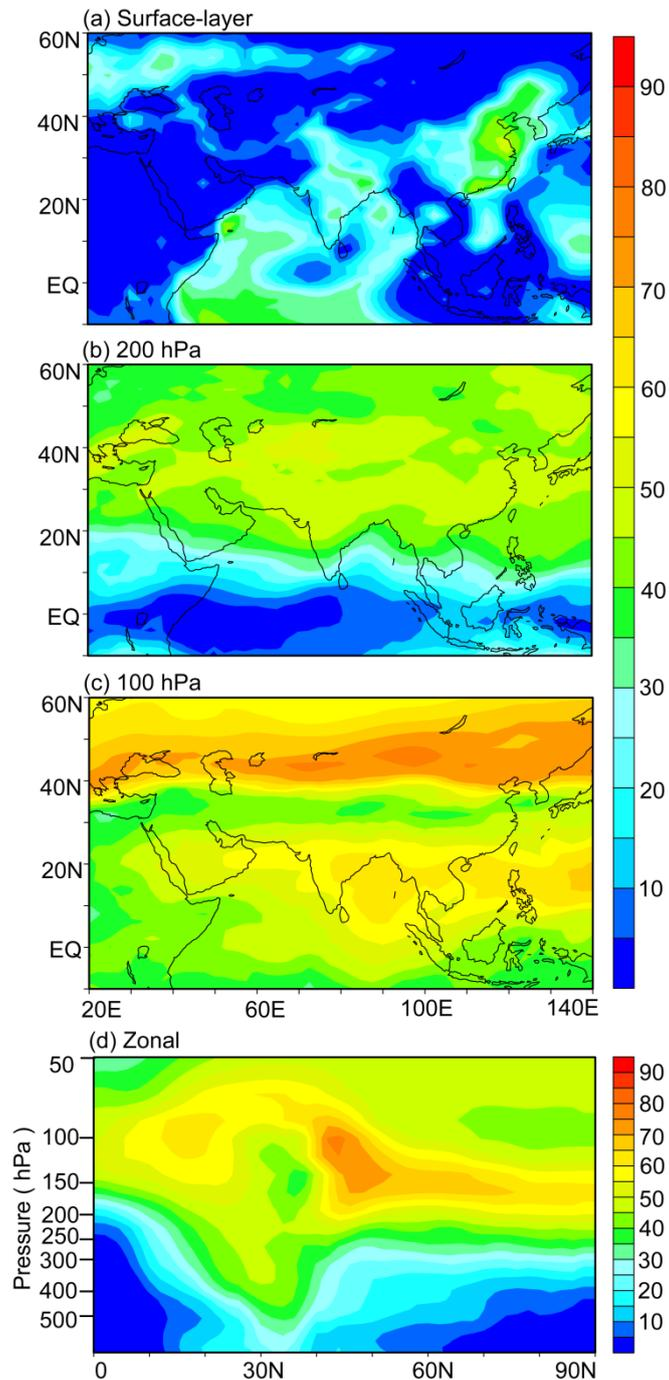
1517  
1518

1519 **Figure 8.** (a) Locations with measured aerosol concentrations from previous  
1520 studies. Also shown are surface winds during summertime. (b)–(f) show the  
1521 comparisons of simulated seasonal mean concentrations of sulfate, nitrate,  
1522 ammonium, OC, and BC with measured values, respectively. Also shown in  
1523 (b)–(f) are the 1:1 line (dashed), linear fit (solid line and equation), correlation  
1524 coefficient between simulated and measured concentrations (R), and  
1525 normalized mean bias (NMB) (defined as  $NMB = \frac{\sum_{i=1}^n (P_i - O_i)}{\sum_{i=1}^n O_i} \times 100\%$ , where  $P_i$   
1526 and  $O_i$  are predicted and observed concentrations at station  $i$  for each aerosol  
1527 species).



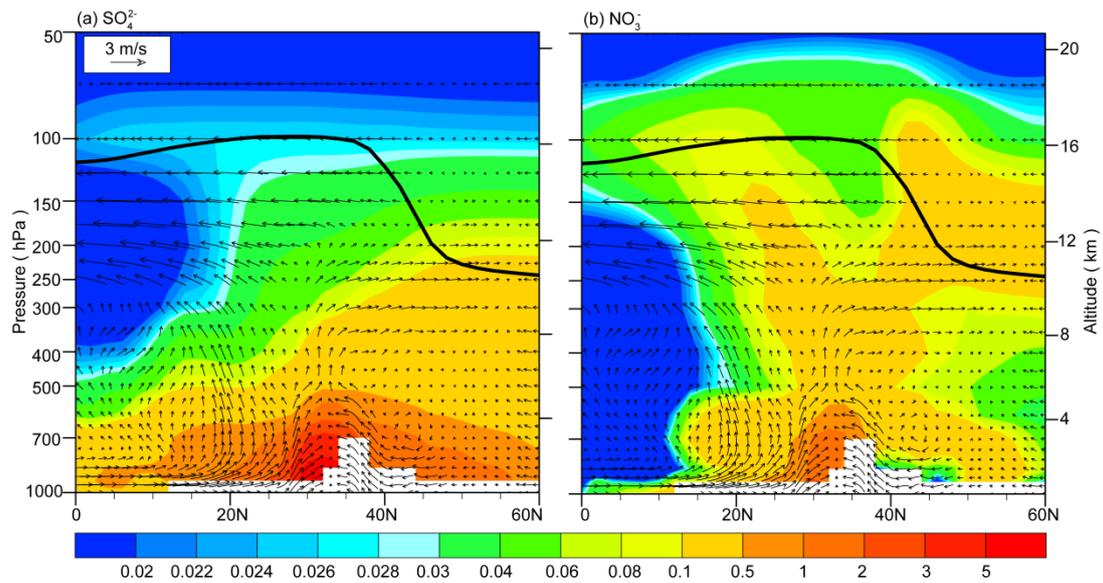
1528  
 1529  
 1530  
 1531  
 1532  
 1533  
 1534  
 1535  
 1536

**Figure. 9.** (a) Monthly mean distribution of aerosol extinction coefficients ( $\text{km}^{-1}$ ) at 100 hPa for July of 2005. (b) Monthly mean vertical distributions of aerosol extinction coefficients (at 525 nm for SAGE II and 550 nm for GEOS-Chem) ( $\text{km}^{-1}$ ) averaged over the Asian monsoon anticyclone region ( $20\text{--}120^\circ\text{E}$ ,  $10\text{--}40^\circ\text{N}$ ) for July of 2005. The horizontal dashed line represents the tropopause averaged over the Asian monsoon anticyclone region simulated by the GEOS-Chem model.



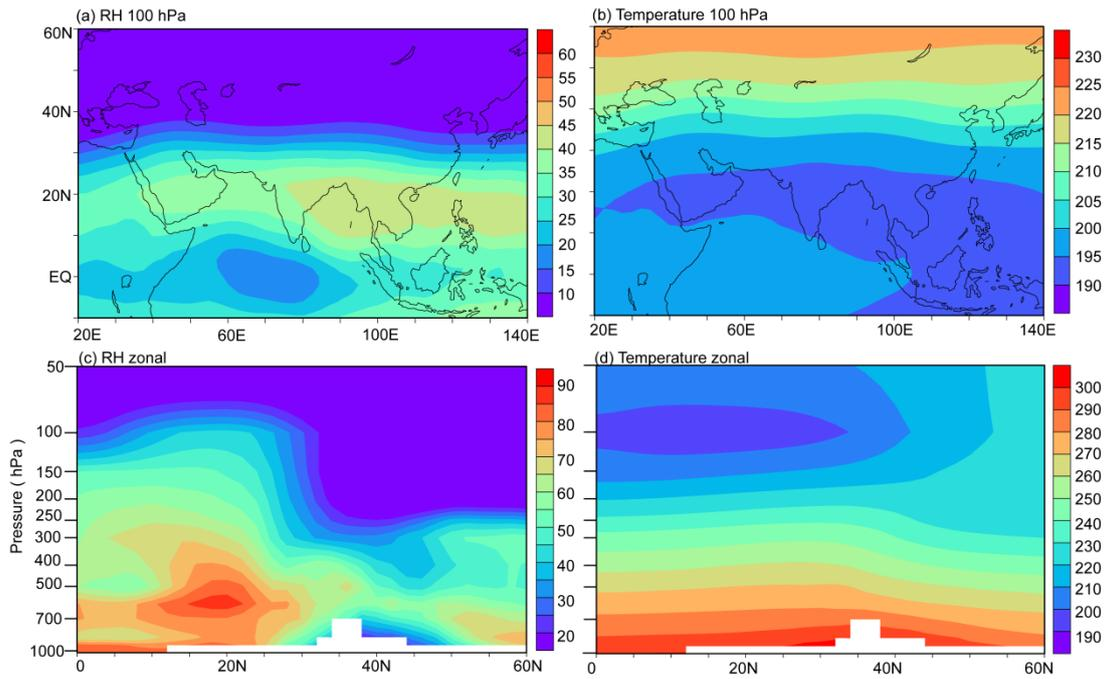
1537  
 1538  
 1539  
 1540  
 1541  
 1542

**Figure. 10.** Simulated contributions of nitrate to PM<sub>2.5</sub> ( $C_{\text{NIT}} = [\text{NIT}] / [\text{PM}_{2.5}] \times 100\%$ ) averaged over summer (June-August) of year 2005 at (a) surface-layer, (b) 200 hPa, and (c) 100 hPa. (d) The latitude-altitude cross section of simulated  $C_{\text{NIT}}$  (%) averaged over 70–105°E.



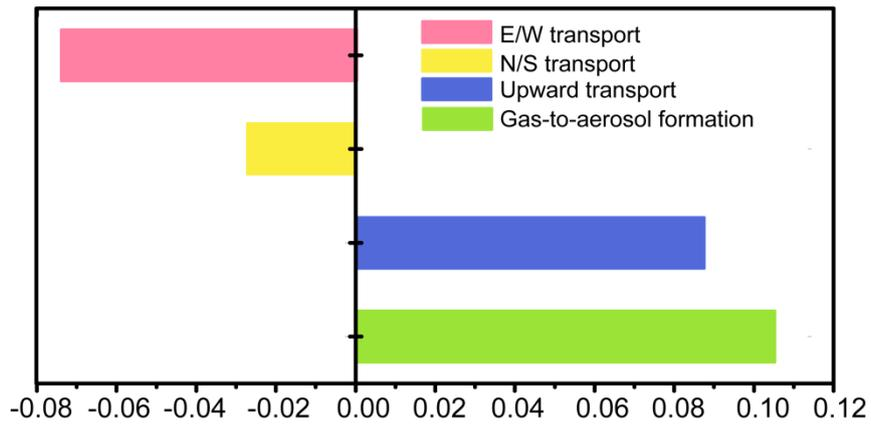
1543  
 1544  
 1545  
 1546  
 1547  
 1548  
 1549

**Figure. 11.** Latitude-altitude cross sections of simulated concentrations (color shades,  $\mu\text{g m}^{-3}$ ) of  $\text{SO}_4^{2-}$  and  $\text{NO}_3^-$  averaged over  $70\text{--}105^\circ\text{E}$  in June-August of 2005, together with the wind vectors obtained from the European Centre for Medium-Range Weather Forecasts (ECMWF) ERA-Interim Reanalysis data. The black line is the tropopause simulated by the GEOS-Chem model.



1550  
 1551  
 1552  
 1553  
 1554  
 1555  
 1556

**Figure. 12.** (a)-(b) Distributions of RH (%) and temperature (K) at 100 hPa. (c)-(d) The latitude-altitude cross sections of RH (%) and temperature (K) averaged over 70–105°E. RH and temperature are from the GEOS5 assimilated meteorological fields, and all the values are the averages over June-August of year 2005.



1557  
 1558  
 1559  
 1560  
 1561  
 1562  
 1563  
 1564  
 1565

**Figure. 13.** Mass budget for nitrate aerosol within the selected box of (70–105°E, 10–40°N, 8–16 km). E/W transport indicates net mass flux through the east and west lateral boundaries, N/S transport indicates net mass flux through the north and south lateral boundaries, and upward transport is the net mass flux through the top and bottom sides of the box. The mass flux is positive if it increases nitrate mass within the box. Unit of fluxes is Tg season<sup>-1</sup>. All the values are the averages over June-August of 2005.